IOP Publishing Journal of Physics A: Mathematical and Theoretical
J. Phys. A: Math. Theor. **55** (2022) 013002 (75pp) https://doi.org/10.1088/1751-8121/ac354e

Topical Review

Variable energy flux in turbulence

Mahendra K Verma*

Department of Physics, Indian Institute of Technology Kanpur, Kanpur 208016, India

E-mail: mkv@iitk.ac.in

Received 14 November 2020, revised 16 October 2021
Accepted for publication 1 November 2021
Published 9 December 2021

Abstract

In three-dimensional hydrodynamic turbulence forced at large length scales, a constant energy flux Π_u flows from large scales to intermediate scales, and then to small scales. It is well known that for multiscale energy injection and dissipation, the energy flux Π_u varies with scales. In this review we describe this principle and show how this general framework is useful for describing a variety of turbulent phenomena. Compared to Kolmogorov's spectrum, the energy spectrum steepens in turbulence involving quasi-static magnetofluid, Ekman friction, stable stratification, magnetohydrodynamics, and solution with dilute polymer. However, in turbulent thermal convection, in unstably stratified turbulence such as Rayleigh–Taylor turbulence, and in shear turbulence, the energy spectrum has an opposite behaviour due to an increase of energy flux with wavenumber. In addition, we briefly describe the role of variable energy flux in quantum turbulence, in binary-fluid turbulence including time-dependent Landau–Ginzburg and Cahn–Hillianrd equations, and in Euler turbulence. We also discuss energy transfers in anisotropic turbulence.

Keywords: turbulence, variable energy flux, energy flux, MHD turbulence, turbulent thermal convection, turbulence modelling, energy transfers

(Some figures may appear in colour only in the online journal)

1. Introduction

Turbulence is observed in most natural flows, for example, in atmospheres and interiors of planets and stars, in oceanic flows, and in stellar and galactic winds. Many engineering flows, as in air conditioners and combustion engines, as well as most kitchen flows are also turbulent. These complex flows have multiple components that could be a combination of velocity, temperature, density, and magnetic fields. The complexities of above turbulent flows appear daunting, yet, the mathematical models and tools developed over the last two centuries

*Author to whom any correspondence should be addressed.

provide reasonable understanding of such flows. In this review article we will describe one such tool called *variable energy flux*.

The nonlinear interactions among the Fourier modes of a turbulent flow cause energy exchange among the modes [1–14]. In one of the pioneering works, Kolmogorov [1, 2] showed that when a hydrodynamic flow is forced vigorously at large scales, it becomes turbulent. In such flows large-scale kinetic energy is transferred to intermediate scales, called *inertial range*, and then to small scales. The flow is *homogeneous* and *isotropic* in the inertial range. For hydrodynamic turbulence, we define *kinetic energy flux* $\Pi_u(k)$ as the net energy transfer from the Fourier modes of a wavenumber sphere of radius k to the Fourier modes outside the sphere. Kolmogorov [1, 2] argued that in the inertial range, an absence of forcing and weak dissipation makes $\Pi_u(k_0)$ constant. In addition, the inertial-range kinetic energy spectrum, $E_u(k)$, varies as $k^{-5/3}$, also called *Kolmogorov's energy spectrum* [5–7]. The above Fourier-space description is directly related to the real-space description proposed by Kolmogorov [1, 2].

The constancy of energy flux in the inertial range of hydrodynamic turbulence is valid only statistically. Researchers have observed strong fluctuations in the inertial-range energy flux due to the singular nature of viscous dissipation [8, 15–17]. This effect is called *intermittency*. Even though significant progress has been made in the understanding of intermittency, yet first-principle derivation of intermittency is still lacking.

Kolmogorov's theory of turbulence describes the energy spectrum and flux of hydrodynamic turbulence without any external force in the intermediate scales. However this assumption is not valid for many complex flows where the forcing and/or dissipation are active in the intermediate scales. For example, gravity acts at all scales in buoyant flows (stably stratified turbulence and thermal convection); the Lorentz force acts at all scales in MHD turbulence; Ekman friction dissipates kinetic energy at all scales. Due to the additional forcing and/or dissipation, the inertial-range energy flux of the such flows varies with wavenumber and the inertial-range kinetic energy spectrum differs from Kolmogorov's $k^{-5/3}$ spectrum. *In the present review, we focus on these variations in the energy flux.*

Interestingly, complex variations in energy spectrum and flux can be quantified using an equation for the variable energy flux: $\mathrm{d}\Pi_u(k)/\mathrm{d}k = \mathcal{F}_u(k) - D_u(k)$, where $\mathcal{F}_u(k)$ is the kinetic energy injection rate by the external force at wavenumber k, and $D_u(k)$ is the dissipation rate at k [8, 9, 11, 14]. This framework of *variable energy flux*, which is the theme of this review, helps us understand a wide range of turbulent phenomena. We introduce these topics in this section and detail them in subsequent sections.

Strong external fields, such as magnetic field and rotation, make a flow anisotropic. Consequently, the modal energy spectrum $E_u(\mathbf{k})$, where $\mathbf{k}$ is the wavenumber, becomes a function of k and θ, which is the angle between the anisotropy direction and $\mathbf{k}$. The shell spectrum $E_u(k)$, which is a sum of $E_u(\mathbf{k})$ over the shell of radius k, does not capture the θ-dependence of $E_u(\mathbf{k})$. A more refined measure called *ring spectrum* $E_u(k, \theta)$ [14, 18] is useful for such flows. The energy flux $\Pi_u(k)$ too has a similar limitation, while the *ring-to-ring energy transfer* achieves this objective [14, 18]. Note however that $E_u(k)$ and $\Pi_u(k)$ are well defined for anisotropic flows as well, and they pick up the multiscale dynamics quite well. For example, in quasi-static magnetohydrodynamic (MHD) turbulence and in the presence of Ekman friction (both being anisotropic flows), $E_u(k)$ is steeper than Kolomogorov's spectrum due to additional dissipation. In stably stratified turbulence, a conversion of kinetic energy to potential energy leads to a steepening of the energy spectrum. In this review we will study such variations in isotropic turbulence, as well as in anisotropic turbulence, using variable energy flux.

Gravity acts at all scales in stably stratified turbulence and in thermal convection and generates variable kinetic energy fluxes in these systems. For the stably stratified turbulence with moderate stratification, Bolgiano [19] and Obukhov [20] showed that $\mathcal{F}_u(k) < 0$ and

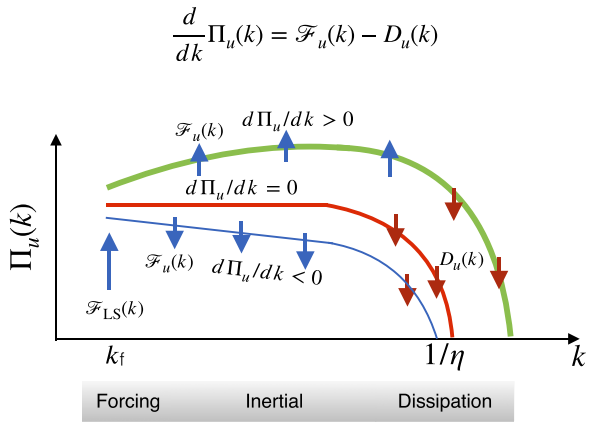

Figure 1. A figure illustrating variable energy flux. The blue and red arrows depict $\mathcal{F}_u(k)$ and $D_u(k)$ respectively. The red curve represents Kolmogorov's model for which $\Pi_u(k) =$ constant in the inertial range because $\mathcal{F}_u(k) = 0$ and $D_u(k) = 0$. The green curve represents the case when $\mathcal{F}_u(k) > 0$ and $\mathrm{d}\Pi_u(k)/\mathrm{d}k > 0$, while the blue curve represents flows with $\mathcal{F}_u(k) < 0$ and $\mathrm{d}\Pi_u(k)/\mathrm{d}k < 0$.

$\mathrm{d}\Pi_u(k)/\mathrm{d}k < 0$ due to a conversion of kinetic energy to potential energy by buoyancy. In particular, $\Pi_u(k) \sim k^{-4/5}$ and $E_u(k) \sim k^{-11/5}$ (different from Kolmogorov's $k^{-5/3}$ spectrum). See figure 1 for an illustration.

The physics of thermal convection, however, is quite different from the stably stratified turbulence even though the equations for the two systems are the same. This is because thermal convection is unstable, while stably stratified turbulence is stable. In the inertial range of turbulent convection, thermal plumes drive the velocity field. Hence, $\mathcal{F}_u(k) > 0$ leading to $\mathrm{d}\Pi_u(k)/\mathrm{d}k > 0$. See figure 1 for an illustration. Detailed studies, however, show that for small and moderate Prandtl numbers, $\mathcal{F}_u(k)$ is primarily concentrated at small wavenumbers, as in Kolmogorov's theory of hydrodynamic turbulence. Consequently, the kinetic energy spectrum and flux of turbulent convection are similar to those predicted by Kolmogorov's turbulence theory [21–23]. Thus, energy flux diagnostics helped in resolving the long-standing problem whether turbulent convection follows Bolgiano–Obukhov spectrum or Kolmgorov spectrum.

Variable energy flux is also useful for describing MHD turbulence and dynamo. Here, the Lorentz force, which is active at all scales, transfers energy from the velocity field to the magnetic field. These energy transfers are responsible for the enhancement of magnetic field in astrophysical objects via dynamo mechanism [14, 24, 25]. These transfers also lead to a reduction in the kinetic energy flux and an enhancement of the magnetic energy flux with wavenumber [14]. In quasi-static MHD turbulence, Joule dissipation is significant at all scales; consequently, the inertial-range kinetic energy flux decreases with k, and $E_u(k)$ is steeper than Kolmogorov's $k^{-5/3}$ spectrum [26–28]. Anas and Verma [29] showed that the variable energy formalism successfully explains the spectral steepening of quasi-static MHD turbulence observed in numerical simulations and experiments [26–28]. For a very strong magnetic field, the Joule dissipation steepens $E_u(k)$ even further and yields an exponential spectrum, which is $\exp(-ck)$, where c is a constant.

In shear turbulence, shear acts at small wavenumbers and injects energy to the flow. This injected energy leads to an increase in the kinetic energy flux with k. This variation in the kinetic energy flux may be responsible for the $1/f$ noise reported for many shearing flows

[30–32]. On the other hand, Ekman friction acts at all scales and depletes the kinetic energy flux in the inertial range leading to a steeper kinetic energy spectrum than $k^{-5/3}$ [33, 34].

In the viscous range of hydrodynamic turbulence, $\mathrm{d}\Pi_u(k)/\mathrm{d}k = -2\nu k^2 E_u(k)$, where ν is the kinematic viscosity. The viscous dissipation leads to steep decline in $\Pi_u(k)$ and $E_u(k)$ in the dissipation range. Researchers [11, 35–37] have attempted to model the energy spectrum in this range. In particular, Pao [35] derived that in the inertial–dissipation range of 3D hydrodynamic turbulence, $\Pi_u(k)$ and $E_u(k)k^{5/3}$ vary as $\exp\{-c(k/k_d)^{4/3}\}$, where c is a constant, and k_d is the Kolmogorov wavenumber. Pao's model for the 3D inertial–dissipation range has been extended to 2D hydrodynamic turbulence [14, 38]. Falkovich [39] and Verma and Donzis [40] showed that the energy flux plays an important role in the bottleneck effect. Recently, Kuchler *et al* [41] performed a detailed experimental study of bottleneck effect.

In most complex flows, one or several secondary fields are coupled to the velocity field. The secondary field could be the density field in buoyant flows, the temperature field in thermal convection, the magnetic field in MHD turbulence, or the conformation tensor of polymers in polymeric flows. The nonlinear term associated with the secondary field also induces energy transfer or secondary-energy flux. The potential-energy fluxes of stably stratified turbulence and turbulent thermal convection are examples of such fluxes. In addition, a coupling between the velocity field with the secondary field often yields energy exchange between the velocity field and the secondary field, as well as variability in the secondary energy flux [42–44]. This phenomena is related to the turbulent drag reduction in polymeric turbulence [45–47] and in MHD turbulence [48].

The enstrophy ($\int \mathrm{d}\mathbf{r}\frac{1}{2}|\boldsymbol{\omega}|^2$, where $\boldsymbol{\omega}$ is the vorticity field) and kinetic helicity ($\int \mathrm{d}\mathbf{r}\frac{1}{2}|[\mathbf{u}\cdot\boldsymbol{\omega}]$) are important quantities of hydrodynamic turbulence. The fluxes of these quantities exhibit interesting properties. For example, the enstrophy flux has a similar structure as those of kinematic dynamo [14, 24]. In MHD turbulence, the flux of magnetic helicity too exhibit interesting properties [25].

Under strong external field, stably stratified turbulence, MHD turbulence, and rotating turbulence become quasi-two-dimensional (quasi-2D) with $|\mathbf{u}_\perp| \gg u_\parallel$, where $\mathbf{u}_\perp$ and $u_\parallel$ are respectively the perpendicular and parallel components of the velocity field in relation to the anisotropy direction. On the other hand, in thermal convection, $|\mathbf{u}_\perp| \ll u_\parallel$. In these flows, the pressure acts as a mediator for the energy exchange between the parallel and perpendicular components of the velocity field [14, 28, 49]. The energy fluxes of $\mathbf{u}_\perp$ and $u_\parallel$ help us model the anisotropic nature of such flows. The secondary fields too have similar anisotropic fluxes, but these quantities have not been analyzed in detail. As described earlier, the other useful tools for anisotropic flows are ring spectrum and ring-to-ring energy transfers.

Quantum systems, such as superfluids and Bose–Einstein condensate, too exhibit turbulent behaviour for a range of parameters. Researchers have studied energy spectra and fluxes of these systems. For example, in helium-4, normal and superfluid components interact with each other that leads to a variability in their energy fluxes (e.g. [50–53] and references therein). The scenario is more complicated in helium-3 that lacks normal component; here phonon coupling at small scales is expected to provide the dissipation [54, 55].

The energy flux is a useful diagnostic tool for other nonequilibrium systems as well. For example, in binary-mixture turbulence, the energy flux provides valuable insights into the field dynamics, especially for phase separation and coarsening [56, 57]. Researchers have also employed time-dependent Ginzburg–Landau and Cahn–Hilliard (CH) equations to model the coarsening process [58, 59], where the energy flux is proving to be a very useful tool [56, 57].

Lee [60] and Kraichnan [61] showed that inviscid hydrodynamic turbulence ($\nu = 0$) exhibits equilibrium behaviour (also called *absolute equilibrium*). The energy flux for this case vanishes due to the detailed energy balance among the Fourier modes [8]. The evolution of such

systems depends quite critically on the initial condition. For example, Cichowlas *et al* [62] showed that Taylor–Green vortex as an initial condition yields a mixture of $k^{-5/3}$ and k^2 spectra, which approaches k^2 spectrum at all wavenumbers asymptotically. On the contrary, for delta-correlated field as an initial condition, the system exhibits k^2 spectrum for the whole range of wavenumbers [63, 64]. The former system exhibits variable energy flux, but the latter system (equilibrium configuration) has no energy flux. The absolute equilibrium theory of hydrodynamics has been extended to MHD turbulence [65, 66], quantum turbulence [67, 68], Burger turbulence [69], and other forms of turbulence [6, 8].

The aforementioned turbulent systems have been studied extensively in the past, including in books [3–11, 14] and review articles [70]. The equation of variable energy flux, $\mathrm{d}\Pi_u(k)/\mathrm{d}k = \mathcal{F}_u(k) - D_u(k)$, too appears in several textbooks, for example [6–9]. In this review article, we illustrate how various turbulent phenomena can be connected via variable energy flux. We also present the scaling laws and energy fluxes of many turbulent systems thematically in the framework of variable energy flux. This perspective helps model and understand several turbulent systems. For example, using variable energy flux, it has been shown that the dynamics of turbulent thermal convection is very different from that of stably stratified turbulence, contrary to a popular view that the Bolgiano–Obukhov scaling for stably stratified turbulence [19, 20] also works for turbulent thermal convection [71–73]. The different behaviour of the energy fluxes of the two systems played a key role in the resolution of this critical puzzle.

The structure of the review is as follows. Section 2 introduces the energy transfers and energy flux in hydrodynamic turbulence. The formalism of variable energy flux is presented in section 3. In this section, we present variable energy fluxes in the dissipation range of hydrodynamic turbulence and in shear turbulence. In section 4 we derive the energy flux for the secondary field that is advected by velocity field and show how it could become variable when a multiscale force is applied to the secondary field. In section 5 we describe the energy exchange between the secondary field and the velocity field, as well as those between the field components in anisotropic turbulence. Section 6 contains discussions on turbulence in stably stratified flows and thermal convection. Section 7 describes variable energy fluxes in MHD turbulence and in quasi-static MHD turbulence. Here, we discuss several exact relations among the fluxes of MHD turbulence. In section 8, we show how energy flux is an useful tool to describe a turbulent flow with dilute polymer. Section 9 describes the fluxes associated with enstrophy and kinetic helicity, while section 10 contains discussions on 2D and quasi-2D turbulence. Variable energy fluxes in dissipationless systems are discussed in section 11, while those in quantum turbulence and binary-mixture turbulence are discussed in section 12. In section 13 we briefly discuss how to compute energy fluxes using field-theoretic tools. We conclude in section 14.

2. Energy flux in hydrodynamics

In this section, we introduce the kinetic energy flux of hydrodynamics. We start with the basic equations of hydrodynamics in real and Fourier spaces.

2.1. Basic equations of hydrodynamics

The Navier–Stokes (NS) equations given below describe an incompressible flow [15]:

$$\frac{\partial \mathbf{u}}{\partial t} + (\mathbf{u}\cdot\nabla)\mathbf{u} = -\frac{1}{\rho}\nabla p + \mathbf{F}_u + \mathbf{F}_{\mathrm{LS}} + \nu\nabla^2\mathbf{u}, \tag{1}$$

$$\nabla\cdot\mathbf{u} = 0, \tag{2}$$

where $\mathbf{u}(\mathbf{r},t)$ is the velocity field, $p(\mathbf{r},t)$ is the pressure field, $\mathbf{F}_{\rm LS}$ is the large-scale external force, $\mathbf{F}_u$ is the force field such as buoyancy, and ν is the kinematic viscosity. Under incompressible limit, the fluid density ρ can be treated as a constant. In this review, without loss of generality, ρ is taken to be unity. We distinguish $\mathbf{F}_{\rm LS}$ and $\mathbf{F}_u$ to clearly demarcate the energy transfers from these forces. Note that $\mathbf{F}_u$ could be a function of the velocity field; for example, Ekman friction is $-\alpha\mathbf{u}$, where α is a constant. For an incompressible flow, the pressure field is determined using

$$p = -\nabla^{-2}\nabla\cdot[(\mathbf{u}\cdot\nabla)\mathbf{u} - \mathbf{F}_u - \mathbf{F}_{\rm LS}]\,. \tag{3}$$

The ratio of the nonlinear term $(\mathbf{u}\cdot\nabla)\mathbf{u}$ and the viscous term $\nu\nabla^2\mathbf{u}$ is called *Reynolds number* Re, which is UL/ν, where U, L are the large-scale velocity and length respectively.

In three-dimensional (3D) inviscid ($\nu = 0$) hydrodynamics, for a periodic or vanishing boundary condition, the total kinetic energy, $E_u = \frac{1}{2}\int \mathrm{d}\mathbf{r}u^2$, and the total kinetic helicity, $H_{\rm K} = \frac{1}{2}\int \mathrm{d}\mathbf{r}(\mathbf{u}\cdot\boldsymbol{\omega})$, are conserved [6, 8, 9]. Here, $\boldsymbol{\omega} = \nabla\times\mathbf{u}$ is the vorticity field. In two-dimensional (2D) hydrodynamics, the total kinetic energy and the total enstrophy, $\frac{1}{2}\int \mathrm{d}\mathbf{r}|\boldsymbol{\omega}|^2$, are conserved. Note that the physics of turbulence in 2D and 3D are quite different. In this review, we will focus on the fluxes of kinetic energy and associated secondary energy in 3D flows. The fluxes of other quantities, such as enstrophy and kinetic helicity, will be discussed briefly.

The multiscale energy transfers and fluxes are conveniently described using the velocity Fourier modes. For compactness, we denote the Fourier transform of $\mathbf{u(r)}$ using $\mathbf{u(k)}$; here $\mathbf{r}$ and $\mathbf{k}$ denote the real and Fourier space coordinates respectively. In a Fourier space convolution, the other wavenumbers are denoted by $\mathbf{p}$ and $\mathbf{q}$. The wavenumbers are discrete for a flow confined in a finite box, but they form a continuum for a flow in an infinite box.

The NS equations are transformed in Fourier space as [6, 8, 9, 23]

$$\frac{\mathrm{d}}{\mathrm{d}t}\mathbf{u}(\mathbf{k}) + \mathbf{N}_u(\mathbf{k}) = -\mathrm{i}\mathbf{k}p(\mathbf{k}) + \mathbf{F}_u(\mathbf{k}) + \mathbf{F}_{\rm LS}(\mathbf{k}) - \nu k^2\mathbf{u}(\mathbf{k}), \tag{4}$$

$$\mathbf{k}\cdot\mathbf{u}(\mathbf{k}) = 0, \tag{5}$$

where

$$\mathbf{N}_u(\mathbf{k}) = \mathrm{i}\sum_{\mathbf{p}}\{\mathbf{k}\cdot\mathbf{u}(\mathbf{q})\}\mathbf{u}(\mathbf{p}) \tag{6}$$

is the Fourier transform of the nonlinear term $(\mathbf{u}\cdot\nabla)\mathbf{u}$. Here $\mathbf{q} = \mathbf{k} - \mathbf{p}$. The equation for the pressure mode $p(\mathbf{k})$ is

$$p(\mathbf{k}) = \frac{\mathrm{i}}{k^2}\mathbf{k}\cdot\{\mathbf{N}_u(\mathbf{k}) - \mathbf{F}_u(\mathbf{k}) - \mathbf{F}_{\rm LS}(\mathbf{k})\}. \tag{7}$$

We define *modal kinetic energy* for wavenumber $\mathbf{k}$ as $E_u(\mathbf{k}) = \frac{1}{2}|\mathbf{u}(\mathbf{k})|^2$. Note that Parseval's theorem yields the following relation for the total kinetic energy:

$$E_u = \frac{1}{2}\langle|\mathbf{u}(\mathbf{r})|^2\rangle = \frac{1}{\mathrm{Vol}}\int \mathrm{d}\mathbf{r}\frac{1}{2}|\mathbf{u}(\mathbf{r})|^2 = \sum_{\mathbf{k}}\frac{1}{2}|\mathbf{u}(\mathbf{k})|^2, \tag{8}$$

where 'Vol' is the volume of the box. We derive the following dynamical equation for $E_u(\mathbf{k})$ by performing a scalar product of equation (4) with $\mathbf{u}^*(\mathbf{k})$ and adding the resulting equation

with its complex conjugate [6, 8, 9, 23]:

$$\begin{aligned}\frac{\mathrm{d}}{\mathrm{d}t}E_u(\mathbf{k}) &= T_u(\mathbf{k}) + \mathcal{F}_u\mathbf{k}) + \mathcal{F}_{\mathrm{LS}}\mathbf{k}) + D_u(\mathbf{k}) \\ &= \sum_{\mathbf{p}} \Im\left[\{\mathbf{k}\cdot\mathbf{u}(\mathbf{q})\}\{\mathbf{u}(\mathbf{p})\cdot\mathbf{u}^*(\mathbf{k})\}\right] + \Re[\mathbf{F}_u(\mathbf{k})\cdot\mathbf{u}^*(\mathbf{k})] \\ &\quad + \Re[\mathbf{F}_{\mathrm{LS}}(\mathbf{k})\cdot\mathbf{u}^*(\mathbf{k})] - 2\nu k^2 E_u(\mathbf{k}),\end{aligned} \tag{9}$$

where $\mathbf{q} = \mathbf{k} - \mathbf{p}$, and $\Re[.]$, $\Im[.]$ stand respectively for the real and imaginary parts of the argument. In the above equation, $T_u(\mathbf{k})$ is the nonlinear energy transfer from all the Fourier modes to $\mathbf{u(k)}$; $\mathcal{F}_u(\mathbf{k}), \mathcal{F}_{\mathrm{LS}}\mathbf{k})$ are the respective energy supply rates from $\mathbf{F}_u$ and $\mathbf{F}_{\mathrm{LS}}$ to $\mathbf{u(k)}$; and $D_u(\mathbf{k})$ is the viscous dissipation rate of $\mathbf{u(k)}$.

The nonlinear interactions of equation (9) induce complex energy transfers among the Fourier modes. However, a peep into a single wavenumber triad provides interesting insights into the nature of nonlinear interactions [74], which will be described below.

2.2. *Triadic energy transfers and energy flux in hydrodynamics*

Kraichnan [74] focussed on a pair of interacting wavenumber triads, $(\mathbf{k}, \mathbf{p}, \mathbf{q})$ and $(-\mathbf{k}, -\mathbf{p}, -\mathbf{q})$ with a condition that $\mathbf{k} = \mathbf{p} + \mathbf{q}$. The corresponding Fourier modes are $\mathbf{u(k)}, \mathbf{u(p)}, \mathbf{u(q)}$ and their complex conjugates: $\mathbf{u}^*(\mathbf{k}), \mathbf{u}^*(\mathbf{p}), \mathbf{u}^*(\mathbf{q})$. For convenience, we set $\nu = 0$ to suppress the viscous dissipation rate, which is a trivial linear term of equation (9). In addition, we assume that $\mathbf{F}_u = 0$ and $\mathbf{F}_{\mathrm{LS}} = 0$.

The wavenumbers $\mathbf{k}, \mathbf{p}, \mathbf{q}$ of equation (9) are not symmetric (note $\mathbf{k} = \mathbf{p} + \mathbf{q}$). The formulas for the energy transfers are best expressed using a symmetric set $(\mathbf{k}', \mathbf{p}, \mathbf{q})$ obeying a constraint, $\mathbf{k}' + \mathbf{p} + \mathbf{q} = 0$. Note that $\mathbf{k}' = -\mathbf{k}$. For this triad, the dynamical equation for the modal energy $E_u(\mathbf{k}')$ is

$$\begin{aligned}\frac{\mathrm{d}}{\mathrm{d}t}E_u(\mathbf{k}') &= -\Im\left[\{\mathbf{k}'\cdot\mathbf{u}(\mathbf{q})\}\{\mathbf{u}(\mathbf{p})\cdot\mathbf{u}(\mathbf{k}')\} + \{\mathbf{k}'\cdot\mathbf{u}(\mathbf{p})\}\{\mathbf{u}(\mathbf{q})\cdot\mathbf{u}(\mathbf{k}')\}\right] \\ &= S^{uu}(\mathbf{k}'|\mathbf{p},\mathbf{q}).\end{aligned} \tag{10}$$

The equations for $E_u(\mathbf{p})$ and $E_u(\mathbf{q})$ are written in a similar manner.

The function $S^{uu}(\mathbf{k}'|\mathbf{p},\mathbf{q})$, called the *combined energy transfer*, represents the net kinetic energy transfer from modes $\mathbf{u(p)}$ and $\mathbf{u(q)}$ to $\mathbf{u}(\mathbf{k}')$. Note that the energy of the mode $\mathbf{u}(\mathbf{k}')$ grows at a rate of $\mathrm{d}E_u(\mathbf{k}')/\mathrm{d}t$. Using equation (10) and the incompressibility condition, $\mathbf{k}'\cdot\mathbf{u}(\mathbf{k}') = 0$, we derive that [6, 74]

$$S^{uu}(\mathbf{k}'|\mathbf{p},\mathbf{q}) + S^{uu}(\mathbf{p}|\mathbf{q},\mathbf{k}') + S^{uu}(\mathbf{q}|\mathbf{k}',\mathbf{p}) = 0 \tag{11}$$

that leads to the conservation of the total energy within a triad.

Even though Kraichnan's combined energy transfer formula has been widely used, it does not provide individual energy transfers among the Fourier modes. This task was first achieved by Dar *et al* [42] who derived the *mode-to-mode energy transfer* from mode $\mathbf{u(p)}$ to mode $\mathbf{u}(\mathbf{k}')$ with the mediation of mode $\mathbf{u(q)}$ as [43].

$$S^{uu}(\mathbf{k}'|\mathbf{p}|\mathbf{q}) = -\Im\left[\{\mathbf{k}'\cdot\mathbf{u}(\mathbf{q})\}\{\mathbf{u}(\mathbf{p})\cdot\mathbf{u}(\mathbf{k}')\}\right]. \tag{12}$$

The formula contains a scalar product between the receiver mode $\mathbf{u}(\mathbf{k}')$ and the giver mode $\mathbf{u(p)}$, and another scalar product between the receiver wavenumber $\mathbf{k}'$ and the mediator mode $\mathbf{u(q)}$.

The successive arguments of S^{uu} are receiver, giver, and mediator wavenumbers respectively. In terms of wavenumbers $\mathbf{k}, \mathbf{p}, \mathbf{q}$ with $\mathbf{k} = \mathbf{p} + \mathbf{q}$, the above formula is written as

$$S^{uu}(\mathbf{k}|\mathbf{p}|\mathbf{q}) = \Im\left[\{\mathbf{k}\cdot\mathbf{u}(\mathbf{q})\}\{\mathbf{u}(\mathbf{p})\cdot\mathbf{u}^*(\mathbf{k})\}\right]. \tag{13}$$

Note that the mode-to-mode energy transfer functions satisfy the following properties:

$$S^{uu}(\mathbf{k}'|\mathbf{p}|\mathbf{q}) + S^{uu}(\mathbf{k}'|\mathbf{q}|\mathbf{p}) = S^{uu}(\mathbf{k}'|\mathbf{p},\mathbf{q}), \tag{14}$$

$$S^{uu}(\mathbf{k}'|\mathbf{p}|\mathbf{q}) = -S^{uu}(\mathbf{p}|\mathbf{k}'|\mathbf{q}). \tag{15}$$

The latter property follows from the incompressibility condition: $\mathbf{k}'\cdot\mathbf{u}(\mathbf{k}') = 0$. Dar *et al* [42] and Verma [43] showed that equation (12) satisfies equations (14) and (15), but it is not a unique solution to equations (14) and (15). A circulating energy transfer that traverses along wavenumbers $\mathbf{p}\to\mathbf{k}'\to\mathbf{q}\to\mathbf{p}$ could be added to the respective mode-to-mode energy transfers of equation (12) without violating equations (14) and (15). The circulating transfer enters and leaves a mode, hence they do not alter the energy flux, which is a measurable quantity. Therefore, the circulating transfer could be safely ignored. Later, using tensor analysis and symmetry arguments, Verma [14] showed that equation (12) provides a unique formula for the mode-to-mode energy transfer.

A fluid flow has many Fourier modes. Hence, the net energy transfer to the mode **u(k)** is a sum of energy transfers from all other modes. In terms of mode-to-mode energy transfer, the net energy transfer to **u(k)** is [42, 43]

$$\frac{\mathrm{d}}{\mathrm{d}t}E_u(\mathbf{k}) = \sum_{\mathbf{p}} S^{uu}(\mathbf{k}|\mathbf{p}|\mathbf{q}) + \mathcal{F}_u(\mathbf{k}) + \mathcal{F}_{\mathrm{LS}}(\mathbf{k}) - D_u(\mathbf{k}), \tag{16}$$

where $\mathbf{q} = \mathbf{k} - \mathbf{p}$. A comparison of equations (16) and (9) shows that

$$T_u(\mathbf{k}) = \sum_{\mathbf{p}} S^{uu}(\mathbf{k}|\mathbf{p}|\mathbf{q}), \tag{17}$$

is the net energy transfer to mode **u(k)** by nonlinearity. Also note that for any wavenumber region A,

$$\sum_{\mathbf{p}\in A}\sum_{\mathbf{k}\in A} S^{uu}(\mathbf{k}|\mathbf{p}|\mathbf{q}) = 0. \tag{18}$$

The above relation hinges on equation (15).

A very useful quantity in turbulence is the energy flux $\Pi_u(k_0)$, which is the total energy transfer from all the modes inside a wavenumber sphere of radius k_0 to all the modes outside the sphere. Starting from Kraichnan [74], researchers have derived a number of formulas for $\Pi_u(k_0)$ [1, 2, 6, 8, 9, 42, 43, 74, 75]. Here we present the flux formula in terms of mode-to-mode energy transfer, which is

$$\Pi_u(k_0) = \sum_{\mathbf{p}\leqslant k_0}\sum_{k>k_0} S^{uu}(\mathbf{k}|\mathbf{p}|\mathbf{q}) = \sum_{\mathbf{p}\leqslant k_0}\sum_{k>k_0} \Im\left[\{\mathbf{k}\cdot\mathbf{u}(\mathbf{q})\}\{\mathbf{u}(\mathbf{p})\cdot\mathbf{u}^*(\mathbf{k})\}\right] \tag{19}$$

with $\mathbf{q} = \mathbf{k} - \mathbf{p}$. In the sum, the giver wavenumber **p** is inside the wavenumber sphere, while the receiver wavenumber **k** is outside the sphere. For the above formula, it does not matter whether the mediator wavenumber **q** is inside or outside the sphere. This liberty does not exist for the combined energy transfer formula in which both **u(p)** and **u(q)** supply energy to **u**($\mathbf{k}'$).

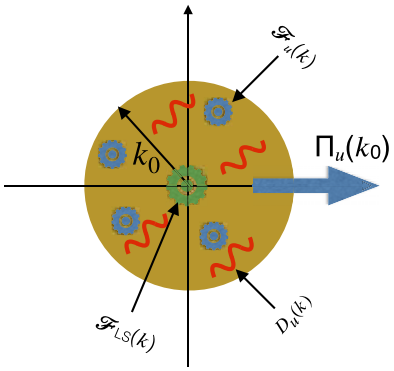

Figure 2. Illustration of the energy flux $\Pi_u(k_0)$, the kinetic energy injection rates by $\mathcal{F}_u(\mathbf{k})$ and $\mathcal{F}_{\rm LS}(\mathbf{k})$ (wheels), and the local viscous dissipation rate $D_u(\mathbf{k})$ (wavy lines). The viscous dissipation is negligible at small wavenumbers.

The ambiguity of $\mathbf{u}(\mathbf{q})$ in the combined energy transfer poses a serious challenge for computing the shell-to-shell energy transfers [42, 43].

We derive another set of formulas for the energy flux using $T_u(\mathbf{k})$. We sum the terms of equation (16) over all the modes inside the sphere that yields [6, 8, 9, 74]

$$\frac{\mathrm{d}}{\mathrm{d}t}\sum_{k\leqslant k_0} E_u(\mathbf{k}) = \sum_{k\leqslant k_0} T_u(\mathbf{k}) + \sum_{k\leqslant k_0} \mathcal{F}_u(\mathbf{k}) + \sum_{k\leqslant k_0} \mathcal{F}_{\rm LS}(\mathbf{k}) - \sum_{k\leqslant k_0} D_u(\mathbf{k}). \tag{20}$$

To the wavenumber sphere of radius k_0, $\sum_{k\leqslant k_0} \mathcal{F}_u(\mathbf{k})$ and $\sum_{k\leqslant k_0} \mathcal{F}_{\rm LS}(\mathbf{k})$ are the net energy supply rates by $\mathbf{F}_u$ and $\mathbf{F}_{\rm LS}$ respectively; and $\sum_{k\leqslant k_0} D_u(\mathbf{k})$ is the net viscous dissipation rate in the sphere (see figure 2). The sum $\sum_{k\leqslant k_0} T_u(\mathbf{k})$ is the net energy transfer due to the nonlinear term from the modes outside the sphere to the modes inside the sphere. Hence, by definition,

$$\Pi_u(k_0) = -\sum_{k\leqslant k_0} T_u(\mathbf{k}). \tag{21}$$

Using equations (20) and (21) we derive

$$\Pi_u(k_0) = -\frac{\mathrm{d}}{\mathrm{d}t}\sum_{k\leqslant k_0} E_u(\mathbf{k}) + \sum_{k\leqslant k_0} \mathcal{F}_u(\mathbf{k}) + \sum_{k\leqslant k_0} \mathcal{F}_{\rm LS}(\mathbf{k}) - \sum_{k\leqslant k_0} D_u(\mathbf{k}). \tag{22}$$

Similarly, using the following equation,

$$\frac{\mathrm{d}}{\mathrm{d}t}\sum_{k>k_0} E_u(\mathbf{k}) = \sum_{k>k_0} T_u(\mathbf{k}) + \sum_{k>k_0} \mathcal{F}_u(\mathbf{k}) + \sum_{k>k_0} \mathcal{F}_{\rm LS}(\mathbf{k}) - \sum_{k>k_0} D_u(\mathbf{k}), \tag{23}$$

one obtains $\Pi_u(k_0) = \sum_{k>k_0} T_u(\mathbf{k})$ [6, 14]. Verma *et al* [76] employed equation (22) to compute the energy fluxes of MHD turbulence.

Note that the energy flux $\Pi_u(k)$ arises due to the nonlinear interactions. Its definition does not hinge on the conservation laws for force-free inviscid flow, contrary to what is argued in some literature. For example, in buoyant flows, $\Pi_u(k)$ is clearly defined, but total kinetic energy is not conserved due to conversion of kinetic energy to potential energy. However, equations (20), (22) and (23) are exact relations based on energy conservation for any region of Fourier space;

the total incident energy to a volume of Fourier space yields rate of change of kinetic energy in that region. The latter conservation law is related to the energy flux.

Interestingly, $T_u(k)$-based energy flux formula can be used for systems whose nonlinear interactions differ from those of incompressible hydrodynamics. For example, for dissipationless Burgers equation, $\partial_t u = -\partial_x u^2/2$, the energy equation is

$$\frac{\mathrm{d}}{\mathrm{d}t}\frac{1}{2}|u(k)|^2 = \sum_{\mathbf{p}} \Im[ku(k-\mathbf{p})u(\mathbf{p})u^*(k)] = T(k). \tag{24}$$

Hence, the energy flux $\Pi(k_0) = -\sum_{k<k_0} T(k)$. We can also use the above procedure to compute the energy flux for ϕ^4 theory where the interaction is quartic, and $T(k) \sim \phi(\mathbf{k}_1)\phi(\mathbf{k}_2)\phi(\mathbf{k}_3)\phi(\mathbf{k}_4)$ with $\mathbf{k}_1 + \mathbf{k}_2 + \mathbf{k}_3 + \mathbf{k}_4 = 0$ [77, 78]. Such schemes are useful for modelling energy transfers in binary fluids, in time-dependent Ginzburg–Landau, and in Cahn-Hilliard equations. (See section 12).

Kraichnan [74], Frisch [8], Alexakis *et al* [44, 75], and others have derived formulas for the energy flux based on nonlinear interactions in Fourier space. These formulas will not be discussed here due to lack of space and due to similarities with those discussed above. In contrast, Kolmogorov's formula for the energy flux [1, 2] is based on the third-order structure function of real space.

For homogeneous, isotropic, and steady hydrodynamic turbulence, under the limit of $\nu \to 0$, Kolmogorov [1, 2] formulated a theory for the third-order structure function. Assuming the fluid to be forced at large scales, the theory predicts that the energy flux is constant in the inertial range, and that the inertial-range energy spectrum is proportional to $k^{-5/3}$. For such systems, the constancy of the inertial-range energy flux can also be deduced using the Fourier-space formalism. Since the flow is forced at large scales, $\mathcal{F}_u(\mathbf{k}) = \mathcal{F}_{\mathrm{LS}}(\mathbf{k}) = 0$ for the inertial-range wavenumbers where $D_u(\mathbf{k})$ is negligible. For the steady state ($\langle \partial_t E(\mathbf{k})\rangle = 0$), using equation (22), we deduce that in the inertial range [8, 14],

$$\langle \Pi_u(k)\rangle = \langle \epsilon_u\rangle = \text{const.}, \tag{25}$$

where ϵ_u is the energy supply rate by the large-scale forcing, and $\langle f\rangle$ denotes the ensemble average of the quantity f. We remark that $\Pi_u(k)$ and ϵ_u exhibit fluctuations with nontrivial probability distribution function (PDF) [8]. Consequently, $\langle [\Pi_u(k)]^q\rangle \neq \langle \Pi_u(k)\rangle^q$ for hydrodynamic turbulence [8].

In Kolmogorov's model, the inertial-range energy flux is constant under steady state because $\mathcal{F}_u(\mathbf{k}) = 0$. The energy flux *varies with* k when the flow is forced in the inertial range ($\mathcal{F}_u(\mathbf{k}) \neq 0$). In this review, we will illustrate various systems with such kind of forcing. In addition, the energy flux does not capture anisotropic effects because it is a sum over the modes of a wavenumber sphere. We will discuss these issues in the next subsection.

2.3. Caveats for energy flux; anisotropic turbulence

In this subsection, we will discuss some more important issues related to the energy flux.

(a) Since $T_u(k)$ is a scalar, the energy flux, which is a sum of $T_u(k)$, is also a scalar. Note that $\Pi_u(k)$ is the net energy transfer from the Fourier modes inside the sphere of radius k to modes outside the sphere.

(b) Several authors (e.g. Nazarenko [79]) have proposed a vectorial energy flux $\vec{\Pi}(\mathbf{k})$ that satisfies the following relation:

$$\nabla \cdot \vec{\Pi}(\mathbf{k}) = -T_u(\mathbf{k}). \tag{26}$$

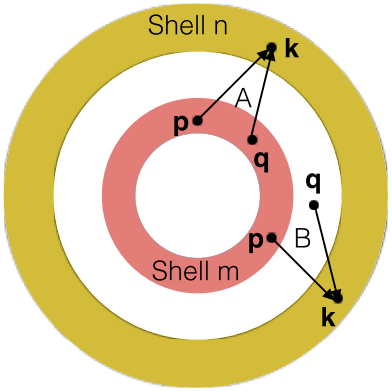

Figure 3. An illustration of the shell-to-shell energy transfer from wavenumber shell m to shell n. The giver wavenumber $\mathbf{p}$ is in shell m, while the receiver wavenumber k is in shell n. From Verma. Reproduced with permission from [14]. © Cambridge University Press.

The vectorial flux $\vec{\Pi}(\mathbf{k})$ is useful for anisotropic flows, where the energy transfers depend on the polar angle. However, we face several difficulties in this definition. Since divergence of a solenoidal vector vanishes, we can always add such functions to $\vec{\Pi}(\mathbf{k})$, which makes this energy flux indeterminate. This issue could be overcome by choosing a gauge (as in electromagnetism).

A major difficulty with $\vec{\Pi}(\mathbf{k})$ is a lack of algorithm to compute this flux. It is hoped that we will have a working definition of $\vec{\Pi}(\mathbf{k})$ in future.

(c) Another energy transfer of interest is that from a wavenumber shell to another shell. The wavenumber space is divided into many shells. A shell with shell index m is defined as a set of wavenumbers,

$$\text{Shell}(m) := \{\mathbf{k} : k_{m-1} \leqslant |\mathbf{k}| < k_m\}, \tag{27}$$

where k_{m-1} and k_m are the inner and outer radii of the shell. The *shell-to-shell energy transfer* from shell m to shell n is [42]

$$T^{u,m}_{u,\mathrm{n}} = \sum_{\mathbf{k}\in n}\sum_{\mathbf{p}\in m} S^{uu}(\mathbf{k}|\mathbf{p}|\mathbf{q}). \tag{28}$$

We illustrate this transfer in figure 3. It is important to contrast the 'shell' of equation (27) with that of the shell spectrum, where the shell width is typically taken to be unity.

(d) Keeping in mind the power-law physics of turbulent flows, typically, the shell radii for the shell-to-shell transfers are logarithmically binned. Numerical simulations and experiments reveal that $T^{u,m}_{u,n}$ is scale invariant in the inertial range of hydrodynamic turbulence, that is, $T^{u,m}_{u,n}$ is a function of $n-m$ [14, 42, 80]. In addition, the inertial-range shell-to-shell energy transfer is forward and dominantly local. That is, in the inertial range, maximal energy flows from shell m to $m+1$ [81]. However, significant energy also gets transferred to other shells (e.g. m to $m+2$ and $m+3$) via nonlocal transfers. See figure 4 for an illustration, where $k_m \propto 2^{m/5}$ for the inertial-range shells. Due to the above reasons, the energy flux is not analogous to real-space fluxes that represent transfers of quantities, such as, mass, momentum, energy, electric field locally across a surface.

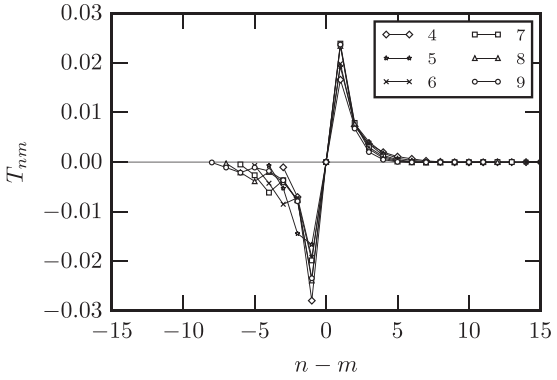

Figure 4. Plot of $T^{u,m}_{u,n}$ vs $n-m$ for 3D hydrodynamic turbulence with Re $= 68\,000$. $k_m \propto 2^{1/5}$ for inertial-range shells. From Verma. Reproduced with permission from [14]. © Cambridge University Press.

(e) External fields or anisotropic geometries typically induce anisotropy in the energy distribution, as well as in the energy transfers. Teaca *et al* [83] introduced *ring spectrum* and *ring-to-ring energy transfers* for an axisymmetric flow. The anisotropy direction is taken to be along $\hat{\mathbf{z}}$, while the polar angle, θ, is the angle between $\mathbf{k}$ and $\hat{\mathbf{z}}$. A ring is an intersection of a shell and a sector. For example, a ring of index (i, j) is defined as

$$\text{Ring}(i, j) := \{\mathbf{k} : \mathbf{k} \in \text{Shell}(i) \cap \text{Sector}(j)\}, \tag{29}$$

where sector(j) is defined as the set,

$$\text{Sector}(j) := \left\{\mathbf{k} : \theta_{j-1} \leqslant \arccos\left(\frac{k_\parallel}{|\mathbf{k}|}\right) < \theta_j\right\}, \tag{30}$$

with θ_j denoting the angular division of the wavenumber space [82]. See figures 5(a) and (b) for an illustration. The kinetic energy spectrum of ring(k, j) in Fourier space is defined as,

$$E_u(k, j) = \frac{1}{A_j} \sum_{k-1<|\mathbf{k}'|\leqslant k;\theta_{j-1}<\theta\leqslant\theta_j} \frac{1}{2}|\mathbf{u}(\mathbf{k}')^2|, \tag{31}$$

where $A_j := |\cos(\theta_j) - \cos(\theta_{j-1})|$ is the normalization constant that compensates for the uneven distribution of modes inside sectors. Note that a sector near the equator contains more modes than those near the pole. The ring-to-ring energy transfer from ring (m, α) to ring (n, β) is defined as

$$T^{(m,\alpha)}_{(n,\beta)} = \frac{1}{A_\alpha A_\beta} \sum_{\mathbf{k}\in\text{Ring}(n,\beta)} \sum_{\mathbf{p}\in\text{Ring}(m,\alpha)} S(\mathbf{k}|\mathbf{p}|\mathbf{q}). \tag{32}$$

We also define *conical energy flux* for Fourier-space cones in the Fourier space (see figure 5(c)). The axis of the cone is aligned along the anisotropy direction. Conical energy flux for a cone with a half-angle of θ is the rate of energy transfer by modes inside the cone to the modes outside the cone; the receiver Fourier modes have polar angle greater

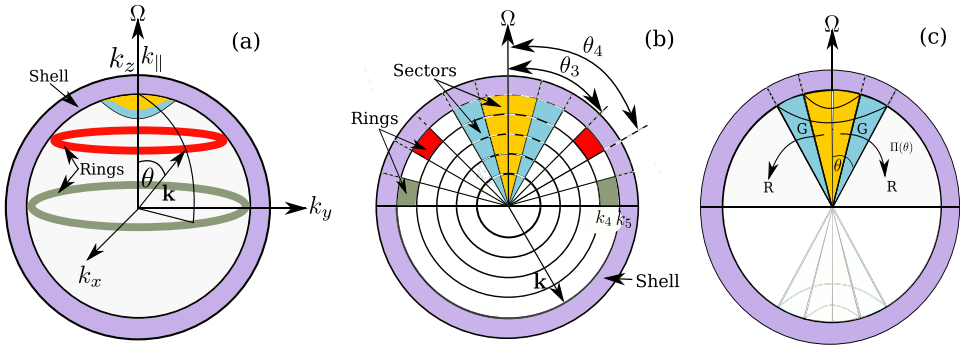

Figure 5. Illustrations of (a) wavenumber rings; (b) shells, sectors, and rings; (c) conical energy transfer from the blue cone. In (c), the modes inside the blue cone transfer energy to the modes outside the cone (the receiving modes have polar angle greater than θ). From Sharma *et al*. Reprinted with permission from AIP. Reprinted from [82], with the permission of AIP Publishing.

than θ. Therefore,

$$\Pi(\theta) = \sum_{\mathbf{k}\in R} \sum_{\mathbf{p}\in \text{cone}} S(\mathbf{k}|\mathbf{p}|\mathbf{q}), \tag{33}$$

where the region R represents the region of receiving Fourier modes (see figure 5(c)).

(f) For isotropic systems, the energy transfers are isotropic. For example, isotropic flows do not exhibit energy transfer (statistically) between any two rings with the same radius (for example, red and green rings of figure 5). However, anisotropic turbulence exhibits energy transfers among such rings. For example, in quasi-static MHD turbulence, energy flows from equatorial rings to ones with lower polar angles (e.g. from green ring to red ring in figure 5). The ring-to-ring energy transfers take place among nearest neighbours (local), as well as among distant rings (nonlocal). Due to the above the nonlocal nature of ring-to-ring energy transfers, the Fourier-space energy transfer for a turbulent flow is not a vector, but it is a scalar.

(g) Note that neither the energy flux and nor the shell-to-shell energy transfer capture the anisotropic energy transfers. However, the formulas of equations (19) and (21) are applicable to isotropic, as well as anisotropic flows. The energy flux, which involves a sum over Fourier modes of a sphere, is well-defined for such flows. Due to these reasons, energy flux remains an important quantity for anisotropic turbulence (e.g. buoyant and MHD turbulence), even though such flows are typically anisotropic. In subsequent sections we will study variability of $\Pi_u(k)$ in anisotropic systems.

In the next section, we will show how the energy flux varies with wavenumbers due to multiscale external force and dissipation.

3. Variable energy flux

The kinetic energy flux varies with wavenumbers in the presence of multiscale forcing and dissipation [6, 8, 9, 11, 23]. In this review we summarise how past works employed this observation to deduce interesting properties of turbulence. We start this section with an equation for the variable energy flux. In this section we assume the wavenumber k to be a continuous variable.

3.1. Formalism

Rewriting equation (20) for spheres of radii k and $k + \mathrm{d}k$, and then taking a difference between the two equations yields

$$\frac{\mathrm{d}}{\mathrm{d}t}\sum_{k<k'\leqslant k+\mathrm{d}k} E_u(\mathbf{k}') = \sum_{k<k'\leqslant k+\mathrm{d}k} T_u(\mathbf{k}') + \sum_{k<k'\leqslant k+\mathrm{d}k} \mathcal{F}_u(\mathbf{k}') + \sum_{k<k'\leqslant k+\mathrm{d}k} \mathcal{F}_{\mathrm{LS}}(\mathbf{k}') - \sum_{k<k'\leqslant k+\mathrm{d}k} D_u(\mathbf{k}'). \tag{34}$$

Using $\sum_{k<k'\leqslant k+\mathrm{d}k} T_u(\mathbf{k}') = [-\Pi_u(k+\mathrm{d}k) + \Pi_u(k)]$ and taking the limit $\mathrm{d}k \to 0$, we obtain the following evolution equation for one-dimensional energy spectrum $E_u(k)$ [6, 8, 9, 11, 23]:

$$\frac{\partial}{\partial t}E_u(k,t) = -\frac{\partial}{\partial k}\Pi_u(k,t) + \mathcal{F}_u(k,t) + \mathcal{F}_{\mathrm{LS}}(k,t) - D_u(k,t), \tag{35}$$

where

$$E_u(k)\mathrm{d}k = \sum_{k<k'\leqslant k+\mathrm{d}k} E_u(\mathbf{k}'), \tag{36}$$

$$\mathcal{F}_u(k)\mathrm{d}k = \sum_{k<k'\leqslant k+\mathrm{d}k} \Re[\mathbf{F}_u(\mathbf{k}')\cdot\mathbf{u}^*(\mathbf{k}')], \tag{37}$$

$$\mathcal{F}_{\mathrm{LS}}(k)\mathrm{d}k = \sum_{k<k'\leqslant k+\mathrm{d}k} \Re[\mathbf{F}_{\mathrm{LS}}(\mathbf{k}')\cdot\mathbf{u}^*(\mathbf{k}')], \tag{38}$$

$$D_u(k)\mathrm{d}k = 2\nu\sum_{k<k'\leqslant k+\mathrm{d}k} k'^2 E_u(\mathbf{k}'). \tag{39}$$

Figure 6 illustrates the above quantities for a wavenumber shell whose inner and outer radii are k and $k + \mathrm{d}k$ respectively. Also note that $T_u(k,t)$ is defined as [5, 6]

$$T_u(k,t) = -\frac{\partial}{\partial k}\Pi_u(k,t). \tag{40}$$

Equation (35) describes how $\Pi_u(k)$ varies with k in an unsteady flow. Note that equation (35) is based on energy conservation. The net rate of energy supply to a wavenumber shell determines the rate of change of energy in that shell. This is an exact relation.

In this review we focus on the behaviour of the kinetic energy flux under a *statistical* steady state. Setting $\langle\partial E_u(k,t)/\partial t\rangle = 0$, where $\langle.\rangle$ represents averaging, in equation (34) yields the following equation for the wavenumber shell of radius k:

$$\frac{\mathrm{d}}{\mathrm{d}k}\langle\Pi_u(k)\rangle = \langle\mathcal{F}_u(k)\rangle + \langle\mathcal{F}_{\mathrm{LS}}(k)\rangle - \langle D_u(k)\rangle\,. \tag{41}$$

That is, the energy flux $\Pi_u(k)$ varies with k due to the energy injection rates $\mathcal{F}_u(k)$ and $\mathcal{F}_{\mathrm{LS}}(k)$, and the viscous dissipation rate $D_u(k)$. For brevity, we avoid writing the angular brackets throughout the review. We remark that equation (41) is an exact relation in a statistical sense. That is, the quantities $\Pi_u(k)$, $\mathcal{F}_u(k)$, $\mathcal{F}_{\mathrm{LS}}(k)$, and $D_u(k)$ fluctuate around their mean, but equation (41) holds on an average. The structure of the equation is local, that is, the local variation of the energy flux depends on the local energy injection by forcing and by the dissipation rate. This feature yields complimentary insights compared to Kolmogorov's four-fifth law [8, 14] in which real-space interactions are nonlocal, as we describe below.

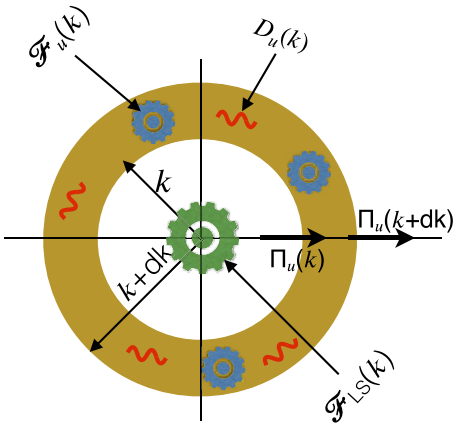

Figure 6. A figure illustrating the energy flux difference, $\Pi_u(k+\mathrm{d}k) - \Pi_u(k)$; the energy injection rates $\mathcal{F}_u(k)\mathrm{d}k$ and $\mathcal{F}_{\mathrm{LS}}(k)\mathrm{d}k$ are represented by wheels; and the viscous dissipation rate $D_u(k)\mathrm{d}k$ is represented by wavy lines. Refer to equation (35).

Starting from NS equation, under the assumption of homogeneity and isotropy, Karman and Howarth [84] (also see [4, 8]) derived the following evolution equation for $\langle u_i u_j' \rangle$:

$$\begin{aligned}\frac{\partial}{\partial t}\frac{1}{2}\langle u_i u_i' \rangle &= \frac{1}{2}\left\langle u_i' \frac{\partial}{\partial t} u_i \right\rangle + \frac{1}{2}\left\langle u_i \frac{\partial}{\partial t} u_i' \right\rangle \\ &= \frac{1}{4}\nabla_l \cdot \left\langle |\mathbf{u}' - \mathbf{u}|^2 (\mathbf{u}' - \mathbf{u}) \right\rangle + \langle F_{\mathrm{LS},i} u_i' \rangle + \nu \nabla'^2 \langle u_i u_i' \rangle \\ &= T_u(\mathbf{l}) + \mathcal{F}_{\mathrm{LS}}(\mathbf{l}) - D_u(\mathbf{l}). \end{aligned} \tag{42}$$

In the above equation, u and u′ represent velocities at two different locations. The above derivation makes use of tensorial and symmetry properties (homogeneity and isotropy) of the correlation functions. For example, $\langle p u_i' \rangle = \langle p' u_i \rangle = 0$ due to isotropy. For details, refer to [2, 8, 15, 85, 86].

Fourier transform of equation (42) yields equation (16). The Fourier transform of $\frac{1}{4}\nabla_l \cdot \left\langle |\mathbf{u}' - \mathbf{u}|^2 (\mathbf{u}' - \mathbf{u}) \right\rangle$ yields $T_u(\mathbf{k})$, while those of $\mathcal{F}_{\mathrm{LS}}(\mathbf{l})$ and $D_u(\mathbf{l})$ yield $\mathcal{F}_{\mathrm{LS}}(\mathbf{k})$ and $D_u(\mathbf{k})$ respectively. See figure 7(a) for an illustration. Thus, the Fourier and real space formalisms are equivalent, as expected. Further, the term $T_u(\mathbf{l})$ is a product of three velocity differences. Among them, the product $|\mathbf{u}' - \mathbf{u}|^2$ includes the gier and receiver fields, while the third $\delta\mathbf{u}$ is the mediator field (see figure 7(b)). Hence, the structure of the nonlinear energy transfer in real and Fourier space are similar.

Coming back to Fourier space, in the intermediate wavenumber range, the nonlinear term dominates the viscous term, a reason for which this is called the *inertial range*. In addition, $\mathcal{F}_{\mathrm{LS}}(k) = 0$ and $D_u(k) \approx 0$ in this range. Therefore,

$$\frac{\mathrm{d}}{\mathrm{d}k}\Pi_u(k) = \mathcal{F}_{u,\mathrm{in}}(k), \tag{43}$$

where the subscript 'in' stands for the inertial range. Thus, the energy flux varies due to $\mathcal{F}_{u,\mathrm{in}}(k)$. Behaviour of $\Pi_u(k)$ can be classified into the following four categories (see figure 8):

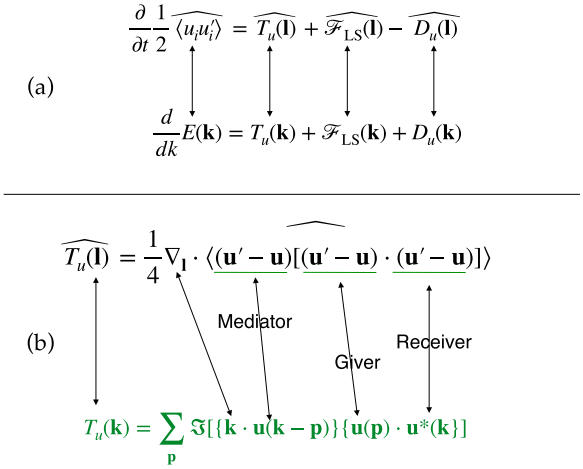

Figure 7. (a) A figure illustrating connection between the terms of the energy equations in real and Fourier spaces. (b) Similarity between the nonlinear energy terms $T_u(\mathbf{l})$ and $T_u(\mathbf{k})$. Here $\hat{f}$ represents Fourier transform operation of the real function f.

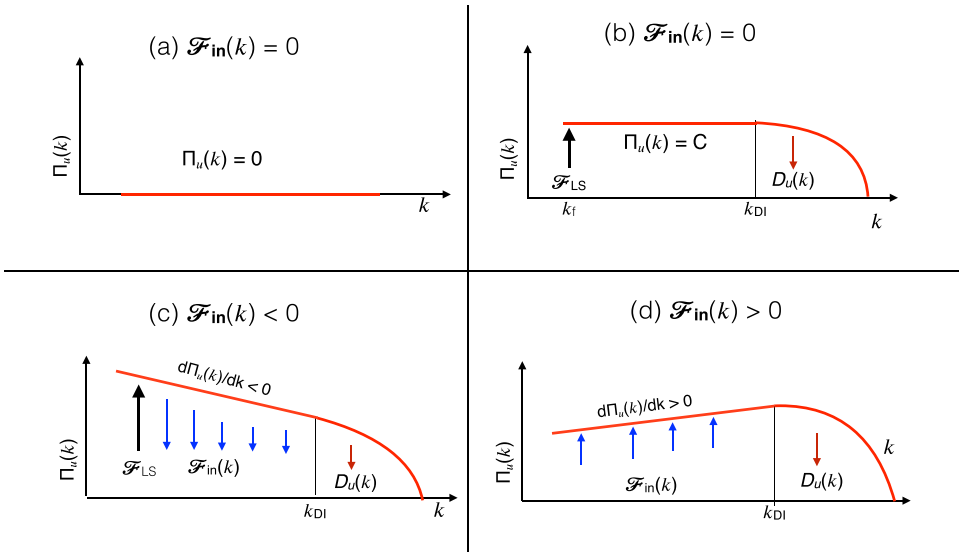

Figure 8. Four categories of $\Pi_u(k)$ depending on the inertial-range forcing $\mathcal{F}_{u,\rm in}(k)$: (a) $\mathcal{F}_{u,\rm in}(k) = 0$ and $\Pi_u(k) = 0$ (equilibrium); (b) $\mathcal{F}_{u,\rm in}(k) = 0$ and $\Pi_u(k) = C > 0$ (nonequilibrium); (c) $\mathcal{F}_{u,\rm in}(k) < 0 \Rightarrow {\rm d}\Pi_u(k)/{\rm d}k < 0$; (d) $\mathcal{F}_{u,\rm in}(k) > 0 \Rightarrow {\rm d}\Pi_u(k)/{\rm d}k > 0$. Viscous dissipation $D_u(k)$ dominates the nonlinear term beyond wavenumber $k_{\rm DI}$.

(a) $\mathcal{F}_{u,\rm in}(k) = 0$ and $\Pi_u(k) = 0$: this case corresponds to the *absolute equilibrium* scenario of Euler's equation (Navier Stokes equation with $\nu = 0$) [60, 61]. For this case, the average energy exchange between any two Fourier modes is zero. That is, $\langle S^{uu}(\mathbf{k}'|\mathbf{p}|\mathbf{q})\rangle = 0$ for any triad, thus satisfying detailed balance of kinetic energy transfer. Therefore, as in thermodynamics, the modal kinetic energy spectrum $E_u(\mathbf{k})$ = constant, leading to $E_u(k) \sim k^2$ and $\sim k$ for 3D and 2D hydrodynamic turbulence respectively [6, 12, 43, 60,

61, 70]. We will discuss these cases in more detail in section 11. A related phenomenon to this cases is flux loop cascade [87, 88], which will be discussed in section 10.

(b) $\mathcal{F}_{u,\text{in}}(k) = 0$ and $\Pi_u(k) = C > 0$: this regime is described by Kolmogorov's theory of turbulence. For this nonequilibrium case, $\langle S^{uu}(\mathbf{k}'|\mathbf{p}|\mathbf{q})\rangle > 0$ for $k' > p$ and vice versa. We briefly describe this case in in section 3.2.

(c) $\mathcal{F}_{u,\text{in}}(k) < 0$ and $\mathrm{d}\Pi_u(k)/\mathrm{d}k < 0$: for $\mathcal{F}_{\text{in}}(k) < 0$, the kinetic energy flux decreases with k. Notable examples in this category are quasi-static MHD turbulence, flows with Ekman friction, and stably-stratified turbulence. These flows are described in subsequent sections.

(d) $\mathcal{F}_{u,\text{in}}(k) > 0$ and $\mathrm{d}\Pi_u(k)/\mathrm{d}k > 0$: the kinetic energy flux increases in this case. Leading examples for this case are turbulent thermal convection and shear turbulence that will be described in later sections.

In the above four cases, the nature of energy fluxes in the inertial range is the *asymptotic behaviour* with the effects of large-scale forcing and dissipative effects suppressed.

In literature, it has been argued that the energy flux in turbulence is related to the conserved quantities [6, 8]. For an inviscid force-free hydrodynamics, all the terms in the right-hand-side of equation (41) vanish. Hence, $\Pi_u(k)$ is a constant, in fact *zero*, as we describe for case (a). This is a consequence of conservation of kinetic energy, and it yields an equilibrium solution.

However, a more interesting scenario is case (b) that includes large-scale forcing and viscous dissipation. Here, the total kinetic energy is not conserved. But, the equation for the variable energy flux hinges on the principle of energy conservation: the net energy injected into a wavenumber shell alters the energy fluxes at the two surfaces of the shell. A direct consequence of the above is that $\Pi_u(k)$ is a nonzero constant in the inertial range when $\mathcal{F}_u = 0$. Note that the absence of $\mathcal{F}_u$ plays a key role in the energy conservation for the inviscid and force-free hydrodynamics. This is the connection between the conservation law and constancy of energy flux in the inertial range where the large-scale forcing and dissipative effects have a minimal role.

In later parts of the paper we will show that secondary fields (e.g. magnetic field and buoyancy) induce $\mathcal{F}_u$ (see cases (c) and (d) described above). Consequently, the total kinetic energy is not conserved for such systems in the inviscid and force-free limit. Following the arguments described above, we observe that such systems do not exhibit constant $\Pi_u(k)$ in the inertial range. However, some systems with secondary field exhibit conserved quantities that are function of velocity and secondary fields. For example, in stably stratified turbulence, the total energy, which is a sum of kinetic and potential energies, is conserved in the inviscid limit. We show in section 6 that the flux associated with the total energy is constant in the inertial range. Thus, conservation laws are connected to the constancy of inertial-range fluxes of appropriate quantities. In addition, we can derive certain exact relations using the equations for variable energy fluxes for the velocity and secondary fields (see sections 4, 6 and 7). Thus, the formalism of variable energy flux provides interesting insights into the physics of turbulence.

In the following discussion, we provide several examples of variable energy flux in hydrodynamic turbulence. We start with a brief description of energy flux in inertial–dissipation range of hydrodynamic turbulence.

3.2. Variable energy flux in the inertial–dissipation range

According to Kolmogorov's theory of turbulence [1, 2, 8], a homogeneous, isotropic, and steady 3D hydrodynamic turbulent flow with large-scale forcing exhibits a constant energy flux in the inertial range. Kolmogorov simplified equation (42) under the above assumptions and

arrived at the four-fifth law. Note that the constancy of inertial-range energy flux for hydrodynamic turbulence with large-scale forcing follows from equation (43) with $\mathcal{F}_{u,\mathrm{in}}(k) = 0$. Thus, the equation representing variable energy flux is very useful.

A key assumption in Kolmogorov's theory is that the flow is forced at large scales. Another important assumption of Kolmogorov's theory of turbulence is that the physics in the inertial range is independent of the forcing and dissipative mechanisms [5, 6, 8]. Hence, the energy spectrum $E_u(k)$ is isotropic, and it depends only on ϵ_u and local wavenumber k. Absence of any external length scale implies that $E_u(k)$ is a power law in k. This assumption is related to the locality of interactions in hydrodynamic turbulence [80, 89, 90], which was briefly discussed in the previous section.

The above inputs and dimensional analysis yield

$$E_u(k) = K_{\mathrm{Ko}}\epsilon_u^{2/3}k^{-5/3}, \tag{44}$$

where ϵ_u is the viscous dissipation rate. Note that the dissipation rate matches with the inertial-range energy flux under steady state. We remark that equation (44) is an approximate relation. Experiments and numerical simulation reveal small correction to spectral exponent (from $5/3$ to 1.70) due to intermittency [8, 91]. However, equations (41) and (43) are exact relations in the statistical sense, similar to Karman–Howarth relation [84] and Kolmogorov's four-fifth law [1, 2].

Kolmogorov's $k^{-5/3}$ energy spectrum is observed in the inertial range of hydrodynamic turbulence, but not in the dissipative range. Using the data from numerical simulations, Chen *et al* [36] and Martinez *et al* [37] proposed that in the far-dissipation range, the energy spectrum varies as $k^{\alpha}\ \exp\left(-ck/k_d\right)$, where α, c are constants, and $k_d = (\epsilon_u/\nu^3)^{1/4}$ is Kolmogorov's wavenumber. Pao [35] argued in favour of $k^{-5/3}\ \exp(-c(k/k_d)^{4/3})$ spectrum. Pope [11] showed that the following energy spectrum is a good fit to many experimental observations (see e.g. [92]):

$$E_u(k) = K_{\mathrm{Ko}}\epsilon^{2/3}k^{-5/3}f_{\mathrm{L}}(kL)f_{\eta}(k/k_d), \tag{45}$$

where $f_{\mathrm{L}}(kL), f_{\eta}(\tilde{k})$ represent the large-scale and dissipative-scale components respectively. Recently, using numerical simulations, Buaria and Sreenivasan [93] argued that $E(k) \sim k^{-5/3}\ \exp(-c(k/k_d)^{2/3})$. The exponent 2/3 is determined using the best-fit curve on the function $\phi(k) = \mathrm{d}\log E(k)/\mathrm{d}\log k = \alpha - \beta\gamma(k\eta)^{\gamma}$. See figure 9 for an illustration.

Here we present Pao's model [35], which is based on the variable energy flux. In the inertial–dissipation range, where $\mathcal{F}_u = \mathcal{F}_{\mathrm{LS}} = 0$, equation (41) yields

$$\frac{\mathrm{d}}{\mathrm{d}k}\Pi_u(k) = -2\nu k^2 E_u(k). \tag{46}$$

Pao's model makes the following ansatz to close the equation: in the inertial-dissipative range, $\Pi_u(k)/E_u(k)$ is independent of ν and is function only of k and ϵ_u (also see [5]). Under these assumptions, dimensional analysis with an aid of equation (44) yields

$$\frac{E_u(k)}{\Pi_u(k)} = K_{\mathrm{Ko}}\epsilon_u^{-1/3}k^{-5/3}. \tag{47}$$

Substitution of equation (47) in (46) yields

$$\Pi_u(k) = \epsilon_u\ \exp\left(-\frac{3}{2}K_{\mathrm{Ko}}(k/k_d)^{4/3}\right), \tag{48}$$

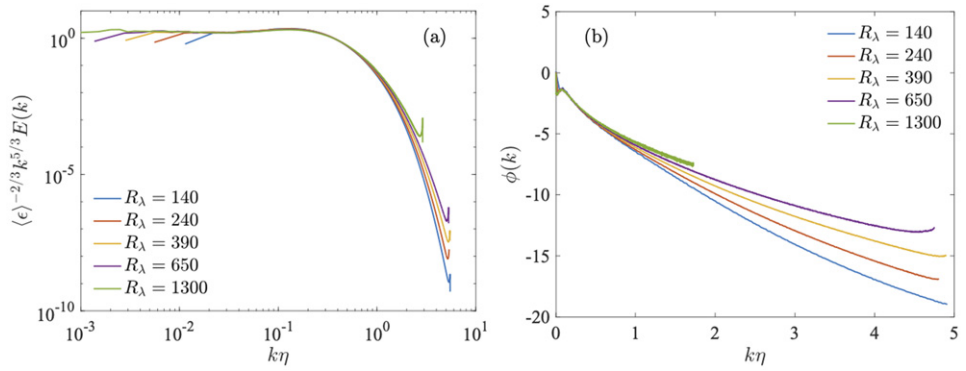

Figure 9. (a) Normalized energy spectrum ($E(k)k^{5/3}\epsilon_u^{-2/3}$) in the inertial–dissipation range, computed using numerical simulations with Taylor-scale Reynolds number ranging from 140 to 1300. (b) The log-derivative of energy spectrum $\phi(k) = \mathrm{d}\log E(k)/\mathrm{d}\log k$, which is modelled as $\alpha - \beta\gamma(k\eta)^\gamma$, with α, β, γ as constants. The green curve at the top indicates the best-fit curve with $\gamma = 2/3$. From Buaria and Sreenivasan. Reproduced from [93]. CC BY 4.0.

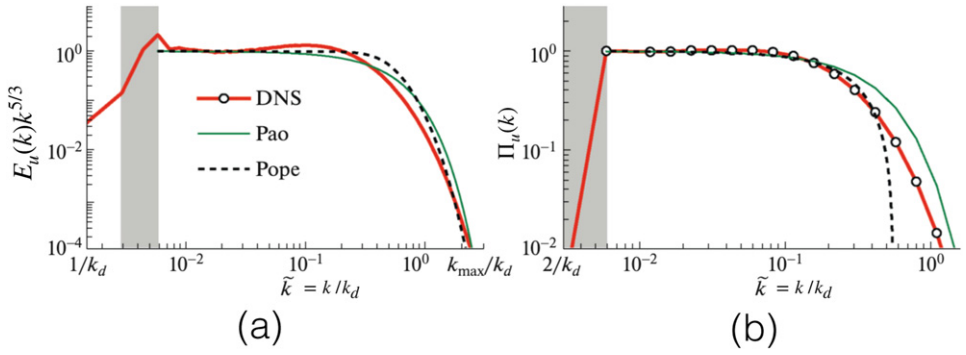

Figure 10. (a) and (b) The energy spectra and fluxes of hydrodynamic turbulence for a 4096^3 DNS exhibited as a red curve. Predictions of Pao's model (green curve) and Pope's model (dashed curve) are also shown in the figure. Figures (a) and (b) are adopted from a figure of Verma *et al*. Reprinted by permission from Springer Nature Customer Service Centre GmbH: Springer. Fluid Dyn. [81] © 2018.

$$E_u(k) = K_{\mathrm{Ko}}\epsilon_u^{2/3}k^{-5/3}\,\exp\left(-\frac{3}{2}K_{\mathrm{Ko}}(k/k_d)^{4/3}\right). \tag{49}$$

Pao [35] showed that the above energy spectrum describes many experimental observations [94] reasonably well. Recently, Verma *et al* [81] showed that the above spectrum and flux describe the results of high-resolution numerical simulations reasonably well, but it marginally overpredicts the energy flux and spectrum in the dissipation range (see figure 10). This discrepancy arises because the numerical results indicate that equation (47) is not strictly valid (see the discussion in the following subsection and figure 12).

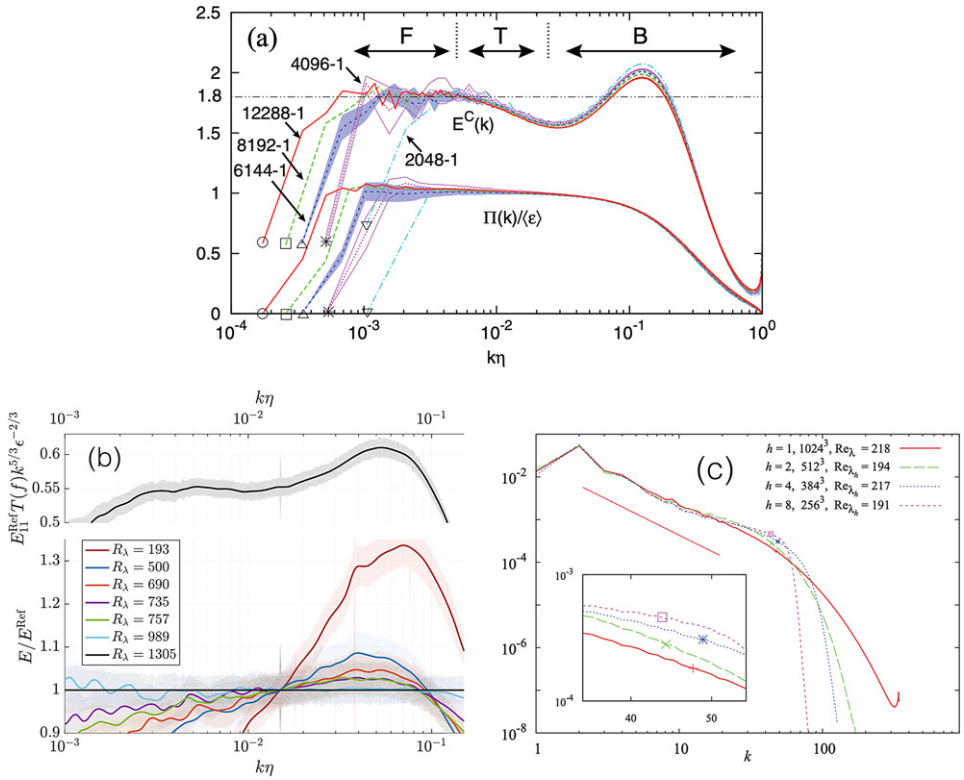

Figure 11. (a) Bottleneck effect observed by Ishihara *et al* in high-resolution simulations on grids ranging from 2048^3 to $12\,888^3$. From Ishihara *et al*. Reprinted figure with permission from [95], Copyright (2016) by the American Physical Society. (b) Bottleneck effect observed by Kuchler *et al* in an experiment on hydrodynamic turbulence over a wide range of Reynolds number. From Kuchler *et al*. Reproduced from [41]. CC BY 4.0. (c) Spyksma *et al* showed that Bottleneck effect is enhanced in the presence of hyperviscosity: higher the hyperviscous effect, higher the bottleneck effect. From Spyksma *et al*. Reprinted from [96], with the permission of AIP Publishing. Figures (a) and (c) reproduced with permission from APS and AIP respectively; Figure (b) reproduced under the terms of the Creative Commons CC BY license.

3.3. Bottleneck effect and variable energy flux

In hydrodynamic turbulence, the normalised energy spectrum $E_u(k)k^{5/3}$ exhibits a hump between the inertial range and the dissipation range [39–41, 92, 97] (see figures 9(a) and 10(a)). This phenomena, called *bottleneck effect*, is not yet fully understood. Falkovich [39] related the bottleneck effect to the nonlinear energy transfer $T_u(k)$ of equation (40). Verma and Donzis [40] argued that the observed bottleneck effect in most experiments and simulations is due to the insufficient inertial range available for facilitating the energy transfer from the large scales to small scales. Ishihara *et al* [95] observed bottleneck effect in their high-resolution numerical simulations with the strength of bottleneck decreasing with the increase of grid resolution. Kuchler *et al* [41] performed an experimental study of bottleneck effect and arrived at a similar conclusion. Spyksma *et al* [96] showed that the bottleneck effect gets enhanced by hyperviscosity. These results are illustrated in figure 11. Interestingly, as shown in figure 10, Pao's model does not exhibit bottleneck effect.

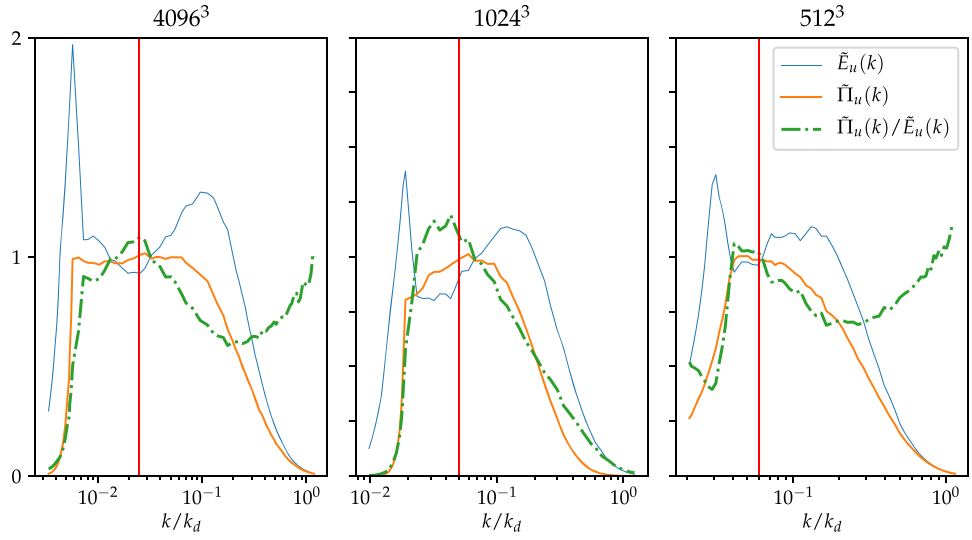

Figure 12. For the DNS of Verma *et al* [81], the normalized energy spectrum $\tilde{E}(k) = E(k)k^{5/3}\epsilon_u^{-2/3}/K_{\rm Ko}$ (blue solid curve), normalized flux $\tilde{\Pi}_u(k) = \Pi_u(k)/\epsilon_u$ (red solid curve), and the ratio $\tilde{\Pi}_u(k)/\tilde{E}_u(k)$ (green chained curve). The hump in $\tilde{E}(k)$ commenses when $\tilde{\Pi}_u(k)/\tilde{E}_u(k)$ starts to decrease.

The energy flux provides complimentary inputs to the present understanding of the bottleneck effect. In the inertial range, $\Pi_u(k) \propto E_u(k)k^{2/3}$, meaning that the energy flux is proportional to the normalized energy spectrum. However, $\Pi_u(k)$ decreases sharply in the dissipation range. This sharp decrease in the energy flux leads to a pile up of energy near the junction between the inertial range and the dissipation range, as in wave shoaling, as suggested by Sheremet *et al* [98]. This connection however needs more careful investigation.

To quantify the connection between the energy flux and bottleneck effect further, in figure 12 we plot the normalized flux $\tilde{\Pi}_u(k) = \Pi_u(k)/\epsilon_u$, the normalized energy spectrum $\tilde{E}(k) = E(k)k^{5/3}\epsilon_u^{-2/3}/K_{\rm Ko}$, and their ratio for the numerical data of Verma *et al* [81]. For the three datasets, the ratio $\tilde{\Pi}_u(k)/\tilde{E}(k)$ exhibits significant variations in the inertial and dissipation range, which is contrary to the assumptions of Pao [35]. Interestingly, the bottleneck effect (the hump in $\tilde{E}(k)$) commences when $\tilde{\Pi}_u(k)/\tilde{E}(k)$ starts to decrease, which is near the vertical red lines in figure 12. This is an important diagnostics that needs to be investigated even further using more numerical and experimental datasets.

The curves of figure 12 indicate that $\tilde{\Pi}_u(k)/\tilde{E}(k)$ is not a constant in the inertial–dissipation range. This is the reason why the predictions of Pao's model deviate from the numerical data. This observation provides us clues for a better modelling of the dissipation range of a turbulent energy spectrum.

The above discussion on Pao's model and the bottleneck effect illustrates the usefulness of the energy flux.

3.4. k^{-1} spectrum in shear turbulence

Many turbulent systems exhibit k^{-1} energy spectrum at small wavenumbers or $1/f$ frequency spectrum at small frequencies. For example, Tichen [30] and Pereira *et al* [32] observed k^{-1} energy spectrum in shear-driven turbulence. In the solar wind, Matthaeus and Goldstein [31]

reported $1/f$ spectrum for small frequencies where solar wind jets may create shear turbulence. Recently, Duguid *et al* [99] reported $1/f$ spectrum for the total kinetic energy of thermal convection at large time scales. To explain the k^{-1} spectrum at small k's, Tchen [30] modelled shear turbulence at large scales using Heisenberg's turbulence model [100]; he argued that the shear induces *strong resonance* in the flow, which in turn yields $u_k \sim$ constant. Hence, $E_u(k) \sim u_k^2/k \sim k^{-1}$.

In the following discussion we derive k^{-1} spectrum using variable energy flux. The velocity shear injects kinetic energy to the small-wavenumber modes of the flow. Hence, we expect that $\mathcal{F}_{\rm LS}(k) > C$ that leads to an increase in the energy flux $\Pi_u(k)$ with k, as in case (d) discussed in section 3.1. Consequently, we make an ansatz that the energy spectrum $E_u(k) \sim [\Pi_u(k)]^{2/3}k^{-5/3}$. Since $\Pi_u(k)$ will increase with k, it is expected that $E_u(k)$ will be shallower than $k^{-5/3}$. In particular, for $\mathcal{F}_{\rm LS}(k) = C$, equation (43) yields $\Pi_u(k) = \int^k \mathcal{F}_{\rm LS}(k')\mathrm{d}k' = Ck$. Now, using dimensional analysis we derive that

$$E_u(k) \sim C^{2/3}k^{-1}. \tag{50}$$

As argued in section 2, the energy flux can be defined for shear turbulence even though it is anisotropic. The above wavenumber-dependent $\mathcal{F}_{\rm LS}(k)$ is tune with the earlier works by Yakhot and Orszag [101] and Sain *et al* [102].

The above mechanism provides a plausible explanation for the k^{-1} energy spectrum in shear turbulence [30–32]. The low-frequency $1/f$ spectrum in the solar wind may be due to the shear experienced by wind jets [31], while that in thermal convection may be due to shear among the large-scale thermal plumes [99]. Note that we convert the wavenumber spectrum to the frequency spectrum using Taylor's hypothesis, which is applicable to the solar wind because it is much faster than spacecrafts [103]. In thermal convection, Taylor's hypothesis is expected to work under certain conditions [104–106].

The above theory of k^{-1} spectrum in shear turbulence hinges on the assumption that $\mathcal{F}_u(\mathbf{k}) = C$, which needs to be tested using experiments and/or numerical simulations. Interestingly, $1/f$ noise has been reported in a large number of physical systems—electric currents, ion-channel currents, music, earthquakes, etc (see [107–109], and references therein). It is possible that $1/f$ spectrum in the electric and ion-channel currents are connected to shear in the electron flow. This conjecture, however, needs to be tested.

In addition to the above, there are many more examples of variable energy flux. In stably-stratified turbulence, $\Pi_u(k)$ decreases as $k^{-4/5}$ due to buoyancy [19, 20]. On the contrary, $\Pi_u(k)$ increases marginally in turbulent thermal convection. We will describe these fluxes in section 6. In MHD turbulence, the kinetic energy flux varies in the inertial range itself due to the Lorentz force. Similar variations are observed in solvents with polymers, quantum turbulence, binary-mixture turbulence, etc. We will discuss these systems in sections 7 and 12. In addition, the energy flux variations can be generalised to other quantities such as enstrophy and kinetic helicity; these issues will be discussed in section 9.

With this, we close our brief discussion on variable energy flux in hydrodynamic turbulence. In the next section, we will discuss variable energy flux in the presence of a secondary field.

4. Variable energy flux in flows with a secondary field: formalism

Consider a secondary field ζ advected by the velocity field $\mathbf{u}$. This secondary field could be a scalar, a vector, or a tensor. Leading examples of a scalar field are density and temperature of a fluid; that of a vector field are magnetic field, dipolar field, and flock velocity; and that of

Table 1. Energy (E_ζ) and modal energy ($E_\zeta(\mathbf{k})$) of a secondary field.

	Scalar	Vector	Tensor
E_ζ	$\frac{1}{2}\langle\zeta^2\rangle$	$\frac{1}{2}\langle\boldsymbol{\zeta}\cdot\boldsymbol{\zeta}\rangle$	$\frac{1}{2}\langle\zeta_{ij}\zeta_{ij}\rangle$
$E_\zeta(\mathbf{k})$	$\frac{1}{2}\lvert\zeta(\mathbf{k})\rvert^2$	$\frac{1}{2}\lvert\boldsymbol{\zeta}(\mathbf{k})\rvert^2$	$\frac{1}{2}\zeta_{ij}(\mathbf{k})\zeta^*_{ij}(\mathbf{k})$

a tensor are the configuration tensor of a polymer and stress tensor of an elastic fluid. In this section, we present energy fluxes associated with a secondary field and those arising due to the interactions between the velocity and secondary fields. As we describe below, many features of energy transfers are common among the scalar, vector, and tensor secondary fields.

4.1. Variable energy flux associated with a secondary field

The equations for the velocity field $\mathbf{u}$ are same as those covered in section 2, except that the force field for the velocity field ($\mathbf{F}_u$) could be a function of $\mathbf{u}$, ζ, $\mathbf{r}$, and t. The equations for the secondary field are

$$\text{Scalar}: \frac{\partial\zeta}{\partial t} + (\mathbf{u}\cdot\nabla)\zeta = F_\zeta(\mathbf{u},\zeta) + \kappa\nabla^2\zeta, \tag{51}$$

$$\text{Vector}: \frac{\partial\boldsymbol{\zeta}}{\partial t} + (\mathbf{u}\cdot\nabla)\boldsymbol{\zeta} = \mathbf{F}_\zeta(\mathbf{u},\boldsymbol{\zeta}) + \kappa\nabla^2\boldsymbol{\zeta}, \tag{52}$$

$$\text{Tensor}: \frac{\partial\zeta_{ij}}{\partial t} + (\mathbf{u}\cdot\nabla)\zeta_{ij} = F_{\zeta,ij}(\mathbf{u},\zeta) + \kappa\nabla^2\zeta_{ij}, \tag{53}$$

where κ is the diffusion coefficient of the secondary field, and F_ζ is the force field for the secondary field. Two important nondimensional parameters are Prandtl number, $\text{Pr} = \nu/\kappa$, and Pélet number, Pe, which is the ratio of the nonlinear term and the diffusion term in the equation for the secondary field, that is,

$$\text{Pe} = \frac{(\mathbf{u}\cdot\nabla)\zeta}{\kappa\nabla^2\zeta} = \frac{UL}{\kappa}, \tag{54}$$

where U, L are the large-scale velocity and length respectively.

Similar to the kinetic energy, we define secondary energy and associated modal energy, as listed in table 1. For discrete wavenumbers, one-dimensional secondary energy spectrum is defined as $E_\zeta(k) = \sum_{k-1<k'\leqslant k} E_\zeta(\mathbf{k}')$, but for continuum wavenumbers, $E_\zeta(k)\mathrm{d}k = \sum_{k<k'\leqslant k+\mathrm{d}k} E_\zeta(\mathbf{k}')$. The evolution equation for the modal secondary energy of a scalar is

$$\begin{aligned}\frac{\mathrm{d}}{\mathrm{d}t}E_\zeta(\mathbf{k}) &= T_\zeta(\mathbf{k}) + \mathcal{F}_\zeta(\mathbf{k}) - D_\zeta(\mathbf{k})\\ &= \sum_{\mathbf{p}} \Im\left[\{\mathbf{k}\cdot\mathbf{u}(\mathbf{q})\}\{\zeta(\mathbf{p})\zeta^*(\mathbf{k})\}\right] + \Re[F_\zeta(\mathbf{k})\zeta^*(\mathbf{k})] - 2\kappa k^2 E_\zeta(\mathbf{k}).\end{aligned} \tag{55}$$

In the above equation, $T_\zeta(\mathbf{k})$ is the nonlinear transfer of secondary energy to $\zeta(\mathbf{k})$, $\mathcal{F}_\zeta(\mathbf{k})$ is the secondary energy transfer to $\zeta(\mathbf{k})$ by $F_\zeta(\mathbf{k})$, and $D_\zeta(\mathbf{k})$ is the diffusion or dissipation rate of $\zeta(\mathbf{k})$. The equations for the vector and tensor fields are very similar to the above equations, except that the field multiplication is performed appropriately (scalar product or tensor product).

Several important points regarding the secondary field are

(a) When F_ζ is a *linear function* of $\mathbf{u}$, the scalar energy injection rate $\mathcal{F}_\zeta(\mathbf{k}) = \Re[F_\zeta(\mathbf{k})\zeta^*(\mathbf{k})]$ is a function of $\mathbf{u(k)}$ and $\zeta(\mathbf{k})$. We encounter such forms of $F_\zeta(\mathbf{k})$ in stably stratified turbulence and in thermal convection where $F_\zeta \propto u_z$. Similar properties hold for $\mathcal{F}_u(\mathbf{k})$ when $\mathbf{F}_u$ is a linear function of ζ.

(b) When F_ζ is a *nonlinear function* of $\mathbf{u}$ and/or ζ, the scalar energy injection rate $\mathcal{F}_\zeta(\mathbf{k})$ is a convolution. Therefore, $\mathcal{F}_\zeta(\mathbf{k})$ involves wavenumbers other than $\mathbf{k}$. For example, in MHD turbulence, where $\mathbf{F}_\zeta = \boldsymbol{\zeta} \cdot \nabla \mathbf{u}$ with $\boldsymbol{\zeta}$ as the magnetic field,

$$\mathcal{F}_\zeta(\mathbf{k}) = \sum_{\mathbf{p}} -\Im\left[\{\mathbf{k}\cdot\boldsymbol{\zeta}(\mathbf{k}-\mathbf{p})\}\{\mathbf{u}(\mathbf{p})\cdot\boldsymbol{\zeta}^*(\mathbf{k})\}\right] \tag{56}$$

is a convolution. The nonlinear F_u yields a similar convolution.

The nonlinear term $(\mathbf{u}\cdot\nabla)\zeta$ (and similar ones for vector and tensor) for the secondary field facilitates scalar energy transfer. For a wavenumber triad $(\mathbf{k}', \mathbf{p}, \mathbf{q})$, the *mode-to-mode secondary energy transfer* from wavenumber $\mathbf{p}$ to wavenumber $\mathbf{k}$ with the mediation of wavenumber $\mathbf{q}$ is [22, 23, 110]:

$$\text{Scalar}: S^{\zeta\zeta}(\mathbf{k}'|\mathbf{p}|\mathbf{q}) = -\Im\left[\{\mathbf{k}'\cdot\mathbf{u}(\mathbf{q})\}\{\zeta(\mathbf{p})\zeta(\mathbf{k}')\}\right], \tag{57}$$

$$\text{Vector}: S^{\zeta\zeta}(\mathbf{k}'|\mathbf{p}|\mathbf{q}) = -\Im\left[\{\mathbf{k}'\cdot\mathbf{u}(\mathbf{q})\}\{\boldsymbol{\zeta}(\mathbf{p})\cdot\boldsymbol{\zeta}(\mathbf{k}')\}\right], \tag{58}$$

$$\text{Tensor}: S^{\zeta\zeta}(\mathbf{k}'|\mathbf{p}|\mathbf{q}) = -\Im\left[\{\mathbf{k}'\cdot\mathbf{u}(\mathbf{q})\}\{\zeta_{ij}(\mathbf{p})\zeta_{ij}(\mathbf{k}')\}\right]. \tag{59}$$

In the above equations, the giver and receiver modes are from the secondary field, while a velocity mode acts as a mediator for the secondary energy transfer. The aforementioned form of energy transfer also follows from the structure of nonlinear term $(\mathbf{u}\cdot\nabla)\zeta$ where $\mathbf{u}$ advects the scalar field ζ. Also, the superscript of $S^{\zeta\zeta}$ refer to the receiver and giver fields, both being ζ.

Using incompressibility condition, we can show that the mode-to-mode secondary energy transfer functions satisfy the following property:

$$S^{\zeta\zeta}(\mathbf{k}'|\mathbf{p}|\mathbf{q}) = -S^{\zeta\zeta}(\mathbf{p}|\mathbf{k}'|\mathbf{q}). \tag{60}$$

Using equation (60) we deduce that for a wavenumber region A (including a triad),

$$\sum_{\mathbf{k}'\in A}\sum_{\mathbf{p}\in A} S^{\zeta\zeta}(\mathbf{k}'|\mathbf{p}|\mathbf{q}) = 0. \tag{61}$$

This relation also implies that E_ζ is conserved when $F_\zeta = 0$ and $\kappa = 0$. Using the formula for the mode-to-mode energy transfers, we define the secondary energy flux for a wavenumber sphere of radius k_0 as [5, 6, 8, 22, 23, 110]:

$$\Pi_\zeta(k_0) = \sum_{k'>k_0}\sum_{\mathbf{p}\leqslant k_0} S^{\zeta\zeta}(\mathbf{k}'|\mathbf{p}|\mathbf{q}). \tag{62}$$

Here, $\Pi_\zeta(k_0)$ is the net secondary energy transfer from all the modes inside the sphere to all the modes outside the sphere.

Following similar lines of arguments as in section 3, we derive the following evolution equation for the scalar energy spectrum $E_\zeta(k)$ [6, 14]:

$$\frac{\partial}{\partial t}E_\zeta(k,t) = -\frac{\partial}{\partial k}\Pi_\zeta(k,t) + \mathcal{F}_\zeta(k,t) - D_\zeta(k,t), \tag{63}$$

where

$$E_\zeta(k)\mathrm{d}k = \sum_{k<k'\leqslant k+\mathrm{d}k} E_\zeta(\mathbf{k}'), \tag{64}$$

$$\mathcal{F}_\zeta(k)\mathrm{d}k = \sum_{k<k'\leqslant k+\mathrm{d}k} \Re[F_\zeta(\mathbf{k}')\zeta^*(\mathbf{k}')], \tag{65}$$

$$D_\zeta(k)\mathrm{d}k = \sum_{k<k'\leqslant k+\mathrm{d}k} 2\kappa k'^2 E_\zeta(\mathbf{k}'). \tag{66}$$

Here, $\mathcal{F}_\zeta(k)$ represents the scalar energy supply rate by F_ζ to shell k, and $D_\zeta(k)$ represents the diffusion or dissipation rate of the scalar energy in shell k. For the vector and tensor secondary fields, equation (65) involves vector and tensor products respectively. For a steady state ($\partial E_\zeta(k)/\partial t = 0$), equation (63) yields

$$\frac{\mathrm{d}}{\mathrm{d}k}\Pi_\zeta(k) = \mathcal{F}_\zeta(k) - D_\zeta(k). \tag{67}$$

Thus, the energy flux of a secondary field is affected by $\mathcal{F}_\zeta(k)$ and $D_\zeta(k)$. We may obtain a steady state when ζ field is forced at large scales.

In the inertial range, $D_\zeta(k) \approx 0$, hence

$$\frac{\mathrm{d}}{\mathrm{d}k}\Pi_\zeta = \mathcal{F}_{\zeta,\mathrm{in}}(k), \tag{68}$$

where the subscript 'in' of $\mathcal{F}_{\zeta,\mathrm{in}}$ represents the inertial range. Therefore, in the inertial range, similar to the description of section 3, variations of $\Pi_\zeta(k)$ can be classified into four categories:

(a) $\mathcal{F}_{\zeta,\mathrm{in}}(k) = 0$ and $\Pi_\zeta(k) = 0$,
(b) $\mathcal{F}_{\zeta,\mathrm{in}}(k) = 0$ and $\Pi_\zeta(k) = C > 0$,
(c) $\mathcal{F}_{\zeta,\mathrm{in}}(k) < 0$ and $\mathrm{d}\Pi_\zeta(k)/\mathrm{d}k < 0$,
(d) $\mathcal{F}_{\zeta,\mathrm{in}}(k) > 0$ and $\mathrm{d}\Pi_\zeta(k)/\mathrm{d}k > 0$.

The interpretation of the above four cases are very similar to those for the kinetic energy flux discussed in section 3 and exhibited in figure 8. Note that the first case corresponds to the equilibrium configuration for the secondary field. We will describe these cases in the subsequent sections.

4.2. Cross energy transfers between the velocity and secondary fields

In this subsection we describe the energy transfers from the velocity field to the secondary field and vice versa. We consider k_0 beyond k_f and rewrite equation (20) as [6, 14]

$$\begin{aligned}\frac{\mathrm{d}}{\mathrm{d}t}\sum_{k\leqslant k_0} E_u(\mathbf{k},t) &= \sum_{k\leqslant k_0} T_u + \sum_{k\leqslant k_0} \mathcal{F}_u(\mathbf{k}) + \sum_{k\leqslant k_0} \mathcal{F}_{\mathrm{LS}}(\mathbf{k}) - \sum_{k\leqslant k_0} D_u(\mathbf{k}) \\ &= -\Pi_u(k_0) + \Pi^\zeta_{u<}(k_0) + \varepsilon_{\mathrm{inj}} - \sum_{k\leqslant k_0} D_u(\mathbf{k}),\end{aligned} \tag{69}$$

where $\varepsilon_{\mathrm{inj}}$ is the kinetic energy injection rate by the large-scale force, and $\Pi^\zeta_{u<}(k_0)$ is the net energy transfer from all the $\boldsymbol{\zeta}$ modes to the velocity modes within the sphere of radius

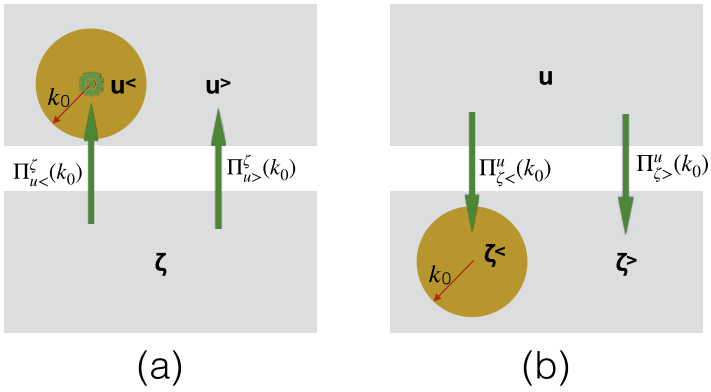

Figure 13. (a) The flux $\Pi^{\zeta}_{u<}(k_0)$ ($\Pi^{\zeta}_{u>}(k_0)$) represents the energy transfer from ζ modes to the velocity modes inside (outside) the sphere. (b) The flux $\Pi^{u}_{\zeta<}(k_0)$ ($\Pi^{u}_{\zeta>}(k_0)$) represents the reverse energy transfers, i.e. from all the velocity modes to ζ modes inside (outside) the sphere.

k_0. In $\Pi^{\zeta}_{u<}(k_0)$, the superscript and subscripts denote the giver and receiver field variables respectively, while $<$ denotes the modes within the sphere. In the same vein, we define

$$\Pi^{\zeta}_{u>}(k_0) = \sum_{k>k_0} \mathcal{F}_u(\mathbf{k}) \tag{70}$$

as the net energy transfer from all the $\boldsymbol{\zeta}$ modes to the velocity modes outside (represented by the symbol $>$) the sphere of radius k_0. Using the evolution equation for $E_\zeta(\mathbf{k})$ we deduce that

$$\Pi^{u}_{\zeta<}(k_0) = \sum_{k\leqslant k_0} \mathcal{F}_\zeta(\mathbf{k}); \qquad \Pi^{u}_{\zeta>}(k_0) = \sum_{k>k_0} \mathcal{F}_\zeta(\mathbf{k}) \tag{71}$$

are the respective energy transfers from all the velocity modes to the ζ modes inside and outside of the sphere of radius k_0. Figure 13 illustrates these fluxes.

The net energy transfer from ζ to $\mathbf{u}$ is

$$\mathcal{F}_u = \sum_{\mathbf{k}} \mathcal{F}_u(\mathbf{k}) = \Pi^{\zeta}_{u<}(k) + \Pi^{\zeta}_{u>}(k). \tag{72}$$

Since $\mathcal{F}_u$ is a fixed number, the sum $\Pi^{\zeta}_{u<}(k) + \Pi^{\zeta}_{u>}(k)$ is constant in k. Similarly, the net energy transfer from $\mathbf{u}$ to ζ is

$$\mathcal{F}_\zeta = \sum_{\mathbf{k}} \mathcal{F}_\zeta(\mathbf{k}) = \Pi^{u}_{\zeta<}(k) + \Pi^{u}_{\zeta>}(k). \tag{73}$$

with the sum $\Pi^{u}_{\zeta<}(k) + \Pi^{u}_{\zeta>}(k)$ as a constant in k. Note however that the individual fluxes (e.g. $\Pi^{u}_{\zeta<}(k)$) may vary with k.

Using the definitions of the above fluxes, we derive the following relations [14]:

$$\begin{aligned} \frac{\mathrm{d}}{\mathrm{d}k}\Pi^{\zeta}_{u>}(k) &= -\mathcal{F}_u(k); \qquad \frac{\mathrm{d}}{\mathrm{d}k}\Pi^{\zeta}_{u<}(k) = \mathcal{F}_u(k); \\ \frac{\mathrm{d}}{\mathrm{d}k}\Pi^{u}_{\zeta>}(k) &= -\mathcal{F}_\zeta(k); \qquad \frac{\mathrm{d}}{\mathrm{d}k}\Pi^{u}_{\zeta<}(k) = \mathcal{F}_\zeta(k). \end{aligned} \tag{74}$$

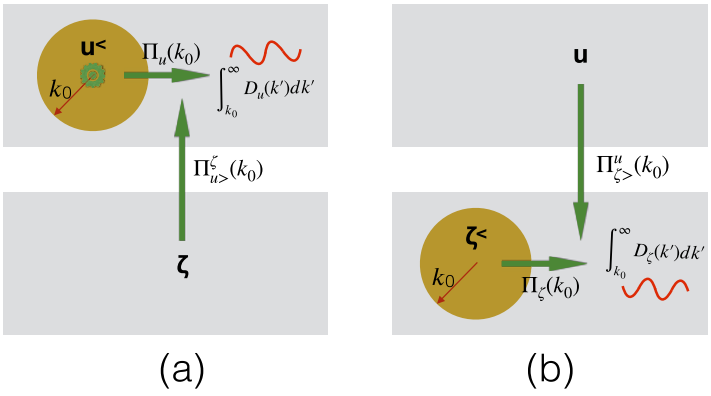

Figure 14. Schematic diagram illustrating the identities (a) $\Pi_u(k_0) + \Pi^{\zeta}_{u>}(k_0) = \int_{k_0}^{\infty} \mathrm{d}k' D_u(k')$; (b) $\Pi_\zeta(k_0) + \Pi^{u}_{\zeta>}(k_0) = \int_{k_0}^{\infty} \mathrm{d}k' D_\zeta(k')$. The wheel in the centre of (a) represents kinetic energy injection rate $\varepsilon_{\mathrm{inj}}$.

If we assume an absence of large scale forcing for ζ, then the fluxes obey the following properties under steady state:

$$\Pi_u(k_0) + \Pi^{\zeta}_{u>}(k_0) = \int_{k_0}^{\infty} \mathrm{d}k D_u(k', t), \tag{75}$$

$$\Pi_\zeta(k_0) + \Pi^{u}_{\zeta>}(k_0) = \int_{k_0}^{\infty} \mathrm{d}k D_\zeta(k), \tag{76}$$

$$\int_0^{k_0} \mathrm{d}k \mathcal{F}_u(k) = \Pi_u(k_0) + \Pi^{u<}_{\zeta}(k_0) + \int_0^{k_0} \mathrm{d}k D_u(k) \tag{77}$$

$$\Pi^{u}_{\zeta<}(k_0) = \Pi_\zeta(k_0) + \int_0^{k_0} \mathrm{d}k D_\zeta(k). \tag{78}$$

The dissipative terms become significant only in the dissipation range. Hence, for k_0 in the inertial range, $\int_0^{k_0} \mathrm{d}k D_{u,\zeta}(k', t) \approx 0$ and $\int_{k_0}^{\infty} \mathrm{d}k D_{u,\zeta}(k', t) \approx \epsilon_{u,\zeta}$. In addition, we assume that the forcing is at large scales, hence, $\int_0^{k_0} \mathrm{d}k \mathcal{F}_u(k) \approx \varepsilon_{\mathrm{inj}}$. Therefore, for a inertial-range spheres of radius k_0,

$$\Pi_u(k_0) + \Pi^{\zeta}_{u>}(k_0) = \epsilon_u, \tag{79}$$

$$\Pi_\zeta(k_0) + \Pi^{u}_{\zeta>}(k_0) = \epsilon_\zeta, \tag{80}$$

$$\varepsilon_{\mathrm{inj}} = \Pi_u(k_0) + \Pi^{u<}_{\zeta}(k_0), \tag{81}$$

$$\Pi^{u}_{\zeta<}(k_0) = \Pi_\zeta(k_0). \tag{82}$$

Note that some of the fluxes, such as $\Pi_u(k_0)$ and $\Pi^{\zeta}_{u>}(k_0)$, vary with k, hence, they are *variable energy fluxes*. However, the above combinations of fluxes are constants (*statistically*) due to the conservation of energy. We call the above equations as *exact relations of energy fluxes*. These relations are illustrated in figures 14 and 15.

Physical interpretations of the above identities are as follows. As shown in figure 14(a), the energy incident to the velocity modes outside the wavenumber sphere is destroyed in the

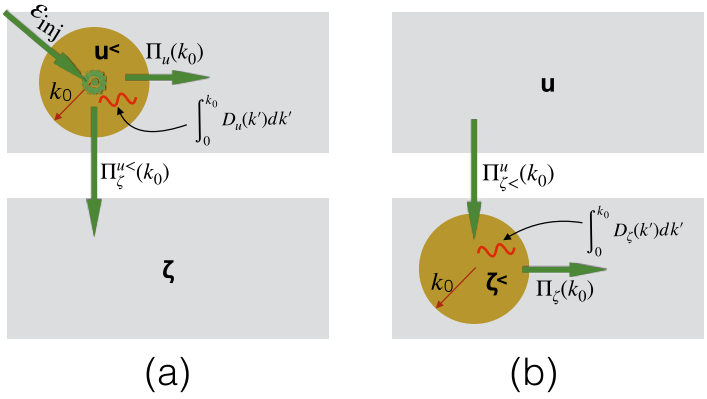

Figure 15. Schematic diagram illustrating identities for a steady state: (a) $\varepsilon_{\rm inj} = \Pi_u(k_0) + \Pi^{u<}_{\zeta}(k_0) + \int_0^{k_0} {\rm d}k D_u(k)$; (b) $\Pi^{u}_{\zeta<}(k_0) = \Pi_\zeta(k_0) + \int_0^{k_0} {\rm d}k D_\zeta(k)$. The wheel in the centre of (a) represents kinetic energy injection rate $\varepsilon_{\rm inj}$.

dissipation range by viscosity. Similar energetics are observed for the secondary field, as shown in figure 14(b). These conservation laws refer to exact relations of equations (75) and (76) respectively. Figures 15(a) and (b) illustrate that the energy incident at large-scale velocity and secondary fields get cascaded as energy fluxes to inertial range, and gets dissipated in the large scales. These equalities refer to exact relations of equations (77) and (78) respectively. These identities have important consequences in MHD turbulence and in drag reduction in polymeric flows [47]. We will discuss these issues is section 7.

Conservation laws are related to the exact relations for the energy fluxes. In addition, for some systems, the total energy, $\int {\rm d}\mathbf{r}(u^2 + \zeta^2)/2$, is conserved in the inviscid limit. For example, for MHD turbulence, the sum of kinetic and magnetic energies is conserved; the sum of kinetic and potential energies is also conserved for stably stratified flows. Energetically, these conditions corresponds to

$$\mathcal{F}_u + \mathcal{F}_\zeta = 0. \tag{83}$$

Consequently, equations (72) and (73) yield the following exact relation:

$$\Pi^{\zeta}_{u<}(k) + \Pi^{\zeta}_{u>}(k) + \Pi^{u}_{\zeta<}(k) + \Pi^{u}_{\zeta>}(k) = 0. \tag{84}$$

We will describe these fluxes and exact relation in later sections of this review.

In subsequent discussion, we will describe the role of variable energy flux in several turbulent flows with secondary fields, namely, passive scalar flow, buoyancy driven flows, MHDs, and polymer solution. Note that in the turbulent limit, the nonlinear terms $(\mathbf{u}\cdot\nabla)\mathbf{u}$ and $(\mathbf{u}\cdot\nabla)\boldsymbol{\zeta}$ dominate the respective dissipation terms, and hence Re $\gg 1$ and Pe $\gg 1$.

In the next subsection, we describe the scaling of passive secondary turbulence.

4.3. Turbulence with a passive secondary field

Consider a flow whose $\mathcal{F}_u$ is independent of the secondary field ζ and, hence, the velocity field is unaffected by the secondary field. However, the secondary field ζ is affected by $\mathbf{u}$. This is the reason why such a ζ is called a *passive secondary field* [3–8]. We will discuss the properties of such flows in this subsection.

If the forces on the velocity and the passive secondary fields are active only at large scales, then $\mathcal{F}_{u,\text{in}}(k) = 0$ and $\mathcal{F}_{\zeta,\text{in}}(k) = 0$, where the subscript 'in' refers to the inertial range. For such field configurations, using equations (43) and (68) we deduce that $\Pi_u(k)$ and $\Pi_\zeta(k)$ are constant in the inertial range. Since the velocity field is unaffected by ζ, the kinetic energy is described by Kolmogorov's theory of turbulence (see section 3.2). Therefore, the kinetic energy spectrum is given by equation (44).

In the inertial range, $\Pi_\zeta(k) = \text{const.} = \epsilon_\zeta$, where ϵ_ζ is the energy dissipation rate of the secondary field. Using dimension analysis and similar arguments as in section 3.2, one obtains [6–8]

$$E_\zeta(k) = K_{\text{OC}}\epsilon_\zeta(\epsilon_u)^{-1/3}k^{-5/3}, \tag{85}$$

where K_{OC} is the *Obukhov–Corrsin constant*. The above scaling has been verified using several numerical simulations and experiments [6–9, 111, 112]. For the inertial–dissipation range, using arguments similar to those in section 3.2, Pao [113] derived that

$$\Pi_\zeta(k) = \epsilon_\zeta \exp\left(-\frac{3}{2}K_{\text{OC}}(k/k_c)^{4/3}\right), \tag{86}$$

$$E_\zeta(k) = K_{\text{OC}}\epsilon_\zeta\epsilon_u^{-1/3}k^{-5/3} \exp\left(-\frac{3}{2}K_{\text{OC}}(k/k_c)^{4/3}\right), \tag{87}$$

where $k_c = \left(\epsilon_u/\kappa^3\right)^{1/4}$ is Kolmogorov's diffusion wavenumber. Hence, $k_c/k_d = \text{Pr}^{3/4}$.

The above arguments are valid when $\text{Re} \gg 1$ and $\text{Pe} \gg 1$. The spectral properties are quite different for other regimes (e.g. $\text{Re} \gg 1$ and $\text{Pe} \ll 1$) [23, 114, 115], which are not discussed in this review. In the next section, we will discuss how variable energy flux play an important role in anisotropic turbulence.

5. Variable energy flux in anisotropic turbulence

Typically, a fluid flow becomes anisotropic in the presence of a strong external field (e.g. mean magnetic field, buoyancy, external rotation field). In such flows, we denote the velocity components perpendicular and parallel to the external field as $\mathbf{u}_\perp$ and $u_\parallel$, and the corresponding energy spectra as $E_{u,\parallel}(\mathbf{k}) = \frac{1}{2}|u_\parallel(\mathbf{k})|^2$ and $E_{u,\perp}(\mathbf{k}) = \frac{1}{2}|\mathbf{u}_\perp(\mathbf{k})|^2$ respectively. The corresponding energy fluxes are [23, 28]:

$$\Pi_{u,\parallel}(k_0) = \sum_{k'>k_0}\sum_{\mathbf{p}\leqslant k_0} -\Im\left\{\left[\mathbf{k}'\cdot\mathbf{u}(\mathbf{q})\right]\left[u_\parallel(\mathbf{k}')u_\parallel(\mathbf{p})\right]\right\}, \tag{88}$$

$$\Pi_{u,\perp}(k_0) = \sum_{k'>k_0}\sum_{\mathbf{p}\leqslant k_0} -\Im\left\{\left[\mathbf{k}'\cdot\mathbf{u}(\mathbf{q})\right]\left[\mathbf{u}_\perp(\mathbf{k}')\cdot\mathbf{u}_\perp(\mathbf{p})\right]\right\}, \tag{89}$$

where $\mathbf{k} = \mathbf{p} + \mathbf{q}$ and $\mathbf{k}' = -\mathbf{k}$.

The evolution equations for the one-dimensional spectra $E_{u,\perp}(k)$ and $E_{u,\parallel}(k)$ are

$$\frac{\partial}{\partial t}E_{u,\parallel}(k,t) = -\frac{\partial}{\partial k}\Pi_{u,\parallel}(k,t) + \mathcal{P}(k,t) - 2\nu k^2 E_{u,\parallel}(k,t) + \mathcal{F}_{u,\parallel}(k) + \mathcal{F}_{\text{LS},\parallel}(k), \tag{90}$$

$$\frac{\partial}{\partial t}E_{u,\perp}(k,t) = -\frac{\partial}{\partial k}\Pi_{u,\perp}(k,t) - \mathcal{P}(k,t) - 2\nu k^2 E_{u,\perp}(k,t) + \mathcal{F}_{u,\perp}(k) + \mathcal{F}_{\text{LS},\perp}(k), \tag{91}$$

where

$$\mathcal{P}(k)\mathrm{d}k = \sum_{k<k'\leqslant k+\mathrm{d}k} \Im\left\{k_\parallel \mathbf{p}(\mathbf{k}) u_\parallel^*(\mathbf{k})\right\}, \tag{92}$$

and $\mathcal{F}_{u,\parallel}(k)$, $\mathcal{F}_{\mathrm{LS},\parallel}(k)$, $\mathcal{F}_{u,\perp}(k)$, and $\mathcal{F}_{\mathrm{LS},\perp}(k)$ are the energy injection rates to $u_\parallel$ and $\mathbf{u}_\perp$ by the parallel and perpendicular components of $\mathbf{F}_u$ and $\mathbf{F}_{\mathrm{LS}}$. Under a steady state and in the inertial range with $\mathbf{F}_u = 0$ and $\mathbf{F}_{\mathrm{LS}} = 0$,

$$\frac{\mathrm{d}}{\mathrm{d}k}\Pi_{u,\parallel}(k) = -\frac{\mathrm{d}}{\mathrm{d}k}\Pi_{u,\perp}(k) = \mathcal{P}(k). \tag{93}$$

Thus, $\Pi_{u,\perp}(k)$ and $\Pi_{u,\parallel}(k)$ vary with k. However,

$$\frac{\mathrm{d}}{\mathrm{d}k}\Pi_u(k) = \frac{\mathrm{d}}{\mathrm{d}k}[\Pi_\parallel(k) + \Pi_{u,\perp}(k)] = 0. \tag{94}$$

That is, the energy flux $\Pi_u(k)$ is constant in inertial range, as expected from Kolmogorov's theory of turbulence. Note that $\mathcal{P}(k)$ facilitates energy transfers between the perpendicular and parallel components of the velocity field.

In later sections, we briefly discuss anisotropy in stably stratified turbulence, turbulent thermal convection, quasi-static MHD turbulence, and MHD turbulence. In all these systems, pressure plays an important role in energy exchange between $\mathbf{u}_\perp$ and $u_\parallel$. In section 10.2 we show how the above energy transfers take an active part in quasi-2D turbulence generated by strong rotation, external magnetic field, or gravity. We refer the reader to earlier works [49, 70, 82, 116] for further details. We also remark that similar formulas need to be derived for the secondary fields as well. For example, it will be interesting to investigate how the parallel and perpendicular components of the magnetic field exchange energy among themselves.

In the next section we describe how the ideas of variable energy flux yields interesting insights into the physics of buoyancy-driven turbulence.

6. Variable energy flux in buoyancy-driven turbulence

Buoyancy-driven flows can be broadly classified into two categories: stable and unstable [10, 23, 117, 118]. The properties of these two categories of flows are very different [119]. For brevity, our focus would be on flows with linear stratification, which is a good approximation for a small region of planetary or stellar atmospheres.

In the next two subsections we will review the turbulence phenomenologies of stably-stratified and unstably-stratified flows. Since gravity affects the velocity field, the secondary fields in such flows are called *active fields*. The buoyant flows are typically anisotropic due to external gravity. Still, one-dimensional energy spectrum and flux are often employed to characterize such flows because they provide cumulative effects over the polar angles (angle between the buoyancy direction and wavenumber $\mathbf{k}$). For justification, refer to section 2. More advanced tools like ring spectrum and ring-to-ring energy transfer too have been applied to model such flows, but these topics are beyond the scope of this review.

6.1. Stably stratified turbulence

A flow is said to be stably stratified when the density of a fluid under gravity decreases with height. See figure 16(a) for an illustration. The background density profile is

$$\bar{\zeta}(z) = \zeta_\mathrm{b} + \frac{\mathrm{d}\bar{\zeta}}{\mathrm{d}z}z = \zeta_\mathrm{b} + \frac{\zeta_\mathrm{t} - \zeta_\mathrm{b}}{d}z, \tag{95}$$

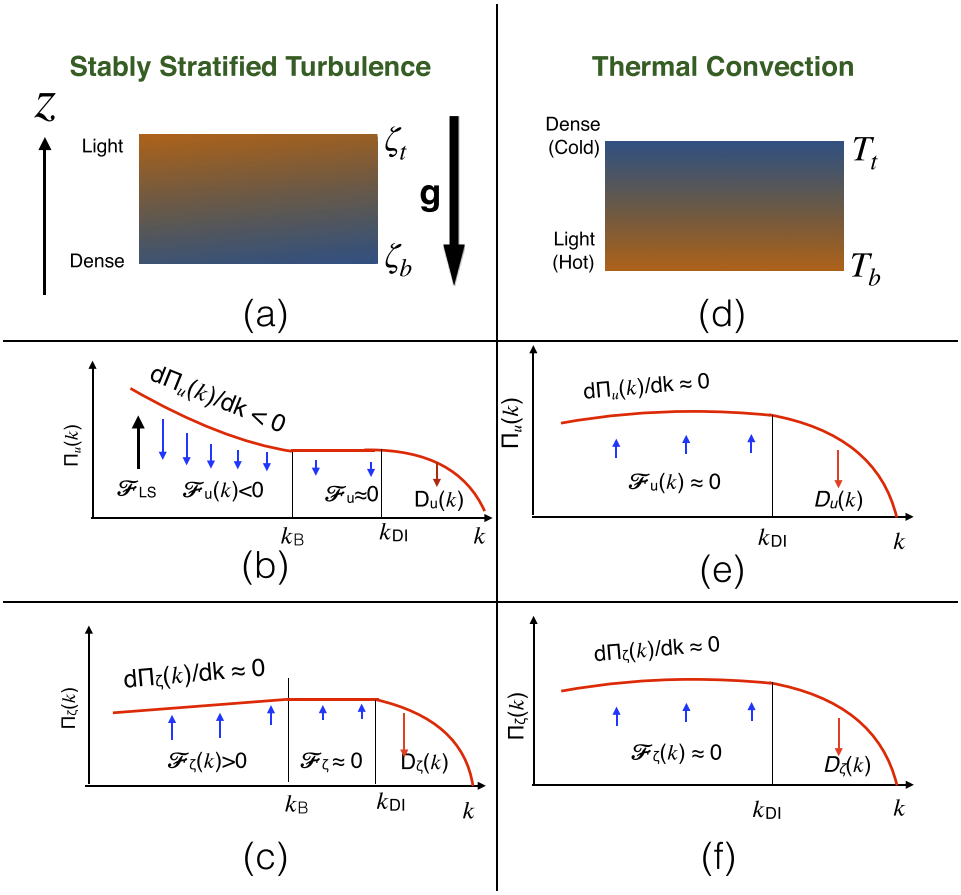

Figure 16. For stably stratified turbulence: (a) a schematic diagram depicting the density $\zeta(z)$ that decreases with height; (b) kinetic energy flux, $\Pi_u(k)$, decreases for $k < k_B$, and is constant for $k_B < k < k_{DI}$, where k_B is the Bolgiano wavenumber, and k_{DI} is the wavenumber beyond which the dissipation range starts. (c) Secondary energy flux, $\Pi_\zeta(k)$, increases marginally for $k < k_B$, and is constant for $k_B < k < k_{DI}$. For turbulent thermal convection: (d) a schematic diagram depicting a fluid between two plates whose temperatures are T_b and T_t ($T_b > T_t$); (e) and (f) $\Pi_u(k)$ and $\Pi_\zeta(k)$ are approximately constant in the inertial range.

where $\bar{\zeta}(z)$ is the vertical density profile, which is assumed to be linear; gravity is along $-\hat{\mathbf{z}}$; and ζ_b, ζ_t are respective densities at the bottom and top layers of the flow that is confined within a vertical distance d. Stably stratified environment supports internal gravity waves with *Brunt–Väisälä frequency*, which is given by [117, 118]

$$N = \sqrt{\frac{g}{\zeta_m}\left|\frac{d\bar{\zeta}}{dz}\right|}, \tag{96}$$

where ζ_m is the mean density of the whole fluid, and g is the acceleration due to gravity. Another useful nondimensional number is *Richardson number*, which is the ratio of buoyancy and nonlinear term.

The governing equations for the system are [10, 23, 117, 118]

$$\frac{\partial \mathbf{u}}{\partial t} + (\mathbf{u}\cdot\nabla)\mathbf{u} = -\nabla\sigma - N\zeta\hat{\mathbf{z}} + \nu\nabla^2\mathbf{u} + \mathbf{F}_{\rm LS}, \tag{97}$$

$$\frac{\partial \zeta}{\partial t} + (\mathbf{u}\cdot\nabla)\zeta = Nu_z + \kappa\nabla^2\zeta, \tag{98}$$

where σ is the pressure, $\zeta \to (g\zeta)/(N\zeta_{\rm m})$ is the density fluctuation in velocity units, and $-N\zeta\hat{z}$ is buoyancy. For periodic or vanishing boundary condition and in the absence of dissipative terms, the total energy,

$$E_u + E_\zeta = \int {\rm d}\mathbf{r}\frac{1}{2}u^2 + \int {\rm d}\mathbf{r}\frac{1}{2}\zeta^2, \tag{99}$$

is conserved [10, 23, 117, 118, 120]. In the above expression, E_ζ is the *total potential energy*.

The forces related to buoyancy are

$$\mathbf{F}_u = -N\zeta\hat{\mathbf{z}}; \qquad F_\zeta = Nu_z, \tag{100}$$

which are linear functions of the field variables. Clearly, the energy injection rates by these two forces are

$$\mathcal{F}_u(\mathbf{k}) = -N\Re[\zeta(\mathbf{k})u_z^*(\mathbf{k})], \tag{101}$$

$$\mathcal{F}_\zeta(\mathbf{k}) = N\Re[\zeta(\mathbf{k})u_z^*(\mathbf{k})]. \tag{102}$$

Hence, $\mathcal{F}_\zeta(\mathbf{k}) + \mathcal{F}_u(\mathbf{k}) = 0$. Therefore, in the inertial range where $D_u(k) = 0$ and $D_\zeta(k) = 0$, adding equations (43) and (68) yields

$$\frac{\rm d}{{\rm d}k}[\Pi_u(k) + \Pi_\zeta(k)] = \mathcal{F}_u + \mathcal{F}_\zeta = 0 \tag{103}$$

leading to constancy of $\Pi_u(k) + \Pi_\zeta(k)$ in the inertial range. Note that $\mathcal{F}_u + \mathcal{F}_\zeta = 0$ plays an important role in the conservation of total energy in the inviscid limit (see equation (99)). For the forced and dissipative equations, the same condition, $\mathcal{F}_u + \mathcal{F}_\zeta = 0$, leads to constancy of total energy flux. Due to the local interactions in $\mathcal{F}_u(\mathbf{k})$ and $\mathcal{F}_\zeta(\mathbf{k})$, the cross fluxes $\Pi_{\zeta>}^{u<}(k)$, $\Pi_{\zeta<}^{u>}(k)$, $\Pi_{u>}^{\zeta<}(k)$, and $\Pi_{u<}^{\zeta>}(k)$ are zeros.

Stably stratified turbulence has complex properties, which are discussed in detail in many books and papers, for example, Lindborg [120], Davidson [118], and references therein. In this review, to present applications of variable energy flux in buoyant flows, we describe the spectral analysis for moderately stratified flows where $|\mathbf{u}\cdot\nabla\mathbf{u}| \approx N\zeta$. For such flows, Richardson number is of the order of unity.

For moderately stratified flows, Bolgiano [19] and Obukhov [20] provided the first phenomenological model. They assumed that for a wavenumber band in the inertial range,

$$ku_k^2 = N\zeta_k; \qquad \Pi_\zeta = k\zeta_k^2 u_k = \epsilon_\zeta \tag{104}$$

that yield the following fluxes and spectra for the velocity and density fields:

$$E_u(k) = c_1\epsilon_\zeta^{2/5}N^{4/5}k^{-11/5}, \qquad \Pi_u(k) = c_3\epsilon_\zeta^{3/5}N^{6/5}k^{-4/5}, \tag{105}$$

$$E_\zeta(k) = c_2\epsilon_\zeta^{4/5}N^{-2/5}k^{-7/5}, \qquad \Pi_\zeta(k) = \epsilon_\zeta. \tag{106}$$

Clearly, the kinetic energy flux $\Pi_u(k)$ decreases with k, in contrast to constant Π_u in the inertial range of 3D hydrodynamic turbulence. The reduction of $\Pi_u(k)$ occurs due to the conversion of kinetic energy to potential energy, and it leads to a steepening of $E_u(k)$ [19–21, 23, 118, 120]. Since the declining $\Pi_u(k)$ is much less than unity, constancy of total energy flux yields $\Pi_\zeta(k) \approx$ const. [121]. See figures 16(b) and (c) for an illustration.

In addition, Obukhov [19] and Obukhov [20] predicted that buoyancy becomes weak for $k > k_\mathrm{B}$, where $k_\mathrm{B} \approx N^{3/2}\epsilon_u^{-5/4}\epsilon_\zeta^{3/4}$ is *Bolgiano wavenumber*. Due to the weak buoyancy, Bolgiano and Obukhov predicted that both kinetic and secondary energies exhibit $k^{-5/3}$ spectrum for $k_\mathrm{B} < k < k_\mathrm{DI}$, where k_DI is the wavenumber beyond which dissipation becomes significant. See figure 16(b) for an illustration. Using the constraint $k_\mathrm{B} \ll k_d$, where k_d is Kolmogorov's wavenumber, Alam *et al* [121] showed that simultaneous presence of both the scaling regimes ($k^{-11/5}$ and $k^{-5/3}$) requires very large Reynolds number. Hence, the $k^{-5/3}$ regime of Bolgiano–Obukhov phenomenology is quite difficult to reproduce in numerical simulations.

Kimura and Herring [122] reported Bolgiano–Obukhov scaling for a narrow wavenumber band in their decaying simulation on a 128^3 grid. Kumar *et al* [21] performed a numerical simulation of stably stratified turbulence on a 1024^3 grid for Richardson number around unity and observed a good agreement between numerical results and the predictions of equations (105) and (106). Rosenberg *et al* [123] reported Bolgiano–Obukhov scaling in their simulation of rotating stratified turbulence.

Strong buoyancy (large Richardson number) makes the flow anisotropic, hence Bolgiano–Obukhov scaling is inapplicable to such flows. Lindborg [120] and Davidson [118] argued that the longitudinal and traverse velocity components exhibit k^{-3} and $k^{-5/3}$ spectra respectively. Variable energy flux may provide interesting clues for this regime as well. For 2D stably stratified turbulence, Kumar *et al* [124] derived several interesting relations using variable energy flux. Also note that buoyancy is weak for flows with small Richardson number. Hence, such flows exhibit Kolmogorov's spectrum [21].

In the next subsection we will employ the ideas of variable energy flux to turbulent thermal convection.

6.2. Turbulent thermal convection

Thermal convection too is driven by buoyancy. However, in contrast to the stably stratified flows, the fluid density increases with height that makes the flow unstable. A setup, exhibited in figure 16(d), consists of a thin fluid layer confined between two thermally conducting plates separated by a distance d. The temperatures of the bottom and top plates are T_b and T_t respectively.

In thermal convection, the temperature is a sum of externally-imposed linearly varying temperature $\bar{T}(z)$ and fluctuation $\zeta(x, y, z)$:

$$T(x, y, z) = \bar{T}(z) + \zeta(x, y, z), \tag{107}$$

where

$$\bar{T}(z) = T_\mathrm{b} + \frac{\mathrm{d}\bar{T}}{\mathrm{d}z}z = T_\mathrm{b} - \frac{T_\mathrm{b} - T_\mathrm{t}}{d}z. \tag{108}$$

The equations for thermal convection under Boussinesq approximation are [125]

$$\frac{\partial \mathbf{u}}{\partial t} + (\mathbf{u}\cdot\nabla)\mathbf{u} = -\frac{1}{\zeta_\mathrm{m}}\nabla\sigma + \alpha g\zeta\hat{\mathbf{z}} + \nu\nabla^2\mathbf{u}, \tag{109}$$

$$\frac{\partial \zeta}{\partial t} + (\mathbf{u}\cdot\nabla)\zeta = \frac{\Delta}{d}u_z + \kappa\nabla^2\zeta, \tag{110}$$

$$\nabla\cdot\mathbf{u} = 0, \tag{111}$$

where α, κ are respectively the thermal expansion coefficient and thermal diffusivity of the fluid, g is the acceleration due to gravity, and $\Delta = T_\mathrm{b} - T_\mathrm{t}$. The two important parameters of turbulent thermal convection are Prandtl number, $\mathrm{Pr} = \nu/\kappa$, and Rayleigh number,

$$\mathrm{Ra} = \frac{\alpha g d^3 \Delta}{\nu\kappa}. \tag{112}$$

Note that the forces

$$\mathbf{F}_u = \alpha g \zeta \hat{\mathbf{z}}, \qquad F_\zeta = \frac{\Delta}{d}u_z \tag{113}$$

are linear functions of the field variables.

In thermal convection, hot plumes ascend and cold ones descend. Hence, $\langle\zeta(\mathbf{r})u_z(\mathbf{r})\rangle > 0$. Therefore, using Parceval's theorem we deduce that

$$\sum_{\mathbf{k}} \Re\left[\langle\zeta(\mathbf{k})u_z^*(\mathbf{k})\rangle\right] > 0. \tag{114}$$

Further, numerical simulations reveals that $\Re\left[\langle\zeta(\mathbf{k})u_z^*(\mathbf{k})\rangle\right] > 0$ for most Fourier modes of thermal convection [22]. Hence,

$$\mathcal{F}_u(\mathbf{k}) = \alpha g \Re[\zeta(\mathbf{k})u_z^*(\mathbf{k})] > 0 \tag{115}$$

$$\mathcal{F}_\zeta(\mathbf{k}) = \frac{\Delta}{d}\Re[\zeta(\mathbf{k})u_z^*(\mathbf{k})] > 0 \tag{116}$$

Therefore, in the inertial range where $D_u(k) = 0$ and $D_\zeta(k) = 0$, subtracting $(\alpha g d/\Delta) \times$ equation (68) from equation (43) yields

$$\frac{\mathrm{d}}{\mathrm{d}k}\left[\Pi_u(k) - \frac{\alpha g d}{\Delta}\Pi_\zeta(k)\right] = 0 \tag{117}$$

leading to

$$\Pi_u(k) - \frac{\alpha g d}{\Delta}\Pi_\zeta(k) = \text{const.} \tag{118}$$

In the dissipationless limit, $\int \mathrm{d}\mathbf{r}\frac{1}{2}[u^2 - (\alpha g d/\Delta)\zeta^2]$, a sum of kinetic energy and potential energy, is conserved. Here, the potential energy, $-\frac{1}{2}(\alpha g d/\Delta)\zeta^2$, is negative because the system is unstable. Since this potential energy can be converted to kinetic energy, it is also called *available potential energy*. Contrast this potential energy with that for stably stratified turbulence [118]. Also, note that constancy of $\Pi_u(k) - (\alpha g d/\Delta)\Pi_\zeta(k)$ is related to the above conservation law, as we argued for the stably stratified turbulence.

Equation (115) implies that $\Pi_u(k)$ should increase with k. However, for $\mathrm{Pr} \sim 1$, Verma *et al* [22] showed that $\mathcal{F}_u(k) \sim (kL)^{-5/3}$, hence, $\mathcal{F}_u(k)$ is small in the inertial range because $kL \gg 1$. The function $\mathcal{F}_u(k)$ is even steeper for small Prandtl numbers [23]. These observations indicate that large-scale thermal plumes drive the flow, similar to the forcing in Kolmogorov's theory for hydrodynamic turbulence. These results falsify the popular statements that thin thermal plumes drive thermal convection.

Based on similarities between the forcing in thermal convection and Kolmogorov's model of turbulence, Kumar *et al* [21] and Verma *et al* [22] argued that for Pr $\lessapprox 1$, $\Pi_u(k)$ remains an approximate constant in the inertial range and $E_u(k) \sim k^{-5/3}$. Kumar *et al* [21] and Verma *et al* [22] verified the above phenomenology using high-resolution numerical simulations. The above flux-based arguments resolve the long impasse in the field regarding the energy spectrum. Note that several past works [71–73, 126] projected that Bolgiano–Obukhov's scaling for stably stratified turbulence ($E_u(k) \sim k^{-11/5}$) holds for turbulent thermal convection as well, while experimental and numerical works were inconclusive. For large Prandtl numbers, the flow is dissipative and $E_u(k) \sim k^{-13/3}$ [23, 127].

However, there is a major difference between hydrodynamic turbulence and turbulent convection. In turbulent convection, inertial-range kinetic energy flux is a fraction of the total viscous dissipation rate. This is because thermal plumes drive the flow at all scales. In particular, under steady state, for wavenumber k in the inertial range,

$$\Pi_u(k) \approx \int_0^k \mathrm{d}k' \mathcal{F}_u(k') = \int_0^\infty \mathrm{d}k' \mathcal{F}_u(k') - \int_k^\infty \mathrm{d}k' \mathcal{F}_u(k')$$
$$= \epsilon_u - \int_k^\infty \mathrm{d}k' \mathcal{F}_u(k'), \tag{119}$$

where ϵ_u is the total viscous dissipation rate. Using equation (119) we deduce that the inertial-range kinetic energy flux $\Pi_u(k) < \epsilon_u$ due to the presence of buoyancy at all scales. Using numerical simulations, Bhattacharya *et al* [128] showed that for Pr $= 1$, the inertial-range $\Pi_u(k)$ is around one-third of ϵ_u.

Turbulent thermal convection has other complex issues, e.g. anisotropy, anomalous heat transport, boundary layers, but these topics are beyond the scope of this review. In the passing we remark that for moderate Prandtl numbers, turbulent thermal convection exhibit near isotropy. Following the analysis of section 5, Nath *et al* [129] showed that for thermal convection, $\mathcal{P}(k)$ of equation (92) is negative implying that energy transfer takes place from $u_\parallel$ to $\mathbf{u}_\perp$. This observation is consistent with the fact that bouyancy drives $u_\parallel$, which in turn provides energy to $\mathbf{u}_\perp$.

There are many turbulent flows with unstable stratification, notably Rayleigh–Taylor turbulence [130], bubbly turbulence [131], Taylor–Couette turbulence [132, 133], etc. Based on the arguments of this subsection, we expect that the turbulence properties of unstable stable stratification are similar to those of hydrodynamic turbulence, e.g. $E_u(k) \sim k^{-5/3}$ [22, 23]. The results on Rayleigh–Taylor turbulence [130, 134, 135] and Taylor–Couette turbulence [132] in some regimes are consistent with the above observations.

In the aforementioned buoyant flows, $\mathbf{F}_u$ and $\mathbf{F}_\zeta$ are linear functions of ζ and $\mathbf{u}$ respectively. Hence the cross energy transfer occurs among the modes with same wavenumbers. Therefore, $\mathcal{F}_u(\mathbf{k})$ and $\mathcal{F}_\zeta(\mathbf{k})$ are functions only of local wavenumber $\mathbf{k}$. However, when $\mathbf{F}_u$ and $\mathbf{F}_\zeta$ are nonlinear functions of $\mathbf{u}$ and/or ζ, the cross energy transfers are convolutions of $\mathbf{u}$ and ζ Fourier modes. In the following section, we illustrate such energy transfers in MHD turbulence.

7. Variable energy fluxes in magnetohydrodynamic turbulence

Magnetohydrodynamic (MHD) turbulence is a vast area of research with many astrophysical and engineering applications. It is covered in several books and review papers, e.g. [25, 43, 70, 136–139] and references therein. The present section does not attempt to summarise vast number of results of MHD turbulence, but focusses on variable energy fluxes of MHD turbulence.

A magnetofluid, which is a quasi-neutral and electrically-conducting collisional plasma, is described using velocity field and magnetic field, which is denoted by $\boldsymbol{\zeta}$. In the following subsection, we describe the governing equations for MHD turbulence.

7.1. MHD turbulence: governing equations and cross transfers

The dynamical equations for the velocity and magnetic fields of MHD are [136–138]

$$\frac{\partial \mathbf{u}}{\partial t} + (\mathbf{u}\cdot\nabla)\mathbf{u} = -\nabla p + (\boldsymbol{\zeta}\cdot\nabla)\boldsymbol{\zeta} + \mathbf{F}_{\rm LS} + \nu\nabla^2\mathbf{u}, \tag{120}$$

$$\frac{\partial \boldsymbol{\zeta}}{\partial t} + (\mathbf{u}\cdot\nabla)\boldsymbol{\zeta} = (\boldsymbol{\zeta}\cdot\nabla)\mathbf{u} + \kappa\nabla^2\boldsymbol{\zeta}, \tag{121}$$

$$\nabla\cdot\mathbf{u} = \nabla\cdot\boldsymbol{\zeta} = 0, \tag{122}$$

where p is the total (thermodynamic + magnetic) pressure, $\mathbf{F}_{\rm LS}$ is the large-scale external force, and ν, κ are the kinematic viscosity and magnetic diffusivity respectively. In the above equation, the magnetic field is in Alfvénic units, which has same dimension as the velocity field; and the forces on $\mathbf{u}$ and $\boldsymbol{\zeta}$ are

$$\mathbf{F}_u = (\boldsymbol{\zeta}\cdot\nabla)\boldsymbol{\zeta}; \qquad \mathbf{F}_\zeta = (\boldsymbol{\zeta}\cdot\nabla)\mathbf{u}. \tag{123}$$

For an inviscid flow ($\nu = \kappa = 0$) with $\mathbf{F}_{\rm LS} = 0$, under periodic or vanishing boundary condition, the total energy,

$$E_u + E_\zeta = \int \mathrm{d}\mathbf{r}\frac{1}{2}u^2 + \int \mathrm{d}\mathbf{r}\frac{1}{2}\zeta^2, \tag{124}$$

is conserved [136–138]. Here, E_ζ is the total magnetic energy.

In Fourier space, the forces of equation (123) are

$$\mathbf{F}_u(\mathbf{k}) = \mathrm{i}\sum_{\mathbf{p}}\{\mathbf{k}\cdot\boldsymbol{\zeta}(\mathbf{q})\}\boldsymbol{\zeta}(\mathbf{p}); \qquad \mathbf{F}_\zeta(\mathbf{k}) = \mathrm{i}\sum_{\mathbf{p}}\{\mathbf{k}\cdot\boldsymbol{\zeta}(\mathbf{q})\}\mathbf{u}(\mathbf{p}), \tag{125}$$

where $\mathbf{q} = \mathbf{k} - \mathbf{p}$. The equation for the kinetic and magnetic modal energies are

$$\begin{aligned}\frac{\mathrm{d}}{\mathrm{d}t}E_u(\mathbf{k}) &= T_u(\mathbf{k}) + \mathcal{F}_u(\mathbf{k}) + \mathbf{F}_{\rm LS}(\mathbf{k}) - D_u(\mathbf{k}) \\ &= \sum_{\mathbf{p}}\Im\left[\{\mathbf{k}\cdot\mathbf{u}(\mathbf{q})\}\{\mathbf{u}(\mathbf{p})\cdot\mathbf{u}^*(\mathbf{k})\}\right] + \mathcal{F}_u(\mathbf{k}) + \mathbf{F}_{\rm LS}(\mathbf{k}) - 2\nu k^2 E_u(\mathbf{k}),\end{aligned} \tag{126}$$

$$\begin{aligned}\frac{\mathrm{d}}{\mathrm{d}t}E_\zeta(\mathbf{k}) &= T_\zeta(\mathbf{k}) + \mathcal{F}_\zeta(\mathbf{k}) - D_\zeta(\mathbf{k}) \\ &= \sum_{\mathbf{p}}\Im\left[\{\mathbf{k}\cdot\mathbf{u}(\mathbf{q})\}\{\boldsymbol{\zeta}(\mathbf{p})\cdot\boldsymbol{\zeta}^*(\mathbf{k})\}\right] + \mathcal{F}_\zeta(\mathbf{k}) - 2\kappa k^2 E_\zeta(\mathbf{k}),\end{aligned} \tag{127}$$

where the kinetic and magnetic energy injection rates by the forces $\mathbf{F}_u(\mathbf{k})$ and $\mathbf{F}_\zeta(\mathbf{k})$ are

$$\mathcal{F}_u(\mathbf{k}) = \sum_{\mathbf{p}} -\Im\left[\{\mathbf{k}\cdot\boldsymbol{\zeta}(\mathbf{q})\}\{\boldsymbol{\zeta}(\mathbf{p})\cdot\mathbf{u}^*(\mathbf{k})\}\right], \tag{128}$$

$$\mathcal{F}_\zeta(\mathbf{k}) = \sum_{\mathbf{p}} -\Im\left[\{\mathbf{k}\cdot\boldsymbol{\zeta}(\mathbf{q})\}\{\mathbf{u}(\mathbf{p})\cdot\boldsymbol{\zeta}^*(\mathbf{k})\}\right]. \tag{129}$$

Note that $\mathbf{F}_u(\mathbf{k})$ facilitates energy transfer from $\boldsymbol{\zeta}$ to $\mathbf{u}$, while $\mathbf{F}_\zeta(\mathbf{k})$ yields energy transfer from $\mathbf{u}$ to $\boldsymbol{\zeta}$. As remarked earlier, $\mathcal{F}_u(\mathbf{k})$, $\mathcal{F}_\zeta(\mathbf{k})$ are convolutions because $\mathbf{F}_u$, $\mathbf{F}_\zeta$ are nonlinear functions of $\mathbf{u}$ and $\boldsymbol{\zeta}$. In contrast, the corresponding transfers for the buoyant flows are functions of fields at local wavenumber (see section 6).

The nonlinear structure of the cross transfers between $\mathbf{u}$ and $\boldsymbol{\zeta}$ can be formulated in terms of mode-to-mode energy transfers. For a triad $(\mathbf{k}', \mathbf{p}, \mathbf{q})$ satisfying $\mathbf{k}' + \mathbf{p} + \mathbf{q} = 0$, Dar *et al* [42] and Verma [43] derived the following formulas for the mode-to-mode energy transfers from $\mathbf{u}$ to $\boldsymbol{\zeta}$ and vice versa:

$$S^{u\zeta}(\mathbf{k}'|\mathbf{p}|\mathbf{q}) = \Im\left[\{\mathbf{k}'\cdot\boldsymbol{\zeta}(\mathbf{q})\}\{\boldsymbol{\zeta}(\mathbf{p})\cdot\mathbf{u}(\mathbf{k}')\}\right] = -\Im\left[\{\mathbf{k}\cdot\boldsymbol{\zeta}(\mathbf{q})\}\{\boldsymbol{\zeta}(\mathbf{p})\cdot\mathbf{u}^*(\mathbf{k})\}\right], \tag{130}$$

$$S^{\zeta u}(\mathbf{k}'|\mathbf{p}|\mathbf{q}) = \Im\left[\{\mathbf{k}'\cdot\boldsymbol{\zeta}(\mathbf{q})\}\{\mathbf{u}(\mathbf{p})\cdot\zeta(\mathbf{k}')\}\right] = -\Im\left[\{\mathbf{k}\cdot\boldsymbol{\zeta}(\mathbf{q})\}\{\mathbf{u}(\mathbf{p})\cdot\zeta^*(\mathbf{k})\}\right]. \tag{131}$$

The former is the mode-to-mode energy transfer from $\boldsymbol{\zeta}(\mathbf{p})$ to $\mathbf{u}(\mathbf{k}')$ with the mediation of $\boldsymbol{\zeta}(\mathbf{q})$, while the latter provides the energy transfer from $\mathbf{u}(\mathbf{p})$ to $\boldsymbol{\zeta}(\mathbf{k}')$ with the mediation of $\boldsymbol{\zeta}(\mathbf{q})$. In $S^{cd}(\mathbf{k}'|\mathbf{p}|\mathbf{q})$, the superscript c and d refer to receiver and giver fields respectively.

These transfers satisfy the property:

$$S^{cd}(\mathbf{k}'|\mathbf{p}|\mathbf{q}) = -S^{dc}(\mathbf{p}|\mathbf{k}'|\mathbf{q}), \tag{132}$$

that is, the energy gained by $\mathbf{c}(\mathbf{k}')$ from $\mathbf{d}(\mathbf{p})$ is negative of the energy gained by $\mathbf{d}(\mathbf{p})$ from $\mathbf{c}(\mathbf{k}')$. This is a property of energy exchange. Using the above property, we can show that for any region A of Fourier space, including a triad,

$$\sum_{\mathbf{k}'\in A}\sum_{\mathbf{p}\in A}[S^{u\zeta}(\mathbf{k}'|\mathbf{p}|\mathbf{q}) + S^{\zeta u}(\mathbf{p}|\mathbf{k}'|\mathbf{q})] = 0. \tag{133}$$

By summing over all the Fourier modes, we deduce that $\mathcal{F}_u + \mathcal{F}_\zeta = 0$, where $\mathcal{F}_u$ and $\mathcal{F}_\zeta$ are respectively the total energy gained by the velocity and secondary fields via cross energy transfers. Note that stably-stratified turbulence too has $\mathcal{F}_u + \mathcal{F}_\zeta = 0$.

In three dimensions, MHD turbulence has two other conserved quantities: cross helicity ($\int \mathrm{d}\mathbf{r}(\mathbf{u}\cdot\boldsymbol{\zeta})/2$) and magnetic helicity ($\int \mathrm{d}\mathbf{r}(\mathbf{A}\cdot\boldsymbol{\zeta})/2$, where $\mathbf{A}$ is the vector potential). In the turbulent regime, both these quantities exhibit turbulent cascades [25, 70]. In this paper, we consider the cross helicity flux (in addition to the energy fluxes), which is detailed in subsection 7.4. The discussion of magnetic helicity flux is too complex too be covered here.

In the next subsection, we define the energy fluxes of MHD turbulence.

7.2. Various energy fluxes of MHD turbulence

Using the mode-to-mode energy transfers of equations (130) and (131), Dar *et al* [42] and Verma [43] derived formulas for the energy fluxes of MHD turbulence for a wavenumber sphere of radius k_0. Note that $\Pi_u(k_0)$ and $\Pi_\zeta(k_0)$ are respective fluxes for the kinetic and magnetic energies, while the energy flux $\Pi^{u<}_{\zeta>}(k_0)$ represents the net energy transfer from all the velocity modes inside the sphere to all the magnetic modes outside the sphere, that is,

$$\Pi^{u<}_{\zeta>}(k_0) = \sum_{\mathbf{p}\leqslant k_0}\sum_{k'>k_0} S^{\zeta u}(\mathbf{k}'|\mathbf{p}|\mathbf{q}). \tag{134}$$

The other fluxes, $\Pi^{\zeta<}_{u>}(k_0)$, $\Pi^{u<}_{\zeta<}(k_0)$, and $\Pi^{u>}_{\zeta>}(k_0)$ are defined similarly. Note that an application of equation (132) yields

$$\Pi^{ua}_{\zeta b}(k_0) = -\Pi^{\zeta b}_{ua}(k_0), \tag{135}$$

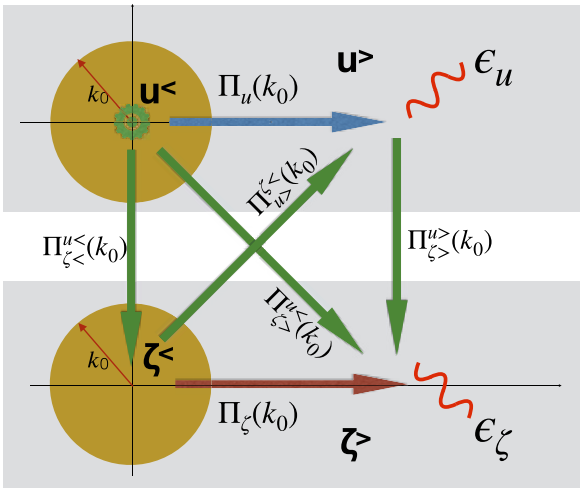

Figure 17. The six energy fluxes of MHD turbulence. $\epsilon_u, \epsilon_\zeta$ are the dissipation rates of the velocity and magnetic fields respectively. The wheel in the centre of the velocity sphere represents the external forcing at large scales.

where a, b represent $<$ or $>$. The above energy fluxes of MHD turbulence, depicted in figure 17, have been studied in great detail [42, 44, 140]. Interestingly, $\Pi^{u<}_{\zeta>}(k)$ and $\Pi^{\zeta<}_{u>}(k)$ are absent in buoyant flows due to the products of field variables with the same wavenumber (see section 6).

Now we relate the above quantities to the fluxes $\Pi^{u}_{\zeta<}$, $\Pi^{u}_{\zeta>}$, $\Pi^{\zeta}_{u<}$, and $\Pi^{\zeta}_{u>}$ discussed in section 4.2. Clearly,

$$\Pi^{\zeta}_{u<}(k_0) = \sum_{k\leqslant k_0} \mathcal{F}_u(\mathbf{k}) = \Pi^{\zeta<}_{u<}(k_0) + \Pi^{\zeta>}_{u<}(k_0), \tag{136}$$

$$\Pi^{\zeta}_{u>}(k_0) = \sum_{k> k_0} \mathcal{F}_u(\mathbf{k}) = \Pi^{\zeta<}_{u>}(k_0) + \Pi^{\zeta>}_{u>}(k_0), \tag{137}$$

$$\Pi^{u}_{\zeta<}(k_0) = \sum_{k\leqslant k_0} \mathcal{F}_\zeta(\mathbf{k}) = \Pi^{u<}_{\zeta<}(k_0) + \Pi^{u>}_{\zeta<}(k_0), \tag{138}$$

$$\Pi^{u}_{\zeta>}(k_0) = \sum_{k\leqslant k_0} \mathcal{F}_\zeta(\mathbf{k}) = \Pi^{u<}_{\zeta>}(k_0) + \Pi^{u>}_{\zeta>}(k_0). \tag{139}$$

The identities of equations (72) and (73) are translated to the following identities for MHD turbulence:

$$\mathcal{F}_u = \Pi^{\zeta<}_{u<}(k) + \Pi^{\zeta<}_{u>}(k) + \Pi^{\zeta>}_{u<}(k) + \Pi^{\zeta>}_{u>}(k) = C_1, \tag{140}$$

$$\mathcal{F}_\zeta = \Pi^{u<}_{\zeta<}(k) + \Pi^{u<}_{\zeta>}(k) + \Pi^{u>}_{\zeta<}(k) + \Pi^{u>}_{\zeta>}(k) = C_2, \tag{141}$$

where C_1 and C_2 are constants. The above two sums are constant in k even though the individual flux in the sum can vary with k. Note that C_1 is the net energy transfer from $\boldsymbol{\zeta}$ to $\mathbf{u}$, while C_2 is the net energy transfer from $\mathbf{u}$ to $\boldsymbol{\zeta}$. Hence, $C_2 = -C_1$ due to the conservation of total energy. The above equality also follows because of the identity of equation (135). Interestingly, the vorticity field has similar properties as the magnetic field (with some important deviations) [141]. In section 9.1 we will describe various fluxes associated with the vorticity field.

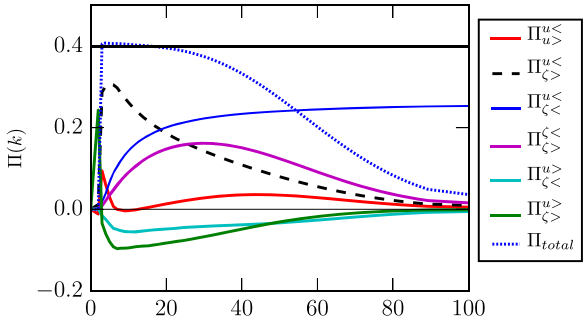

Figure 18. MHD turbulence: various energy fluxes associated with **u** and $\boldsymbol{\zeta}$ computed numerically. The total energy flux, $\Pi_{\rm tot}$, matches with the total energy injection rate of 0.4 in the inertial range ($k = (3, 20)$). But, all other fluxes vary in the inertial range itself. From Verma *et al*. Reproduced from [142]. CC BY 4.0.

Under a steady state with *no* external forcing for $\boldsymbol{\zeta}$, the net nonlinear energy transfer to the magnetic field, $\mathcal{F}_\zeta$, balances the magnetic diffusion or dissipation rate, ϵ_ζ. That is,

$$\mathcal{F}_\zeta = \sum_{\mathbf{k}} 2\eta k^2 E_\zeta(k) = \epsilon_\zeta > 0. \tag{142}$$

Note however that an imbalance in $\mathcal{F}_\zeta$ and ϵ_ζ makes the flow unsteady. For the velocity field, $\mathcal{F}_u = -\mathcal{F}_\zeta < 0$. In addition, the viscous force dissipates the kinetic energy. Hence, for the velocity field, a large-scale force, $\mathbf{F}_{\rm LS}$, is required to maintain a steady state. Using energy balance we obtain

$$\varepsilon_{\rm inj} + \mathcal{F}_u = \sum_{\mathbf{k}} 2\nu k^2 E_u(k) = \epsilon_u, \tag{143}$$

where $\varepsilon_{\rm inj}$ is the total energy injection rate by $\mathbf{F}_{\rm LS}$. In astrophysics, a supernova is an example of one such energy source. Note that under a steady state, the net energy injection rate by $\mathbf{F}_{\rm LS}$ equals the sum of viscous dissipation and Joule dissipation, i.e. $\varepsilon_{\rm inj} = \epsilon_u + \epsilon_\zeta$.

7.3. Variable energy flux in MHD turbulence

The energy fluxes of MHD turbulence vary with k due to cross transfers between **u** and $\boldsymbol{\zeta}$. Recently, Verma *et al* [142] simulated MHD turbulence and analyzed the variations of the above energy fluxes. They employed random forcing to the large-scale velocity modes in the wavenumber band $(2, 3)$. The total kinetic-energy injection rate was taken as 0.4. Their numerically-computed energy fluxes for the *steady state* are illustrated in figure 18. As shown in the figure, all the energy fluxes vary with k due to cross transfers between the u and $\boldsymbol{\zeta}$ [142]. For these reasons, the above fluxes are called *variable energy fluxes*.

However, the total energy flux, which equals the net energy transferred to the inertia-range modes of velocity and magnetic field, is constant. That is,

$$\begin{aligned}\varepsilon_{\rm inj} &= \Pi_u(k) + \Pi^{u<}_{\zeta}(k) = \Pi_u(k) + \Pi^{u<}_{\zeta<}(k) + \Pi^{u<}_{\zeta>}(k) \\ &= \Pi_u(k) + \Pi_\zeta(k) + \Pi^{\zeta<}_{u>}(k) + \Pi^{u<}_{\zeta>}(k) = \Pi_{\rm tot}(k) = \epsilon_u + \epsilon_\zeta.\end{aligned} \tag{144}$$

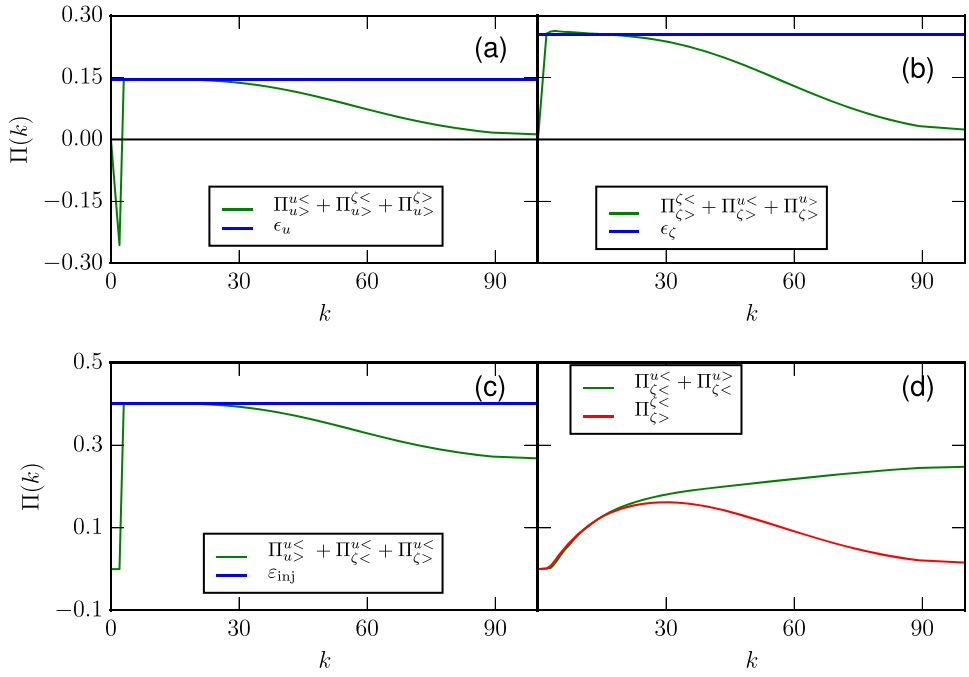

Figure 19. Numerical verification of the exact relations, equations (145)–(148). From Verma *et al*. Reproduced from [142]. CC BY 4.0.

Here, we employ the identity $\Pi^{u<}_{\zeta<} = \Pi_\zeta + \Pi^{\zeta<}_{u>}(k)$. Note however that the above relation does not hold for unsteady flows [6]. The other conserved quantity is $\mathcal{F}_u$.

When k is in the inertial range, an application of equations (136)–(139) to the identities of equations (75)–(78) leads to

$$\Pi_u(k) + \Pi^{\zeta<}_{u>}(k) + \Pi^{\zeta>}_{u>}(k) = \epsilon_u, \tag{145}$$

$$\Pi_\zeta(k) + \Pi^{u<}_{\zeta>}(k) + \Pi^{u>}_{\zeta>}(k) = \epsilon_\zeta, \tag{146}$$

$$\Pi_u(k) + \Pi^{u<}_{\zeta<}(k) + \Pi^{u<}_{\zeta>}(k) = \varepsilon_{\rm inj} \tag{147}$$

$$\Pi_\zeta(k) = \Pi^{u<}_{\zeta<}(k) + \Pi^{u>}_{\zeta<}(k). \tag{148}$$

As described in section 4, the above equations follow from energetics. Equation (145) (equation 146)) represent balance between the energy arriving at the inertial range of velocity (magnetic) field and the viscous (Joule) dissipation. On the other hand, equation (147) (equation (148)) represent balance between the energy arriving at the large-scale velocity (magnetic) field and the energy spreading out of this region. Verma *et al* [142] verified the above exact relations using numerical simulations. Figure 19 illustrates how the left- and right-hand sides of the exact relations match in the inertial range that extends from $k = 3$ to 20.

Equation (147) has important consequence on the dynamo action. Here, the velocity field is forced at large scales by $\mathbf{F}_{\rm LS}$. A part of the injected kinetic energy by $\mathbf{F}_{\rm LS}$ cascades to the inertial range as Π_u, but a fraction of it is transferred to the magnetic energy as $\Pi^{u<}_{\zeta}(k) > 0$ [25, 42–44]. This cross transfer from $\mathbf{u}$ to $\boldsymbol{\zeta}$ amplifies the magnetic field; this mechanism

is responsible for the generation of large-scale magnetic field in planets, stars, and galaxies [24, 25, 43, 143]. Note that this cross energy transfer in MHD turbulence makes the fluxes $\Pi_u(k)$, $\Pi^{u<}_{\zeta<}(k)$, and $\Pi^{u<}_{\zeta>}(k)$ functions of k, in contrast to constant $\Pi_u(k)$ in the inertial range of hydrodynamic turbulence. An important to note that the above relations do not hold for unsteady flows.

The cross energy transfer $\Pi^{u<}_{\zeta}(k)$ is also responsible for the drag reduction in MHD turbulence [48]. Since $\Pi^{u<}_{\zeta}(k) > 0$, using equation (147) we deduce that $\Pi_u(k) < \varepsilon_{\text{inj}}$. Note that in hydrodynamic turbulence, $\Pi_u(k) \approx \varepsilon_{\text{inj}}$. Therefore, for the same ε_{inj}, $\Pi_u(k)$ in MHD turbulence is lower than that for hydrodynamic turbulence. Therefore, the turbulent drag, $F_{\text{D}} \approx \Pi_u/U$, will be lower for MHD turbulence compared to its hydrodynamic counterpart [48]. In the next section we will show that a similar dynamics is a work in turbulent flows with dilute polymer. Thus, variable energy flux provides valuable insights into the dynamics of MHD turbulence and dynamo.

7.4. Energy fluxes associated with Elsäser variables

An alternative formulation of MHD turbulence is in terms of Elsäser variables, $\mathbf{z}^{\pm} = \mathbf{u} \pm \boldsymbol{\zeta}$. The MHD equations in terms $\mathbf{z}^{\pm}$ and a mean magnetic field $\mathbf{B}_0$ are [136, 138]

$$\frac{\partial \mathbf{z}^{\pm}}{\partial t} \mp (\mathbf{B}_0 \cdot \nabla)\mathbf{z}^{\pm} + (\mathbf{z}^{\mp} \cdot \nabla)\mathbf{z}^{\pm} = -\nabla p + \nu_+ \nabla^2 \mathbf{z}^{\pm} + \nu_- \nabla^2 \mathbf{z}^{\mp}, \tag{149}$$

$$\nabla \cdot \mathbf{z}^{\pm} = 0, \tag{150}$$

where $\nu_{\pm} = \frac{1}{2}(\nu \pm \eta)$. For $\mathbf{z}^{+}$, in a triad $(\mathbf{k}', \mathbf{p}, \mathbf{q})$, the mode-to-mode energy transfer from $\mathbf{z}^{+}(\mathbf{p})$ to $\mathbf{z}^{+}(\mathbf{k}')$ with the mediation of $\mathbf{z}^{-}(\mathbf{q})$ is [43]

$$S^{z^+ z^+}(\mathbf{k}'|\mathbf{p}|\mathbf{q}) = -\Im\left[\{\mathbf{k}' \cdot \mathbf{z}^{-}(\mathbf{q})\}\{\mathbf{z}^{+}(\mathbf{p}) \cdot \mathbf{z}^{+}(\mathbf{k}')\}\right]. \tag{151}$$

For $\mathbf{z}^{-}$, the mode-to-mode energy transfer from $\mathbf{z}^{-}(\mathbf{p})$ to $\mathbf{z}^{-}(\mathbf{k}')$ with the mediation of $\mathbf{z}^{+}(\mathbf{q})$ is

$$S^{z^- z^-}(\mathbf{k}'|\mathbf{p}|\mathbf{q}) = -\Im\left[\{\mathbf{k}' \cdot \mathbf{z}^{+}(\mathbf{q})\}\{\mathbf{z}^{-}(\mathbf{p}) \cdot \mathbf{z}^{-}(\mathbf{k}')\}\right]. \tag{152}$$

Note that there is no cross transfer from $\mathbf{z}^{+}$ to $\mathbf{z}^{-}$ and vice versa. The corresponding energy fluxes are

$$\Pi_{z^+}(k_0) = \sum_{\mathbf{p} \leqslant k_0} \sum_{k > k_0} S^{z^+ z^+}(\mathbf{k}|\mathbf{p}|\mathbf{q}), \tag{153}$$

$$\Pi_{z^-}(k_0) = \sum_{\mathbf{p} \leqslant k_0} \sum_{k > k_0} S^{z^- z^-}(\mathbf{k}|\mathbf{p}|\mathbf{q}). \tag{154}$$

Due to the absence of cross transfers between $\mathbf{z}^{+}$ and $\mathbf{z}^{-}$, $\Pi_{z^{\pm}}(k_0)$ are constant in the inertial range of MHD turbulence. In addition, in the inertial range, $\Pi_{z^{\pm}}(k) = \epsilon_{z^{\pm}}$, where $\epsilon_{z^{\pm}}$ are the total dissipation rates of $\mathbf{z}^{\pm}$. Figure 20 illustrates the constancy of $\Pi_{z^{\pm}}(k)$ in the inertial range [142]. In the inertial range, $\Pi_{z^+} = 0.5$ and $\Pi_{z^+} = 0.3$. In contrast, the energy fluxes associated with the velocity and magnetic fields are variable in the inertial range.

Note that total energy and cross helicity (Hc) are related to the energy spectra of the Elsässer variables as follows:

$$E = \frac{1}{2}(E_{z^+} + E_{z^-}); \qquad \text{Hc} = \frac{1}{4}(E_{z^+} - E_{z^-}). \tag{155}$$

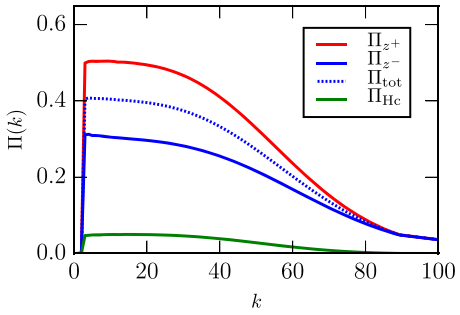

Figure 20. The energy fluxes $\Pi_{z^\pm}(k)$ computed numerically. $\Pi_{z^\pm}(k)$ are nearly constant in the inertial range ($k = (3, 20)$). The figure also shows the fluxes of total energy and cross helicity. From Verma *et al*. Reproduced from [142]. CC BY 4.0.

Hence, the fluxes of the total energy (Π) and cross helicity ($\Pi_{\rm Hc}$) can be deduced from $\Pi_{z^\pm}(k)$ as follows:

$$\Pi(k_0) = \frac{1}{2}[\Pi_{z^+}(k_0) + \Pi_{z^-}(k_0)] \tag{156}$$

$$\Pi_{\rm Hc}(k_0) = \frac{1}{4}[\Pi_{z^+}(k_0) - \Pi_{z^-}(k_0)]. \tag{157}$$

See figure 20 for illustration of these fluxes. In the inertial range, total energy and cross helicity fluxes are 0.4 and 0.05 respectively.

Constancy of $\Pi_{z^\pm}(k)$ in the inertial range makes them suitable candidates for modelling the energy spectrum of MHD turbulence. For example, Marsch [144] argued that

$$E_{z^\pm}(k) = K_{z^\pm}(k)\epsilon_{z^\pm}^{4/3}\epsilon_{z^\mp}^{-2/3}k^{-5/3}, \tag{158}$$

where $K_{z^\pm}(k)$ are nondimensional constants. The energy fluxes related to the velocity and magnetic fields vary with k, hence they are not quite appropriate for spectra modelling. Refer to Biskamp [138] and Verma [43] for further details. In the next subsection, we will study variable energy flux of quasi-static MHD turbulence.

7.5. Quasi-static MHD turbulence

In quasi-static (QS) MHD, which is applicable to liquid metals, the nonlinear term of the induction equation is ignored because RePm $\to 0$, where Pm is the magnetic Prandtl number [27, 28]. For such flows, under a strong mean magnetic field $\mathbf{B}_0$, the Lorentz force is approximated by the following expression [27, 28]:

$$\mathbf{F}_u(\mathbf{k}) = -[N(U/L)\cos^2\theta]\mathbf{u}(\mathbf{k}), \tag{159}$$

where θ is the angle between wavenumber $\mathbf{k}$ and $\mathbf{B}_0$; U, L are the large-scale velocity and length respectively; and $N = B_0^2 L/(U\kappa)$ is the interaction parameter with κ as the magnetic diffusivity.

The effects of the Lorentz force in QS MHD turbulence is an important topic of research. Laboratory experiments [145–149] and numerical simulations [150–153] of QS-MHD turbulence reveal that for small interaction parameters ($N \lessapprox 1$), the Lorentz force has a weak effect

on the flow, thus yielding a weak steepening of the energy spectrum from $k^{-5/3}$. However, for larger N, $E_u(k)$ steepens significantly with the spectral index approaching as low as -5 for $N \approx 30$ [146, 147]. For very large N, $E_u(k) \sim \exp(-bk)$ with b as a positive constant [28, 152].

Several models have been constructed to explain the steepening of the energy spectrum in QS MHD turbulence [26, 27, 29, 145, 147, 148, 154–156]. In particular, many researchers invoked two-dimensionalization of the flow to explain the steepened $E_u(k)$ [26, 148, 154, 155]. However, in the following discussion we present how variable energy flux can explain the steepening of the spectrum [28, 29, 156]. In QS-MHD turbulence, the energy injected by the Lorentz force gets converted to heat by the Joule dissipation $D_J(\mathbf{k})$ (see equation (159)) as shown below:

$$\mathcal{F}_u(\mathbf{k}) = \Re[\mathbf{F}_u(\mathbf{k}) \cdot \mathbf{u}^*(\mathbf{k})] = -[2N(U/L)\cos^2\theta]E_u(\mathbf{k}) = -D_J(\mathbf{k}). \tag{160}$$

In addition, the modal energy spectrum is not isotropic. However, the shell spectrum and energy flux, which is averaged over polar angle, obey the following equation [28, 156]:

$$\frac{\mathrm{d}}{\mathrm{d}k}\Pi_u(k) = -[2\nu k^2 + 2c_2 N(U/L)]E_u(k), \tag{161}$$

where c_2 is a constant.

Anas and Verma [29] solved equation (161) by making an assumption similar to that by Pao [35] for 3D hydrodynamic turbulence and derived the following formulas for the energy flux and spectrum. For $N \lessapprox 1$,

$$\log\left(\frac{\Pi_u(k)}{\Pi_u(k_0)}\right) = -\frac{3}{2}K_{\mathrm{Ko}}[(k/k_d)^{4/3} - (k_0/k_d)^{4/3}] + 3c_2 K_{\mathrm{Ko}}\left[(k/k_{d2})^{-2/3} - (k_0/k_{d2})^{-2/3}\right], \tag{162}$$

$$E_u(k) = K_{\mathrm{Ko}}\Pi_u(k)\epsilon^{-1/3}k^{-5/3}, \tag{163}$$

and for $N \gg 1$,

$$E_u(k) = A\ \exp(-k/\bar{k}_d), \tag{164}$$

$$\Pi_u(k) = A\left[2\nu\bar{k}_d(k^2 + 2k\bar{k}_d + 2\bar{k}_d^2) + 2(NU/L)c_2\bar{k}_d\right]\exp(-k/\bar{k}_d), \tag{165}$$

where $k_{d2}, A, \bar{k}_d$ are constants.

In figures 21 and 22, the energy flux and energy spectrum are plotted for $N = 0$, (b) $N = 0.1$, (c) $N = 0.5$, and (d) $N = 1.0$ [29]. The plots clearly demonstrate steepening of the energy flux and spectrum with the increase of N. Anas and Verma [29] also simulated the QSMHD turbulence for the above parameters. As shown in the figures, the model predictions are in general agreement with the numerical results. It has been also shown that the above formulas describe the experimental results quite well [28, 153]. Thus, variable energy flux helps describe the QS MHD turbulence quite well.

For strong magnetic field or large N, the flow is strong anisotropic. Reddy *et al* [152, 153] studied ring spectra, ring-to-ring energy transfers, as well as energy exchange between $\mathbf{u}_\perp$ and $u_\parallel$. For a strong mean magnetic field, using the formalism of section 5, Reddy *et al* [153] showed that $\mathcal{P}(k)$ of equation (92) is positive, and hence there is an energy transfer from $u_\perp$ to $u_\parallel$. In such flows, $u_\perp$ is stronger than $u_\parallel$. MHD turbulence exhibits a similar behaviour [157].

In the next section we will briefly describe the energy fluxes for a solvent with dilute polymers.

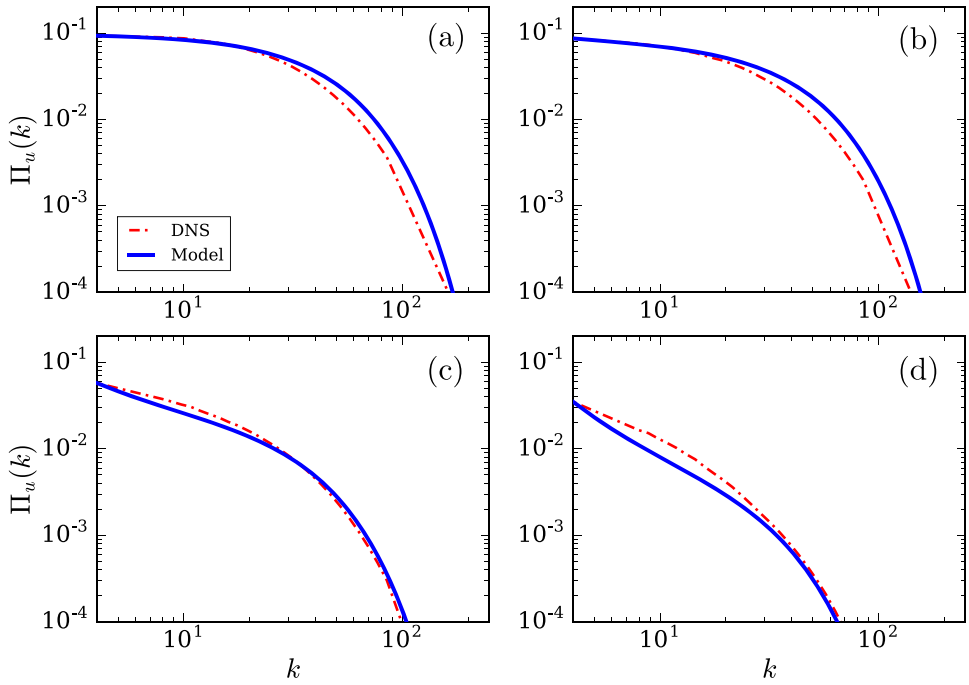

Figure 21. The energy spectra for QSMHD turbulence computed using equation (162) for (a) $N = 0$, (b) $N = 0.1$, (c) $N = 0.5$, and (d) $N = 1.0$. From Anas and Verma. Reprinted figure with permission from [29], Copyright (2019) by the American Physical Society.

8. Variable energy fluxes in a turbulent flow with dilute polymers

In this section, we discuss the energy transfers and drag reduction in a solution of dilute polymers [158–163]. In such flows, the polymer is often described by finitely extensible nonlinear elastic-Peterlin (FENE-P) model. The equations for the velocity field and polymer-conformation tensor ζ of FENE-P model are [164, 165]:

$$\frac{\partial u_i}{\partial t} + u_j \partial_j u_i = -\frac{1}{\rho}\partial_i p + \nu \partial_{jj} u_i + \frac{\mu}{\tau_p}\partial_j (f\zeta_{ij}) + F_{LS,i}, \tag{166}$$

$$\frac{\partial \zeta_{ij}}{\partial t} + u_l \partial_l \zeta_{ij} = \zeta_{il}\partial_l u_j + \zeta_{il}\partial_j u_l + \frac{1}{\tau_p}[f\zeta_{ij} - \delta_{ij}], \tag{167}$$

$$\partial_i u_i = 0, \tag{168}$$

where p is the pressure, ρ is the mean density of the solvent, ν is the kinematic viscosity, μ is an additional viscosity parameter, τ_p is the polymer relaxation time, and f is the renormalized Peterlin's function. We also remark that the energetics of polymer turbulence has many similarities with those for MHD turbulence. As we describe below, there is a preferential energy transfer from the velocity field to the polymer, just like the energy transfer from the velocity field to the magnetic field in dynamos. Refer to deGennes [45], Fouxon and Lebdev [164], and references therein for details.

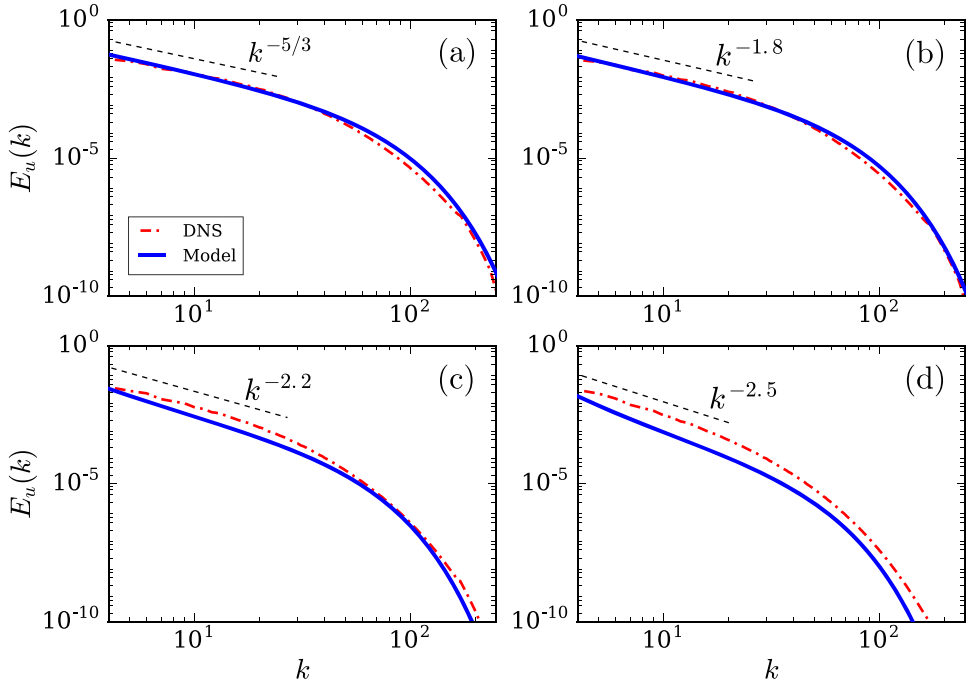

Figure 22. The energy spectra for QSMHD turbulence computed using equation (163) for (a) $N = 0$, (b) $N = 0.1$, (c) $N = 0.5$, and (d) $N = 1.0$. From Anas and Verma [29]. Reprinted with permission from APS.

In the above equations, the following forces (apart from constants) associated with $\mathbf{u}$ and ζ induce cross energy transfers:

$$F_{u,i} = \partial_j(f\zeta_{ij}), \qquad F_{\zeta,ij} = \zeta_{il}\partial_l u_j + \zeta_{il}\partial_j u_l. \tag{169}$$

In Fourier space, the respective energy feed by these forces to the kinetic energy and the tensor energy are

$$\mathcal{F}_u(\mathbf{k}) = -\sum_{\mathbf{p}} \Im\left[k_j f(\mathbf{q})\zeta_{ij}(\mathbf{p})u_i^*(\mathbf{k})\right], \tag{170}$$

$$\mathcal{F}_\zeta(\mathbf{k}) = -\sum_{\mathbf{p}} \Im\left[\zeta_{il}(\mathbf{q})\mathbf{p}_l u_j(\mathbf{p})\zeta_{ij}^*(\mathbf{k}) + \zeta_{il}(\mathbf{q})\mathbf{p}_j u_l(\mathbf{p})\zeta_{ij}^*(\mathbf{k})\right], \tag{171}$$

where $\mathbf{q} = \mathbf{k} - \mathbf{p}$. Both, $\mathcal{F}_u(\mathbf{k})$ and $\mathcal{F}_\zeta(\mathbf{k})$ are the convolutions similar to those in MHD turbulence. However, the structure of the nonlinear terms for the polymers is more complex than that for MHD turbulence. Till date, there are no formulas for the mode-to-mode energy transfers from $\mathbf{u}$ to ζ and vice versa. Yet, the following equations can be used to describe the energy fluxes from the velocity field to the polymer field.

$$\Pi^u_{\zeta<}(k_0) = \sum_{k\leqslant k_0} \mathcal{F}_\zeta(\mathbf{k}); \qquad \Pi^u_{\zeta>}(k_0) = \sum_{k>k_0} \mathcal{F}_\zeta(\mathbf{k}). \tag{172}$$

In fact, equations (75)–(78) too are applicable to the turbulent flows with dilute polymers.

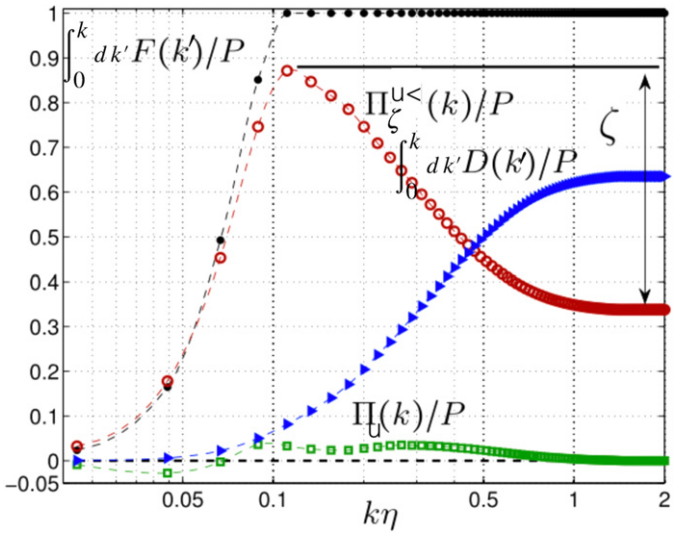

Figure 23. The energy fluxes, energy injected by external force, and dissipation rate computed by Valente *et al* for a polymeric flow. See equation (173). Here, P is the total energy injection by the external force. A fraction of injected energy is transferred to the polymers as $\Pi_\zeta^{u<}(k)$. From Valente *et al*. Reprinted from [47], with the permission of AIP Publishing.

From equation (77), under a steady state, for a wavenumber sphere of radius k,

$$\int_0^k \mathrm{d}k' \mathcal{F}_u(k') = \Pi_u(k) + \Pi_\zeta^{u<}(k) + \int_0^k \mathrm{d}k D_u(k'), \tag{173}$$

where the first term includes the energy injection rate by large-scale forcing to the modes of the sphere, while the last term is the total viscous dissipation inside the sphere. The flux $\Pi_\zeta^{u<}(k)$ is the energy transfer from the large-scale velocity field to ζ. See figure 15(a) for an illustration. Valente *et al* [47] simulated the equations for the dilute polymers and then computed the quantities of equation (173). For a generic parameter, these quantities are illustrated in figure 23. The quantities are normalized with relative to the kinetic energy injection rate by the external force, which is the maximum value of $\int_0^k \mathrm{d}k' \mathcal{F}_u(k')$. As shown in the figure, $\Pi_u \ll P$, where P is the total power injected by the external force. In the inertial range, the balance, $P - \Pi_u$, is transferred to the polymers as $\Pi_\zeta^{u<}$. For the full system, the injected energy by the external force is split between the viscous dissipation and $\Pi_\zeta^{u<}$. Note that the viscous term becomes significant in the dissipation range.

The aforementioned energetics of dilute polymers is very similar to that of MHD turbulence. In the inertial range of both the flows,

$$\Pi_\zeta^{u<}(k) > 0 \Rightarrow \Pi_u(k) < \varepsilon_{\mathrm{inj}}. \tag{174}$$

A physical interpretation of the above result is that in polymeric flows, the velocity field stretches the polymers [158, 159], similar to the stretching of the magnetic field in MHD turbulence and dynamo. Using equation (174) we deduce that for the same $\varepsilon_{\mathrm{inj}}$, the kinetic energy flux in the polymer solution will be reduced compared to hydrodynamic turbulence. Therefore, the turbulent drag, $F_{\mathrm{D}} \approx \Pi_u/U$, for a polymeric flow will be lower than its hydrodynamic

counterpart [48]. Thus, variable energy flux provides interesting insights into the mechanism of turbulent drag reduction in polymer solution and in MHD turbulence.

9. Variable enstrophy and helicity fluxes

In this section we focus on the enstrophy and kinetic-helicity fluxes of 3D hydrodynamics. Note that $\mathbf{F}_u = 0$ for pure hydrodynamics. However, we will retain the large-scale forcing ($\mathbf{F}_{\rm LS}$).

The vorticity field, $\boldsymbol{\omega} = \nabla \times \mathbf{u}$, plays an important role in hydrodynamic turbulence. The dynamical equation of $\boldsymbol{\omega}$ is [6, 8, 9]

$$\frac{\partial \boldsymbol{\omega}}{\partial t} = \nabla \times (\mathbf{u} \times \boldsymbol{\omega}) + \mathbf{F}_{\omega,\rm LS} + \nu \nabla^2 \boldsymbol{\omega}, \tag{175}$$

or

$$\frac{\partial \boldsymbol{\omega}}{\partial t} + (\mathbf{u} \cdot \nabla)\boldsymbol{\omega} = (\boldsymbol{\omega} \cdot \nabla)\mathbf{u} + \mathbf{F}_{\omega,\rm LS} + \nu \nabla^2 \boldsymbol{\omega}, \tag{176}$$

where $\mathbf{F}_{\omega,\rm LS} = \nabla \times \mathbf{F}_{\rm LS}$. The total enstrophy, $E_\omega = \frac{1}{2}\int \mathrm{d}\mathbf{r}\omega^2$, and the modal enstrophy, $E_\omega(\mathbf{k}) = \frac{1}{2}|\boldsymbol{\omega}(\mathbf{k})|^2$, are important quantities of hydrodynamics. The evolution equation for the latter is

$$\frac{\mathrm{d}}{\mathrm{d}t}E_\omega(\mathbf{k}) = \sum_{\mathbf{p}} \left\{ \Im \left[\{\mathbf{k} \cdot \mathbf{u}(\mathbf{q})\} \{\boldsymbol{\omega}(\mathbf{p}) \cdot \boldsymbol{\omega}^*(\mathbf{k})\} \right] - \Im \left[\{\mathbf{k} \cdot \boldsymbol{\omega}(\mathbf{q})\} \{\mathbf{u}(\mathbf{p}) \cdot \boldsymbol{\omega}^*(\mathbf{k})\} \right] \right\} + \mathcal{F}_{\omega,\rm LS}(\mathbf{k}) - 2\nu k^2 E_\omega(\mathbf{k}), \tag{177}$$

where

$$\mathcal{F}_{\omega,\rm LS}(\mathbf{k}) = \Re[\mathrm{i}\mathbf{k} \times \mathbf{F}_{u,\rm LS}(\mathbf{k}) \cdot \boldsymbol{\omega}^*(\mathbf{k})] = k^2 \Re[\mathbf{u}^*(\mathbf{k}) \cdot \mathbf{F}_{\rm LS}(\mathbf{k})] \tag{178}$$

is the enstrophy injection rate by $\mathbf{F}_{\rm LS}$. In equation (177), the first term in the right-hand-side represents the advection of the vorticity field by the velocity field, while the second term represents vortex stretching. For inviscid and force-free 3D hydrodynamics, E_ω is *not* conserved due to the vortex stretching by the velocity field [6, 8, 9]. Note however that E_ω is conserved in 2D hydrodynamics; this issue will be discussed in section 10.

9.1. Variable enstrophy flux

When we compare equation (176) with (52) for the secondary vector $\boldsymbol{\zeta}$, we obtain the following correspondence

$$\boldsymbol{\zeta} \to \boldsymbol{\omega}; \qquad \mathbf{F}_\zeta \to \mathbf{F}_\omega = (\boldsymbol{\omega} \cdot \nabla)\mathbf{u}, \tag{179}$$

and

$$\mathcal{F}_\omega(\mathbf{k}) = \sum_{\mathbf{p}} - \Im \left[\{\mathbf{k} \cdot \boldsymbol{\omega}(\mathbf{q})\} \{\mathbf{u}(\mathbf{p}) \cdot \boldsymbol{\omega}^*(\mathbf{k})\} \right]; \qquad \mathcal{F}_u(\mathbf{k}) = 0. \tag{180}$$

Here, $\mathcal{F}_\omega(\mathbf{k})$ induces enstrophy enhancement via vortex stretching by the velocity field. This process is similar to the magnetic field stretching by the velocity field in MHD turbulence (see section 7), first proposed by Batchelor [141].

The vorticity field does not appear explicitly in the NS equation. This is unlike the appearance of the magnetic field as $(\boldsymbol{\zeta} \cdot \nabla)\boldsymbol{\zeta}$ in the velocity equation of MHD (see equation (120)). Thus, the vorticity field does not back-react on the velocity field, unlike the back-reaction of

the magnetic field on the velocity field in MHD turbulence. Note however that vorticity plays an important role in the evolution of the velocity field, but energetically, it does not back-react on the velocity field. Such comparisons between the vorticity and magnetic fields were made by Batchelor [141] and others.

By making an analogy with MHD turbulence, we define the following enstrophy fluxes for a wavenumber sphere of radius k_0 (see section 7):

$$\Pi^u_{\omega<}(k_0) = \sum_{k\leqslant k_0} \mathcal{F}_\omega(\mathbf{k}); \qquad \Pi^u_{\omega>}(k_0) = \sum_{k>k_0} \mathcal{F}_\omega(\mathbf{k}). \tag{181}$$

Here, $\Pi^u_{\omega<}(k_0)$ ($\Pi^u_{\omega>}(k_0)$) represents the net enstrophy gain by the vorticity modes within (outside) the sphere due to the nonlinear interactions with the velocity modes. Following equation (73), we deduce that the net enstrophy enhancement rate due to the vortex stretching is

$$\Pi^u_{\omega<}(k) + \Pi^u_{\omega>}(k) = \mathcal{F}_\omega = \text{const.} \tag{182}$$

The sum in the above equation is independent of k even though its constituents, $\Pi^u_{\omega<}(k)$ and $\Pi^u_{\omega>}(k)$, may vary with k.

Since $\mathcal{F}_u(\mathbf{k}) = 0$ (no back reaction from the vorticity to the velocity field), both $\Pi^\omega_{u<}(k)$ and $\Pi^\omega_{u>}(k)$ are zeros. Hence, the vortex dynamics is similar to that of *kinematic dynamo* where the magnetic field does not back-react on the velocity field [24]. Note however that in MHD turbulence, the magnetic field back-reacts on the velocity field. Also note that the enstrophy and kinetic energy have different dimensions, unlike MHD where the kinetic energy and magnetic energy have dimension of energy.

The term $(\mathbf{u}\cdot\nabla)\boldsymbol{\omega}$ provides advection to the vorticity field, analogous to the advection of the secondary vector by the term $(\mathbf{u}\cdot\nabla)\boldsymbol{\zeta}$ (see section 4). Consequently, following equation (58), we define the mode-to-mode enstrophy transfer from $\boldsymbol{\omega}(\mathbf{p})$ to $\boldsymbol{\omega}(\mathbf{k}')$ with the mediation of $\mathbf{u}(\mathbf{q})$ as [14, 166]

$$S^{\omega\omega}(\mathbf{k}'|\mathbf{p}|\mathbf{q}) = -\Im\left[\{\mathbf{k}'\cdot\mathbf{u}(\mathbf{q})\}\{\boldsymbol{\omega}(\mathbf{p})\cdot\boldsymbol{\omega}(\mathbf{k}')\}\right]. \tag{183}$$

Hence, the enstrophy flux is (see equation (62))

$$\Pi_\omega(k_0) = \sum_{k'>k_0}\sum_{\mathbf{p}\leqslant k_0} S^{\omega\omega}(\mathbf{k}'|\mathbf{p}|\mathbf{q}). \tag{184}$$

Now, following equations (67) and (74), we deduce that during a steady state, in the inertial range,

$$\frac{\mathrm{d}}{\mathrm{d}k}\Pi_\omega(k) = \mathcal{F}_\omega(k) = -\frac{\mathrm{d}}{\mathrm{d}k}\Pi^u_{\omega>}(k) = \frac{\mathrm{d}}{\mathrm{d}k}\Pi^u_{\omega<}(k). \tag{185}$$

Therefore,

$$\Pi_\omega(k) + \Pi^u_{\omega>}(k) = C_3; \qquad \Pi_\omega(k) - \Pi^u_{\omega<}(k) = C_4, \tag{186}$$

where C_3, C_4 are constants. Since $\Pi^u_{\omega>}(k)$ and $\Pi^u_{\omega<}(k)$ are nonzero, we conclude that $\Pi_\omega(k)$ varies with k, unlike $\Pi_u(k)$ (of hydrodynamic turbulence), which is constant in the inertial range. The above arguments and equation (182) yields $C_3 - C_4 = \mathcal{F}_\omega$.

We derive several new formulas by making an analogy between the vorticity field and the magnetic field. For example, a comparison of vorticity dynamics with equations (130) and (131) yields the following formulas for the mode-to-mode enstrophy transfers:

$$S^{u\omega}(\mathbf{k}'|\mathbf{p}|\mathbf{q}) = 0, \tag{187}$$

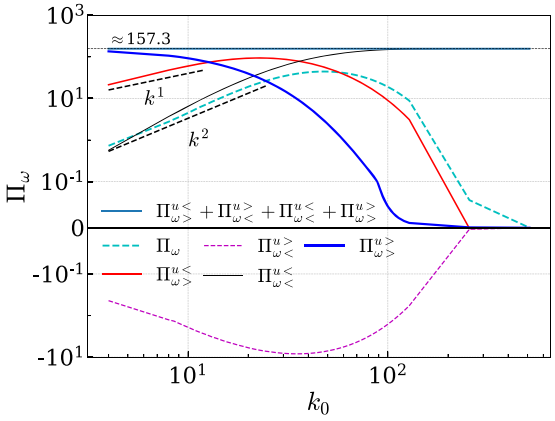

Figure 24. For the numerical simulations by Sadhukhan *et al*, plots of enstrophy fluxes and the conserved flux of equation (190). From Sadhukhan *et al*. Reprinted figure with permission from [166], Copyright (2019) by the American Physical Society.

$$S^{\omega u}(\mathbf{k}'|\mathbf{p}|\mathbf{q}) = \Im\left[\{\mathbf{k}'\cdot\boldsymbol{\omega}(\mathbf{q})\}\{\mathbf{u}(\mathbf{p})\cdot\boldsymbol{\omega}(\mathbf{k}')\}\right]. \tag{188}$$

Vanishing of $S^{u\omega}(\mathbf{k}'|\mathbf{p}|\mathbf{q})$ results from lack of explicit appearance of ω in the NS equation.

Based on the mode-to-mode enstrophy transfers, analogous to MHD fluxes, we can define four enstrophy fluxes: $\Pi^{u<}_{\omega<}$, $\Pi^{u<}_{\omega>}$, $\Pi^{u>}_{\omega<}$, $\Pi^{u>}_{\omega>}$. See figure 17 of section 7 for an illustration. Note that

$$\Pi^{u}_{\omega<}(k) = \Pi^{u<}_{\omega<}(k) + \Pi^{u>}_{\omega<}(k); \qquad \Pi^{u}_{\omega>}(k) = \Pi^{u<}_{\omega>}(k) + \Pi^{u>}_{\omega>}(k). \tag{189}$$

Substitutions of these relations in the identity of equation (182) yields the following relation [166]:

$$\Pi^{u<}_{\omega<}(k) + \Pi^{u>}_{\omega<}(k) + \Pi^{u<}_{\omega>}(k) + \Pi^{u>}_{\omega>}(k) = \mathcal{F}_\omega. \tag{190}$$

The above sum is constant in k (both in inertial and dissipation range), akin to equation (141) for MHD turbulence.

Sadhukhan *et al* [166] performed numerical simulations of hydrodynamic turbulence and computed the aforementioned enstrophy fluxes, as well as the conserved quantity of equation (190). These quantities are exhibited in figure 24. Note that the individual fluxes may vary with k due to cross transfers, but the sum of equation (190) is a constant. Interestingly, $\Pi_\omega(k) \sim k^2$ and $\Pi^{u<}_{\omega>}(k) \sim k$ for small and intermediate wavenumbers. Verma [14] argued that $\Pi_\omega(k) \sim k^2$ due to the term $\boldsymbol{\omega}(\mathbf{p})\cdot\boldsymbol{\omega}(\mathbf{k}')$ of $S^{\omega\omega}(\mathbf{k}'|\mathbf{p}|\mathbf{q})$. At small wavenumbers, $\Pi^{u>}_{\omega>}(k)$ is the most dominant among all the fluxes implying that the intermediate and small-scale vortices are stretched most significantly.

We summarise the similarities and dissimilarities between the vorticity field and magnetic field in table 2. A major difference between the two fields is the back-reaction on the velocity field—vorticity does not back-react, but magnetic field does. Hence, enstrophy dynamics is similar to that of kinematic dynamo where the magnetic field does not affect the velocity field. Note that enstrophy fluxes do not have a relation equivalent to the conservation of total energy flux in MHD turbulence (equation (144)).

In the next subsection, we will the describe variable kinetic-helicity flux.

Table 2. Similarities (first nine rows) and dissimilarities (last two rows) between the energy transfers in magnetic and vorticity fields.

Magnetic field	Vorticity
$S^{\zeta\zeta}$	$S^{\omega\omega}$
$S^{\zeta u}$	$S^{\omega u}$
Π_ζ	Π_ω
Π^u_ζ	Π^u_ω
Stretching of magnetic field lines	Vortex stretching
u-to-ζ transfer	u-to-ω transfer
Growth of magnetic field	Enhancement of enstrophy
ζ-to-ζ transfer (forward for nonhelical)	ω-to-ω transfer (forward)
No dynamo in 2D	No vortex stretching in 2D
$S^{u\zeta} \neq 0$	$S^{u\omega} = 0$
ζ-to-u transfer (back-reaction) except for kinematic dynamo where $S^{u\zeta} = 0$	No ω-to-u transfer (no back-reaction)

9.2. Flux of kinetic helicity

Kinetic helicity, which is defined as $H_K = \frac{1}{2}\int d\mathbf{r}(\mathbf{u}\cdot\boldsymbol{\omega})$, plays a major role in the growth of vorticity and magnetic fields [6, 9, 24]. Using equations (1) and (175) we can show that for $\nu = 0, \mathbf{F}_u = 0, \mathbf{F}_{LS} = 0$, and periodic or vanishing boundary condition, the total kinetic helicity is conserved in 3D hydrodynamics [6, 8, 9]; this is in addition to the conservation of total kinetic energy.

The evolution equation for the modal kinetic helicity, $H_K(\mathbf{k}) = \frac{1}{2}\Re[\mathbf{u}(\mathbf{k})\cdot\boldsymbol{\omega}^*(\mathbf{k})]$, is [6, 8, 9, 14]

$$\frac{d}{dt}H_K(\mathbf{k}) = \sum_{\mathbf{p}} \Re[\mathbf{u}(\mathbf{k}-\mathbf{p})\cdot\{\boldsymbol{\omega}(\mathbf{p})\times\boldsymbol{\omega}^*(\mathbf{k})\}] + \mathcal{F}_{H_K,LS}(\mathbf{k}) - 2\nu k^2 H_K(\mathbf{k}), \tag{191}$$

where $\mathcal{F}_{H_K,LS}(\mathbf{k}) = \Re[\boldsymbol{\omega}^*(\mathbf{k})\cdot\mathbf{F}_{LS}(\mathbf{k})]$ is the kinetic helicity injection rate by $\mathbf{F}_{LS}$. Based on equation (191), researchers have derived various formulas for the kinetic helicity flux. For example, Müller *et al* [167] argued that the kinetic flux is given by

$$\Pi_{H_K}(k_0) = \sum_{k>k_0}\{i\mathbf{k}\times[\mathbf{u}\times\boldsymbol{\omega}](\mathbf{k})\}\cdot\mathbf{u}^*(\mathbf{k}) + \text{c.c.}, \tag{192}$$

where c.c. stands for the complex conjugate. In the following discussion we will describe additional flux formulas for the kinetic helicity.

Following the structure of the nonlinear term of equation (191), Verma [14], Sadhukhan *et al* [166], and Plunian *et al* [168] showed that the mode-to-mode kinetic helicity transfer from wavenumber $\mathbf{p}$ to wavenumber $\mathbf{k}'$ with the mediation of wavenumber $\mathbf{q}$ is

$$S^{H_K}(\mathbf{k}'|\mathbf{p}|\mathbf{q}) = \Re[\mathbf{u}(\mathbf{q})\cdot\{\boldsymbol{\omega}(\mathbf{p})\times\boldsymbol{\omega}(\mathbf{k}')\}]. \tag{193}$$

In terms of $S^{H_K}(\mathbf{k}'|\mathbf{p}|\mathbf{q})$, the kinetic helicity flux for a wavenumber sphere of radius k_0 is

$$\Pi_{H_K}(k_0) = \sum_{\mathbf{p}\leqslant k_0}\sum_{k'>k_0} S^{H_K}(\mathbf{k}'|\mathbf{p}|\mathbf{q}). \tag{194}$$

Following the same lines of arguments as in section 3, we obtain

$$\frac{\mathrm{d}}{\mathrm{d}k}\Pi_{H_\mathrm{K}}(k) = \mathcal{F}_{H_\mathrm{K},\mathrm{LS}}(k) - D_{H_\mathrm{K}}(k), \tag{195}$$

where $D_{H_\mathrm{K}}(k) = 2\nu k^2 H_\mathrm{K}(k)$ is the dissipation rate of kinetic helicity in shell k, and $\mathcal{F}_{H_\mathrm{K},\mathrm{LS}}(k)$ is the kinetic helicity injection rate due to the force $\mathbf{F}_\mathrm{LS}$. In the inertial range, $\mathcal{F}_{H_\mathrm{K},\mathrm{LS}}(k) = 0$ and $D_{H_\mathrm{K}}(k) = 0$, hence $\Pi_{H_\mathrm{K}}(k) = \epsilon_{H_\mathrm{K}} =$ constant, where ϵ_{H_K} is the total dissipation rate of kinetic helicity. Note that kinetic helicity is conserved for inviscid and force-less hydrodynamics because $\mathcal{F}_{H_\mathrm{K}}(\mathbf{k}) = 0$ and $D_{H_\mathrm{K}}(\mathbf{k}) = 0$ for all $\mathbf{k}$, and that $\sum_\mathbf{k}\sum_\mathbf{p}\Re[\mathbf{u}(\mathbf{k}-\mathbf{p})\cdot\{\boldsymbol{\omega}(\mathbf{p})\times\boldsymbol{\omega}^*(\mathbf{k})\}]$ is identically zero (see equation (191)). On the other hand, in a turbulent flow, the kinetic helicity flux in the inertial range is constant because $\mathcal{F}_{H_\mathrm{K},\mathrm{LS}}(k) = 0$ and $D_{H_\mathrm{K}}(\mathbf{k}) = 0$ here. This is the connection between the conservation of kinetic helicity and its constancy in the inertial range. Note that kinetic helicity is not conserved in MHD because the Lorentz force induced a new term in the right-hand-side of equation (191). For the same reason, the kinetic helicity flux is not constant in the inertial range of MHD turbulence.

Using the constancy of $\Pi_{H_\mathrm{K}}(k)$, dimensional analysis and field-theoretic arguments, the following inertial-range spectrum for kinetic helicity has been derived [6, 169, 170]:

$$H_\mathrm{K}(k) = K_\mathrm{H}\epsilon_{H_\mathrm{K}}(\epsilon_u)^{-1/3}k^{-5/3}, \tag{196}$$

where K_H is a nondimensional constant, whose value has been estimated to be of the order of unity. The above scaling has been verified in many numerical simulations [6, 166, 171]. Interestingly, Sadhukhan *et al* [166] also modelled the kinetic helicity spectrum and flux in the inerital–dissipation range using a generalized Pao's model [35].

The helical turbulence is also described using Craya–Herring and helical basis [70, 116, 168, 172, 173]. In Craya–Herring basis [6, 10, 23, 116, 174, 175], the unit vectors for a wavenumber $\mathbf{k}$ are

$$\hat{\mathbf{e}}_3(\mathbf{k}) = \hat{\mathbf{k}}; \quad \hat{\mathbf{e}}_1(\mathbf{k}) = \frac{\hat{\mathbf{k}}\times\hat{\mathbf{n}}}{|\hat{\mathbf{k}}\times\hat{\mathbf{n}}|}; \quad \hat{\mathbf{e}}_2(\mathbf{k}) = \hat{\mathbf{e}}_3(\mathbf{k})\times\hat{\mathbf{e}}_1(\mathbf{k}), \tag{197}$$

where $\hat{\mathbf{k}}$ is the unit vector along wavenumber $\mathbf{k}$, and $\hat{\mathbf{n}}$ could be along any direction, but it is typically chosen along the anisotropy direction. We denote the velocity components along $\hat{\mathbf{e}}_1(\mathbf{k})$, $\hat{\mathbf{e}}_2(\mathbf{k})$, $\hat{\mathbf{e}}_3(\mathbf{k})$ as $u_1(\mathbf{k}), u_2(\mathbf{k}), u_3(\mathbf{k})$ respectively. Among them $u_3(\mathbf{k}) = 0$ due to incompressibility, hence $\mathbf{u}(\mathbf{k}) = u_1(\mathbf{k})\hat{\mathbf{e}}_1(\mathbf{k}) + u_2(\mathbf{k})\hat{\mathbf{e}}_2(\mathbf{k})$. In this basis, the mode-to-mode kinetic energy transfer from wavenumber $\mathbf{p}$ to wavenumber $\mathbf{k}$ with the mediation of wavenumber $\mathbf{q}$ is

$$S^{uu}(\mathbf{k}'|\mathbf{p}|\mathbf{q}) = S^{u_1u_1}(\mathbf{k}'|\mathbf{p}|\mathbf{q}) + S^{u_2u_2}(\mathbf{k}'|\mathbf{p}|\mathbf{q}), \tag{198}$$

where

$$S^{u_1u_1}(\mathbf{k}'|\mathbf{p}|\mathbf{q}) = k'\,\sin\,\bar{\beta}\,\cos\,\bar{\gamma}\Im\{u_1(\mathbf{q})u_1(\mathbf{p})u_1(\mathbf{k}')\}, \tag{199}$$

$$S^{u_2u_2}(\mathbf{k}'|\mathbf{p}|\mathbf{q}) = -k'\,\sin\,\bar{\beta}\Im\{u_1(\mathbf{q})u_2(\mathbf{p})u_2(\mathbf{k}')\}, \tag{200}$$

with $\bar{\alpha}, \bar{\beta}, \bar{\gamma}$ as the internal angles across k, p, q of the triangle formed by the wavenumbers $(\mathbf{k}', \mathbf{p}, \mathbf{q})$ [5, 14].

Another useful basis called *helical basis* [6, 10, 116] is constructed using the Craya–Herring vectors. In this basis, the unit vectors are

$$\hat{\mathbf{e}}_{s_k}(\mathbf{k}) = \frac{1}{\sqrt{2}}[\hat{\mathbf{e}}_2(\mathbf{k}) - \mathrm{i}s_k\hat{\mathbf{e}}_1(\mathbf{k})], \tag{201}$$

where s_k takes values $+1$ or -1. In terms of these unit vectors, the velocity field is $\mathbf{u}(\mathbf{k}) = u_+(\mathbf{k})\hat{e}_+(\mathbf{k}) + u_-(\mathbf{k})\hat{e}_-(\mathbf{k})$, where

$$u_{s_k}(\mathbf{k}) = \frac{1}{\sqrt{2}}[u_2(\mathbf{k}) + \mathrm{i}s_k u_1(\mathbf{k})]. \tag{202}$$

In the helical basis, the mode-to-mode kinetic energy transfer from $\mathbf{u(p)}$ to $\mathbf{u}(\mathbf{k}')$ with the mediation of $\mathbf{u(q)}$ is

$$S^{uu}(\mathbf{k}'|\mathbf{p}|\mathbf{q}) = \sum_{s_\mathbf{p}, s_{k'}} S^{uu}_{s_{k'}s_\mathbf{p}}(\mathbf{k}'|\mathbf{p}|\mathbf{q}), \tag{203}$$

where $S^{uu}_{s_{k'}s_\mathbf{p}}(\mathbf{k}'|\mathbf{p}|\mathbf{q})$, the kinetic energy transfer from mode $u_{s_\mathbf{p}}(\mathbf{p})$ to $u_{s_{k'}}(\mathbf{k}')$ with the mediation of $\mathbf{u(q)}$, is [14]

$$\begin{aligned} S^{uu}_{s_{k'}s_\mathbf{p}}(\mathbf{k}'|\mathbf{p}|\mathbf{q}) &= -\Im\left[\{\mathbf{k}'\cdot\mathbf{u}(\mathbf{q})\}u_{s_\mathbf{p}}(\mathbf{p})u_{s_{k'}}(\mathbf{k}')\{\hat{e}_{s_\mathbf{p}}(\mathbf{p})\cdot\hat{e}_{s_{k'}}(\mathbf{k}')\}\right] \\ &= -\frac{k'}{2}\,\sin\,\bar{\beta}(1 + s_\mathbf{p}s_{k'}\,\cos\,\bar{\gamma})\Im\{u_1(\mathbf{q})u_{s_\mathbf{p}}(\mathbf{p})u_{s_{k'}}(\mathbf{k}')\}. \end{aligned} \tag{204}$$

Similarly, the mode-to-mode kinetic helicity transfer from wavenumber $\mathbf{p}$ to wavenumber $\mathbf{k}'$ with the mediation of wavenumber $\mathbf{q}$ is [14]

$$S^{H_\mathrm{K}}(\mathbf{k}'|\mathbf{p}|\mathbf{q}) = \sum_{s_\mathbf{p}, s_{k'}} S^{H_\mathrm{K}}_{s_{k'}s_\mathbf{p}}(\mathbf{k}'|\mathbf{p},\mathbf{q}), \tag{205}$$

where $S^{H_\mathrm{K}}_{s_{k'}s_\mathbf{p}}(\mathbf{k}'|\mathbf{p},\mathbf{q})$, the elemental helicity transfer from $u_{s_\mathbf{p}}(\mathbf{p})$ to $u_{s_{k'}}(\mathbf{k}')$ with the mediation of $\mathbf{u(q)}$, is

$$\begin{aligned} S^{H_\mathrm{K}}_{s_{k'}s_\mathbf{p}}(\mathbf{k}'|\mathbf{p},\mathbf{q}) &= -\frac{1}{2}\mathbf{p}k'[s_{k'}\,\sin\,\bar{\beta} + s_\mathbf{p}\,\sin\,\bar{\alpha}]\Im\{u_1(\mathbf{q})u_{s_\mathbf{p}}(\mathbf{p})u_{s_{k'}}(\mathbf{k}')\} \\ &\quad + \frac{1}{2}\mathbf{p}k'\,\sin\,\bar{\gamma}\Re\{u_2(\mathbf{q})u_{s_\mathbf{p}}(\mathbf{p})u_{s_{k'}}(\mathbf{k}')\}. \end{aligned} \tag{206}$$

The kinetic energy flux from helical mode u_{s_g} to mode u_{s_r}, where s_g and s_r are the signs of giver and receiver modes respectively, can be written as

$$\Pi^{u_{s_\mathrm{g}}<}_{u_{s_\mathrm{r}}>}(k_0) = \sum_{\mathbf{p}\leqslant k_0}\sum_{k'>k_0} S^{uu}_{s_\mathrm{g}s_\mathrm{r}}(\mathbf{k}'|\mathbf{p}|\mathbf{q}). \tag{207}$$

The corresponding kinetic helicity flux is

$$\Pi^{H_\mathrm{K}s_\mathrm{g}}_{H_\mathrm{K}s_\mathrm{r}}(k_0) = \sum_{\mathbf{p}\leqslant k_0}\sum_{k'>k_0} S^{H_\mathrm{K}}_{s_\mathrm{r},s_\mathrm{g}}(\mathbf{k}'|\mathbf{p}|\mathbf{q}). \tag{208}$$

Alexakis and Biferale [70] and Sahoo *et al* [173] constructed another set of formulas for the energy flux, which is

$$\Pi^{s_1s_2s_3}_u = \left\langle \mathbf{u}^{<k}\cdot\mathcal{P}^{s_1}[\mathbf{u}^{s_2}\times\boldsymbol{\omega}^{s_3}]\right\rangle, \tag{209}$$

where s_i takes values ± 1 depending on the sign of kinetic helicity, and $\mathcal{P}^{s_1}$ represents projection along $\hat{\mathbf{e}}_{s_1}$. The above flux formula is related to equation (204).

As described earlier in this section, for large-scale external force, the energy and helicity spectra exhibit $k^{-5/3}$ spectra and constant fluxes [6, 8]. However, the energy transfers

become more complex when the external force is employed at intermediate scales, or when only homochiral modes (modes with same sign of kinetic helicity) are present. Biferale *et al* [176] showed that the nonlinear interactions among homochiral modes yield an inverse cascade of kinetic energy in 3D hydrodynamic turbulence. Sahoo *et al* [177] varied the strengths of different triadic interactions involving helical modes and observed a discontinuous transition from inverse energy cascade to forward energy cascade. Plunian *et al* [178] performed numerical simulations with realistic helical modes (rather than homochiral modes) and obtained similar results as Sahoo *et al* [177]. Thus, injection of kinetic helicity at intermediate scales affects the turbulence dynamics as well as kinetic energy spectrum and flux. Detailed discussions on these issues are beyond the scope of this review. For details, refer to references [70, 172, 173, 178–180].

We close this subsection with a comment that the secondary fields also induces kinetic helicity. For example, bouyancy and Lorentz force induce kinetic helicity. These topics, however, are too complex to be discussed here. Refer to the references [6, 10, 14, 116] for further details.

In the next section, we describe energy transfers and 2D and quasi-2D turbulence.

10. Brief review of variable energy fluxes in 2D and quasi-2D turbulence

In this section, we present a brief review of variable energy fluxes in 2D and in quasi-2D turbulence. The latter is observed in buoyancy-driven, rotating, and MHD turbulence. We start with a description of the energy and enstrophy fluxes of 2D hydrodynamic turbulence.

10.1. Fluxes of 2D hydrodynamic turbulence

For a 2D flow field $\mathbf{u} = u_x\hat{x} + u_y\hat{y}$, the vorticity field $\boldsymbol{\omega} = \omega\hat{z} = (\partial_x u_y - \partial_y u_x)\hat{z}$ is perpendicular to the plane of the flow. Hence, equation (176) yields the following evolution equation for 2D vorticity:

$$\frac{\partial\omega}{\partial t} + (\mathbf{u}\cdot\nabla)\omega = F_{\omega,\mathrm{LS}} + \nu\nabla^2\omega. \tag{210}$$

Note the absence of vortex stretching term in the above equation. For a 2D field, the total enstrophy, $E_\omega = \int \mathrm{d}\mathbf{r}\frac{1}{2}\omega^2$, is conserved [6, 8, 9], which is in addition to the conservation of total energy. Note that in 2D hydrodynamics, the total kinetic helicity vanishes identically because $\mathbf{u}$ and $\boldsymbol{\omega}$ are perpendicular to each other.

In 2D hydrodynamics, $\Pi^u_{\omega>}(k) = \Pi^u_{\omega<}(k) = 0$ due to the absence of $\boldsymbol{\omega}\cdot\nabla\mathbf{u}$ term in equation (210) (see section 9.1). Here, we assume that the external force supplies kinetic energy and enstrophy at large scales (see equation (178)). Following equation (186), we deduce that $\Pi_\omega(k)$ is constant in the inertial range, and it equals the enstrophy dissipation rate (ϵ_ω). This is in contrast to 3D hydrodynamic turbulence where $\Pi_\omega(k)$ varies with k due to the variability of $\Pi^u_{\omega<}(k)$ and $\Pi^u_{\omega>}(k)$. Kraichnan [181] showed that the above enstrophy flux yields $E_\omega(k) \sim \epsilon_\omega^{2/3}k^{-1}$ in the inertial-range. Note that $\Pi_u(k)$ is small in the inertial range with constant enstrophy flux [38, 70, 182]. The above picture is a part of Kraichnan [181]'s framework for 2D turbulence that will be described below.

Two-dimensional turbulence gets more complex when it is forced at an intermediate wavenumber k_f. Using conservation laws and field-theoretic tools, Kraichnan [181] constructed a phenomenology for such a scenario. In the inertial range of $k < k_f$ region, $\Pi_u(k) = -\epsilon_u$ and $E_u(k) = K_{2\mathrm{D}}\epsilon_u^{2/3}k^{-5/3}$, where ϵ_u is the magnitude of the kinetic energy flux, and $K_{2\mathrm{D}}$ is a constant whose numerical value is observed in the range 5.5 and 7.0. However, in the inertial range of $k > k_f$ regime, $\Pi_\omega(k) = \epsilon_\omega > 0$ and $E_u(k) = K'_{2\mathrm{D}}\epsilon_\omega^{2/3}k^{-3}$, where $K'_{2\mathrm{D}}$

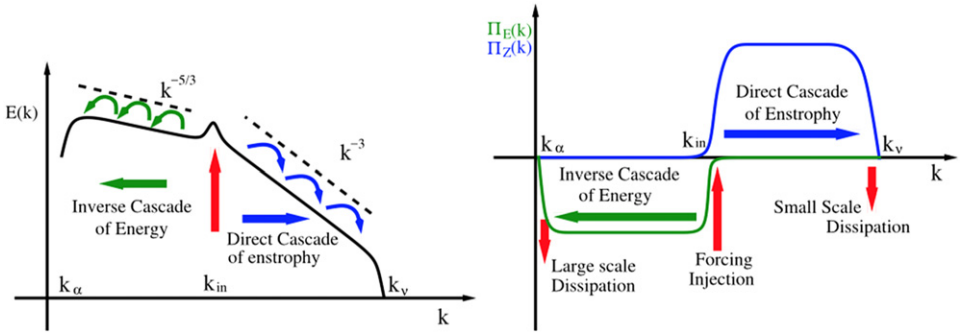

Figure 25. For 2D turbulence, (left panel) schematic illustrations of energy and entropy spectra; (right panel) energy and enstrophy fluxes. Note that $k_{\rm in} \equiv k_f$, $k_\nu \equiv k_d$, and $\Pi_Z(k) \equiv \Pi_\zeta(k)$. From Alexakis and Biferale. Reprinted from [70], Copyright (2018), with permission from Elsevier.

is another constant whose numerical value lies in the range of 1.3 and 1.7. See figure 25 for an illustration. The results of many experiments (see [183–186] and references therein) and numerical simulations (see [186, 187], and references therein) are consistent with the above predictions. We do not detail these results here.

Sharma *et al* [49] and Gupta *et al* [38] extended Kraichnan's phenomenology [181] beyond the inertial range by extrapolating Pao's model [35] to 2D turbulence. In the following we extend their calculations by including Ekman friction. For a steady state, away from the forcing band, the kinetic energy and enstrophy fluxes obey the following equations:

$$\frac{\mathrm{d}}{\mathrm{d}k}\Pi_u(k) = -2(\nu k^2 + \alpha)E_u(k), \tag{211}$$

$$\frac{\mathrm{d}}{\mathrm{d}k}\Pi_\omega(k) = -2(\nu k^2 + \alpha)E_\omega(k) = -2(\nu k^2 + \alpha)k^2 E_u(k). \tag{212}$$

For $k < k_f$, it is assumed that $E_u(k)/\Pi_u(k)$ depends only on the kinetic energy dissipation rate (ϵ_u) and k, but not on ν. Hence,

$$\frac{E_u(k)}{\Pi_u(k)} = -K_{2\rm D}\epsilon_u^{-1/3}k^{-5/3}, \tag{213}$$

where $\epsilon_u = -\Pi_u(k_0)$ with k_0 being a wavenumber near k_f. Substitution of the above in equation (211) and integration from k to k_0 yields

$$\Pi_u(k) = -\epsilon_u \exp\left(\frac{3}{2}K_{2\rm D}[(k/k_d)^{4/3} - (k_0/k_d)^{4/3}]\right) \times \exp\left(-\frac{3\alpha K_{2\rm D}}{\nu k_d^2}[(k_d/k)^{2/3} - (k_d/k_0)^{2/3}]\right), \tag{214}$$

$$E_u(k) = -K_{2\rm D}\Pi_u(k)\epsilon_u^{-1/3}k^{-5/3}, \tag{215}$$

where $k_d = (\epsilon_u/\nu^3)^{1/4}$ is Kolmogorov's wavenumber for 2D turbulence. Interestingly, $\Pi_u(k) \to 0$ as $k \to 0$ due to the Ekman friction. Substitution of the above $E_u(k)$ in equation (212) yields

the following enstrophy flux:

$$\Pi_\omega(k) = \Pi_\omega(k_0) + 2K_{2D}\epsilon_u^{1/3}\int_{k_0}^{k}(\nu k'^2 + \alpha)\Pi_u(k')k'^{1/3}\mathrm{d}k'. \tag{216}$$

Anas and Verma [29] derived the energy spectrum and flux for $k > k_f$ region. We reproduce their result here. For $k > k_f$, following Pao [35], it has been argued that $E_\omega(k)/\Pi_\omega(k)$ depends only on the enstrophy dissipation rate (ϵ_ω) and k, but not on ν. Hence,

$$\frac{E_\omega(k)}{\Pi_\omega(k)} = K'_{2D}\epsilon_\omega^{-1/3}k^{-1}. \tag{217}$$

Under this assumption, using equation (212) we obtain

$$\Pi_\omega(k) = \Pi_\omega(k_0)\left(\frac{k}{k_0}\right)^{-2\alpha K'_{2D}\epsilon_\omega^{-1/3}} \exp\left(-\frac{K'_{2D}}{k_{d2D}^2}(k^2 - k_0^2)\right), \tag{218}$$

where $k_{d2D} = \epsilon_\omega^{1/6}/\sqrt{\nu}$, and $\Pi_\omega(k_0)$ is the reference value of the enstrophy flux at $k = k_0$ [29, 34]. We choose $k_0 \approx k_f$ and $\Pi_\omega(k_f) \approx \epsilon_\omega$, where ϵ_ω is the enstrophy injection rate. Substitution of the above in the equations for variable flux yields

$$E_u(k) = K'_{2D}\epsilon_\omega^{2/3}k^{-3}\left(\frac{k}{k_0}\right)^{-2\alpha K'_{2D}\epsilon_\omega^{-1/3}} \exp\left(-\frac{K'_{2D}}{k_{d2D}^2}(k^2 - k_0^2)\right), \tag{219}$$

$$\Pi_u(k) = K'_{2D}\,\exp(x_0)\frac{\epsilon_\omega}{k_{d2D}^2}\int_x^\infty \frac{1}{x'}\left(1 + \frac{\beta}{x'}\right)\left(\frac{x'}{x_0}\right)^{-\beta} \exp(-x')\mathrm{d}x', \tag{220}$$

where $x = K'_{2D}(k/k_{d2D})^2$, $x_0 = K'_{2D}(k_0/k_{d2D})^2$, and $\beta = K'_{2D}\alpha/\nu k_{d2D}^2$. Note that $E_u(k)$ is steeper than k^{-3} due to the Ekman friction and the viscous dissipation. Asymptotically,

$$\frac{\Pi_u(k)}{\epsilon_\omega} \approx \frac{K'_{2D}}{k_{d2D}^2}E_1(K'_{2D}(k/k_{d2D})^2) \ll 1. \tag{221}$$

That is, $\Pi_u(k) \ll \epsilon_\omega$ for $k \gg k_f$, and $\Pi_u(k) \sim \log k$ for $\alpha = 0$.

The aforementioned scaling relations are consistent with the analytical results of Gotoh [182], numerical results of Gupta *et al* [38] and Anas and Verma [29], as well as the experimental results of Boffetta *et al* [33]. In particular, Boffetta *et al* [33] performed experiments on a thin layer of electrolyte solution with an electromagnetic driving for $\alpha = 0.037, 0.059$, and 0.069. As shown in figure 26, they observed an steepening of the energy spectra with the increase of α. Interestingly, as demonstrated by Anas and Verma [29], the above experimentally-observed energy spectra are described by equation (219) to a good accuracy. The differences between the model predictions and the experimental results are possibly due to bottleneck effects.

Thus, the above phenomenology describes how the viscous and Ekman dissipation steepens the 2D energy spectrum beyond the inertial range scaling. Variable energy flux formalism captures some of these features quite well.

10.2. Fluxes in quasi-2D turbulence

Strong rotation, gravity, magnetic field, and shear tend to make the flows quasi-2D with dominant velocity field perpendicular to the direction of the external field. Note that the above flows are stably stratified. However, unstable stratification, as in thermal convection, tends

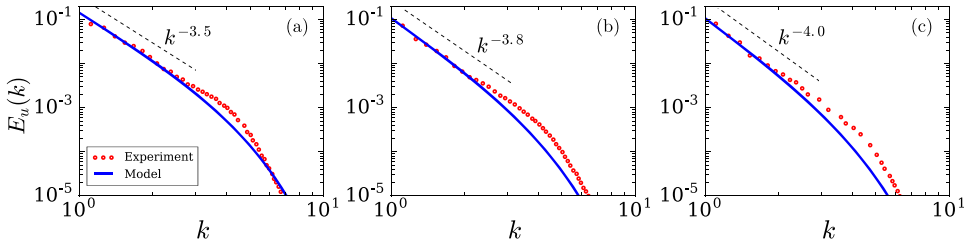

Figure 26. The energy spectra for 2D turbulence with Ekman friction with (a) $\alpha = 0.037$, (b) $\alpha = 0.059$, and (c) $\alpha = 0.069$. The experimental results of Boffetta *et al* [33] are shown as red dotted curves, while the model predictions of equation (219) are shown as solid blue curves. From Anas and Verma [29]. Reprinted figure with permission from [29], Copyright (2019) by the American Physical Society.

to strengthen the parallel component of the velocity field. In such flows, pressure facilitates energy exchange between the parallel and perpendicular components of the velocity fields (see section 5). In this subsection, we sketch some past work in this area without getting into complex details.

For fast rotation, researchers have reported strong two-dimensionalization of the flow [49, 188, 189]. Such flows contain strong vortical structures. They exhibit inverse energy cascade at small wavenumbers and forward energy cascade at large wavenumbers [49, 190]. Similar energy transfers and fluxes are observed in liquid-metal MHD turbulence under strong external magnetic field [26–28, 153, 191]. MHD turbulence too exhibits similar anisotropic behaviour under similar circumstances [157, 191–193]. In contrast, buoyancy destabilizes convective flows and generates plume structures; here, the velocity field parallel to buoyancy is stronger than the perpendicular component.

Boffetta *et al* [87] and Bartello [194] studied the energy fluxes of stably-stratified turbulence; they observed an inverse cascade of kinetic energy and a forward cascade of potential energy. They termed these forward and backward fluxes as a *flux-loop*. Kumar *et al* [124] simulated 2D stably-stratified turbulence and observed variety of flow patterns. Falkovich and Kristsuk [88] studied compressible turbulence and observed that planar structures and wave turbulence exhibit inverse and forward energy cascades respectively. In an another development, Biferale *et al* [195] showed how flows transform from 2D to quasi-2D turbulence when the helical modes are truncated.

In the above examples, variations of certain parameters lead to transition from 3D turbulence to quasi-2D turbulence. The control parameters for stably stratified turbulence and rotation are Richardson number and Rossby number respectively. Another way to make the above transition is by decreasing the height of the box. See Alexais *et al* [70, 196] for further discussion on this topic, which has been termed as *dimension transition*.

In all such flows, pressure plays an important role in the energy transfer between the parallel and perpendicular components. In addition, there are interesting works on 2D turbulence with buoyancy and MHD turbulence. However, these topics have been skipped in this review.

11. Variable energy flux in dissipationless turbulence

11.1. Hydrodynamic systems

An inviscid or dissipationless fluid flow is described using *Euler equation*, which is NS equation with $\nu = 0$. Euler turbulence exhibits either zero kinetic energy flux

[6, 12, 43, 60, 61, 70] or a combination of nonzero and zero fluxes [62]. Passive scalars turbulence and MHD turbulence without dissipation too exhibit similar properties. We describe these systems in the present section.

In the following discussion, we will focus on the properties of truncated Euler turbulence in which Fourier modes beyond certain wavenumber are absent. Kraichnan [61] and Lee [60] showed that the Liouville theorem is applicable to the phase space formed by the Fourier modes of truncated Euler turbulence. Based on the fact that Gibbs measure is invariant measures of systems satisfying Liouville's theorem (similar to that of equilibrium thermodynamics), and using conservation of kinetic energy and kinetic helicity, Kraichnan [61] and Lee [60] showed that $E_u(\mathbf{k})$ and $H_{\mathrm{K}}(\mathbf{k})$ are random variables with the following probability distribution:

$$P(E_u(\mathbf{k}), H_{\mathrm{K}}(\mathbf{k})) = \frac{1}{Z}\,\exp[-\beta E_u(\mathbf{k}) - \gamma H_{\mathrm{K}}(\mathbf{k})], \tag{222}$$

where $E_u(\mathbf{k})$ and $H_{\mathrm{K}}(\mathbf{k})$ are the modal kinetic energy and kinetic helicity respectively, and Z is a prefactor.

It is convenient to write down distribution functions for the helical energy spectra, $E_{u\pm}(\mathbf{k})$, where $u_\pm$ are the helical variables discussed in section 9.2 [14, 116]. These distribution functions are

$$P(E_{u_+}(\mathbf{k}), E_{u_-}(\mathbf{k})) = \beta_+\beta_-\,\exp[-\beta_+ E_{u_+}(\mathbf{k}) - \beta_- E_{u_-}(\mathbf{k})] \tag{223}$$

that lead to $\langle E_{u_\pm}(\mathbf{k})\rangle = 1/\beta_\pm$ (because $u_\pm$ are independent variables). Using a change of variable, $\beta_\pm = \beta \mp \gamma k$, we obtain [60, 61],

$$\langle E_u(\mathbf{k})\rangle = \left\langle E_{u_+}(\mathbf{k})\right\rangle + \langle E_{u_-}(\mathbf{k})\rangle = \frac{2\beta}{\beta^2 - \gamma^2 k^2}, \tag{224}$$

$$\langle H_{\mathrm{K}}(\mathbf{k})\rangle = k(\left\langle E_{u_+}(\mathbf{k})\right\rangle - \langle E_{u_-}(\mathbf{k})\rangle) = \frac{2\gamma k^2}{\beta^2 - \gamma^2 k^2}. \tag{225}$$

One-dimensional shell spectrum, $E_u(k)$, is a sum of the modes in a shell of radius k. Therefore, in 3D, $E_u(k)$ is proportional to k^2 for small and moderate k's, but it gets an upward bend for large k's [60, 61, 70]. The above forms of energy and kinetic helicity arise due to the conservation laws.

Detailed balance is an important property of systems under equilibrium. Consequently, under equilibrium, we expect no energy exchange among the Fourier modes and, hence, the energy flux $\Pi_u(k) = 0$ (see figure 27(a)). This observation is consistent with the fact that the phases of the Fourier modes of a turbulent flow are random [63] [1]. Contrast the above property with that of Kolmogorov's theory of turbulence where $\Pi_u(k) = C > 0$ and the phases of the

[1] The mode-to-mode energy transfer from mode **u(p)** to **u(k)** with the mediation of **u(q)** in Craya–Herring basis is (see section 9.2)

$$\begin{aligned}
\langle S^{u_1u_1}(\mathbf{k}|\mathbf{p}|\mathbf{q})\rangle &= k\,\sin\bar{\beta}\,\cos\bar{\gamma}\,\langle\Im[u_1(\mathbf{p})u_1(\mathbf{q})u_1^*(\mathbf{k})]\rangle\\
&= k\,\sin\bar{\beta}\,\cos\bar{\gamma}\,\langle|u_1(\mathbf{p})u_1(\mathbf{q})u_1^*(\mathbf{k})|\,\sin(\phi_{1\mathbf{p}} + \phi_{1q} - \phi_{1k})\rangle\,,\\
\langle S^{u_2u_2}(\mathbf{k}|\mathbf{p}|\mathbf{q})\rangle &= -k\,\sin\bar{\beta}\,\langle\Im[u_1(\mathbf{p})u_2(\mathbf{q})u_2^*(\mathbf{k})]\rangle\\
&= -k\,\sin\bar{\beta}\,\langle|u_1(\mathbf{p})u_2(\mathbf{q})u_2^*(\mathbf{k})|\,\sin(\phi_{2\mathbf{p}} + \phi_{1q} - \phi_{2k})\rangle\,,
\end{aligned}$$

where ϕ_{1k} and ϕ_{2k} are the phases of modes $u_1(\mathbf{k})$ and $u_2(\mathbf{k})$ respectively. These energy transfers become zero for random phases.

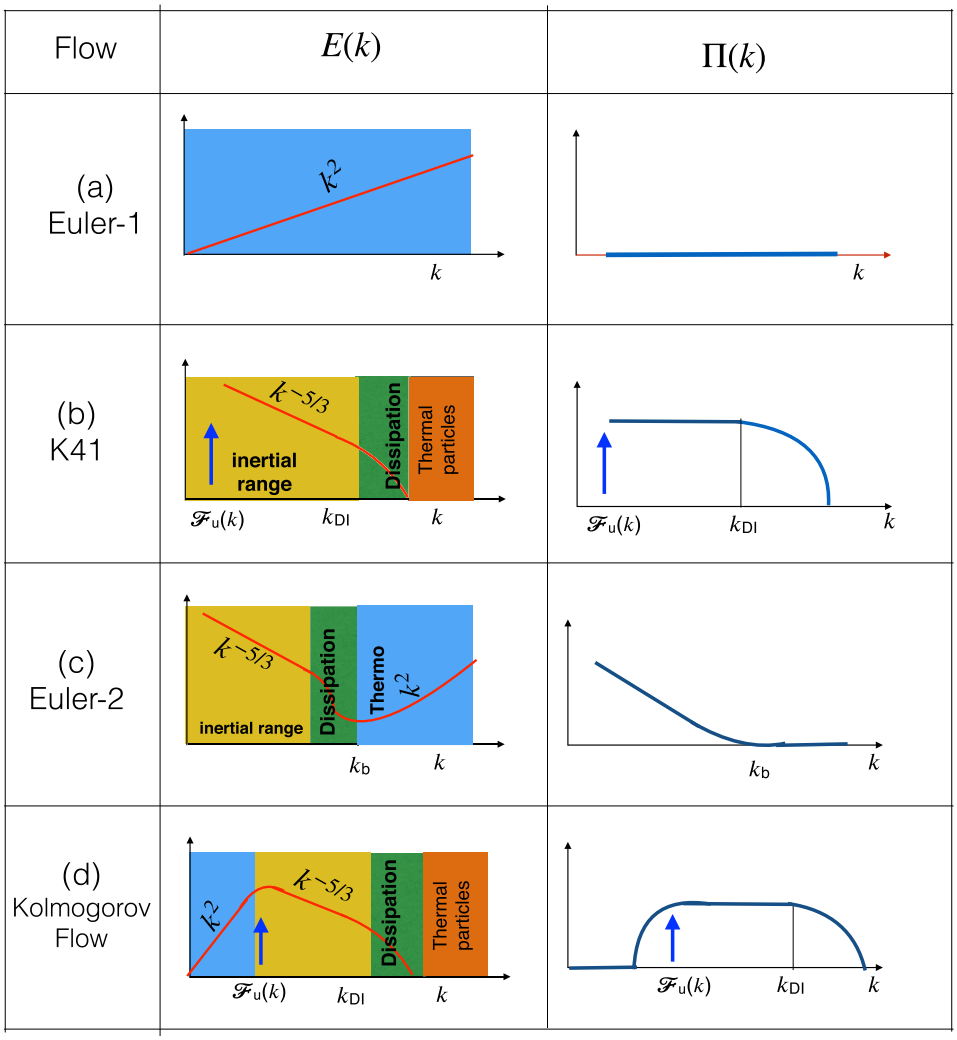

Figure 27. Schematic energy spectra and fluxes for various flows: (a) Euler-1: unforced Euler turbulence exhibiting k^2 for delta-correlated noise as an initial condition. (b) K41: turbulent flow of Kolmogorov model. Such flows with small viscosity are forced at large scales. (c) Euler-2: unforced Euler turbulence with large-scale Taylor–Green vortices as an initial condition. (d) Kolmogorov-flow: a flow that is forced at an intermediate scale. The yellow, green, and blue colours represent inertial, dissipative, and equilibrium ranges respectively. The orange colour represents the thermal or microscopic scales where particles move randomly.

Fourier modes are correlated (see figure 27(b)). Hence, the phase space for flows satisfying Kolmogorov's theory is not expected to be ergodic.

A number of numerical simulations have been performed to verify the equilibrium spectra of equations (224) and (225). Cichowlas *et al* [62] were the first to simulate Euler turbulence with large-scale Taylor–Green vortices as initial condition. They observed a combination of Kolmogorov's $k^{-5/3}$ spectrum in the intermediate range and k^2 spectrum in the dissipative range, as shown in figure 27(c). Over time, the $k^{-5/3}$ regime shrinks at the expense of k^2 regime.

Asymptotically, at large times, the whole range of spectrum is expected to become k^2, consistent with the predictions of Lee [60] and Kraichnan [61]. This is the process of *thermalization* [62, 68, 197]. Recently, Verma *et al* [63, 64] simulated Euler turbulence using white noise as an initial condition and observed k^2 spectrum throughout the duration of the simulation.

Note that the energy flux vanished identically for k^2 spectrum, in line with the arguments of Lee [60] and Kraichnan [61]. However, as transient, the energy flux is nonzero for the $k^{-5/3}$ regime due to the energy cascade from the large-scale structures to the intermediate scales. The asymptotic state of Cichowlas *et al* [62] exhibits k^2 spectrum and zero energy flux, which is the property of equilibrium state.

Connaughton and Nazarenko [198] started with Leith's equation and constructed a mixture of constant-flux Kolmogorov solution and flux-less thermodynamic solution, which is also called *warm cascade*. Numerical solution of Leith's equation with appropriate constants yielded the above mixed solution (a mixture of $k^{-5/3}$ and k^2 spectra), which is similar to the numerical solution of Cichowlas *et al* [62]. Shukla *et al* [199] also worked on a similar theme; they simulated time-reversible NS equation and tuned the solutions using a nondimensional control parameter $R_\tau = f_0 l_f / E_0$, where f_0 is the forcing amplitude, l_f is the energy injection length scale, and E_0 is the total energy. In Shukla *et al* [199]'s simulations, warm solution ($E_u(k) \sim k^2$) was obtained for small values of the control parameter, but Kolmogorov's cascade was observed for large values of the control parameter.

Kolmogorov flow, which is forced at intermediate length scales ($k \approx k_f$), also exhibits equilibrium behaviour for $k \leqslant k_f$. For such flows, Prasath *et al* [200], Dallas *et al* [201], and Alexakis and Biferale [70] showed that $E_u(k) \sim k^2$ and $\Pi_u(k) \approx 0$ for $k < k_f$, and $E_u(k) \sim k^{-5/3}$ and $\Pi_u(k) \approx$ const. > 0 for $k > k_f$. These authors argue that the modes in $k < k_f$ regime are in absolute equilibrium. See figure 27(d) for an illustration. Note that in Kolmogorov flow, the large scales, rather than small scales, are in equilibrium. This is in contrast to flows corresponding to K41 and Euler-2 of figure 27 where the modes at small scales are in equilibrium. Recently, Alexakis and Brachet [202] showed that the nature of forcing can strongly affect the behaviour of the large scales. They observed that spectrally dense forcing with long correlation times may yield spectrum different from the k^2 energy spectrum, while forcing with short correlated time scale is likely to reproduce the thermal spectrum.

Thus, Euler turbulence provides valuable insights into the thermalization process, which is an important area of research in quantum and classical physics. In Euler-2 and K41 flows, the energy at large scales cascades to intermediate and dissipation ranges. The energy flux of the dissipative scale is transferred to the thermal energy of the particles, who move randomly. In Euler-2 flow, thermal energy of the particles appear as k^2 spectrum, but thermal spectrum is not present in the K41 flow. We present various regimes in figure 27 using different colours. The yellow, green, and blue colours represent the inertial, dissipative, and equilibrium regimes respectively, while the orange colour represents the thermodynamic regime or microscopic scales where the particles are in equilibrium. Interestingly, $E_u(k)$ of Cichowlas *et al* [62] exhibits a small exponential transition regime (similar to that of hydrodynamic turbulence) between the $k^{-5/3}$ and k^2 regimes.

Based on these examples, it has been argued that in 3D hydrodynamics, thermalization occurs via a multiscale energy transfer from large and intermediate scales (noequilibrium) to small scales (equilibrium). Here, the coherent fluid energy of inertial-dissipative regime is converted to the thermal energy of constituents molecules. This mechanism provides a scenario for the emergence of friction or dissipation in generic systems, including Hamiltonian and quantum systems [203].

The above formalism for Euler turbulence has been extended to secondary fields advected by the velocity field. For diffusionless passive scalar turbulence, conservation of $\sum_{\mathbf{k}} E_\zeta(\mathbf{k})$

leads to the following distribution for $E_\zeta(\mathbf{k})$:

$$P(E_\zeta(\mathbf{k})) = \beta_\zeta \exp[-\beta_\zeta E_\zeta(\mathbf{k})] \tag{226}$$

that leads to $\langle E_\zeta(\mathbf{k})\rangle = 1/\beta_\zeta$ [6, 8]. The formulas for inviscid MHD turbulence are more complex due the conservation of total energy, cross helicity, and magnetic helicity. The reader is referred to the original papers by Frisch *et al* [65] and Stribling *et al* [66]. For these systems too, the equilibrium spectra and fluxes are easier to obtain using white noise as an initial condition. Burgers turbulence too exhibits similar properties during thermalization [204].

The energy flux vanishes in the equilibrium regime of hydrodynamic turbulence. It is important to contrast this effect from the suppression of the net energy flux by two opposite fluxes, as observed in quasi-2D stably stratified turbulence [87] and in compressible turbulence [88]. In the latter systems, the detailed balance of energy transfers is broken by opposing energy fluxes, called *flux loops*.

In addition to Euler turbulence and other dissipationless turbulent systems, many energy-conserving nonequilibrium systems exhibit strong fluctuations or turbulence, which will be described below.

11.2. Thermalization in miscellaneous dissipationless systems

In this section, we describe some generic properties of thermalization in Hamiltonian systems and dissipationless partial differential equations. But, first we discuss the dynamics of dissipationless Burgers equation.

For a wave (e.g. $\sin(x)$) as an initial condition, one-dimensional dissipative Burgers equation yields shocks [205]. Such flows exhibit k^{-2} spectrum followed by a dissipative spectrum [206]. In contrast, Frisch *et al* [69] and Ray *et al* [204] studied thermalization of Burgers equation by employing a minimal dissipation with small viscosity or hyperviscosity. In these works, they report a mixed spectrum: k^{-2} for intermediate wavenumbers (nonequilibrium regime) and k^0 for large wavenumbers (equilibrium regime), similar to the findings of Cichowlas *et al* [62] for Euler turbulence. Note however that a random initial condition yields an equilibrium state with $E(k) \sim k^0$ and zero energy flux throughout the wavenumber range.

For more than half a century, researchers have been studying thermalization in Fermi–Pasta–Ulam–Tsingou model [207]. In this model, the energy cascades to higher modes when a large-scale excitation is chosen as an initial condition. The system eventually reaches a state where the energy is equipartitioned among all the Fourier modes. However, after some time, the system returns to the initial configuration, consistent with Poincaré recurrence theorem [208–210]. On the contrary, for random initial condition, the system reaches an equilibrium state with energy equipartitioned among all Fourier modes [209, 210]. This observation again demonstrates how random initial condition aids in taking a dynamical system towards thermalization. Similar behaviour has been observed for the KdV equation, which is related to the Fermi–Pasta–Ulam–Tsingou model [210].

Thermalization processes in quantum systems, such as Bose–Einstein condensate and superfluids, are more complex [67, 197]. Still, these systems have certain similarities with Euler turbulence and other related systems. Thus, Euler turbulence provides valuable insights into the thermalization process. More work is being carried to address the following questions among others: Do Euler turbulence and related turbulent systems become ergodic under thermalization? What are the consequences of Poincaré recurrence theorem on thermalization? In Euler turbulence with Taylor–Green vortex as an initial condition [62], would the system return to the initial configuration after thermalization.

In the next section, we describe the properties of energy flux in quantum turbulence and in binary-mixture turbulence.

12. Variable energy flux in quantum turbulence and binary-mixtures turbulence

Bose–Einstein condensates and superfluids, which are quantum systems, exhibit turbulent behaviour for some set of parameters [53, 211–213]. Binary-mixtures too become turbulent for some parameters. As we show below, variable energy flux formulation sheds important light into these complex systems.

12.1. Quantum turbulence

To describe quantum systems, we often employ macroscopic wavefunction $\zeta(x,t) = \sqrt{n}$ exp(iS), where n is the number density of atoms and S is the phase. The time evolution of the wavefunction $\zeta(x,t)$ is described using Gross–Pitaevskii (GP) equation [53, 55, 211, 213]:

$$\mathrm{i}\hbar\frac{\partial\zeta}{\partial t} = \left[-\frac{\hbar^2}{2m}\nabla^2 + V(\mathbf{r}) + g|\zeta|^2\right]\zeta, \tag{227}$$

where m is the mass of the quantum particle, $V(\mathbf{r})$ is the external potential, and g is the proportionality constant for the interaction term. The GP equation exhibits many interesting features, including entangled quantum vortices, Kelvin waves, etc. However, in this subsection we focus on the energy fluxes of quantum turbulence.

The velocity of a superfluid flow is given by the gradient of its wavefunction, that is, $\mathbf{u}_\mathrm{s} = (\hbar/m)\nabla S$. In terms of the number density, n, and $\mathbf{u}_\mathrm{s}$, the real and imaginary parts of the GP equation are [55]

$$\frac{\partial n}{\partial t} + \nabla(n\mathbf{u}_\mathrm{s}) = 0, \tag{228}$$

$$\frac{\partial\mathbf{u}_\mathrm{s}}{\partial t} + (\mathbf{u}_\mathbf{s}\cdot\nabla)\mathbf{u}_\mathbf{s} = -\frac{1}{mn}\nabla p - \frac{1}{m}\nabla\left(\frac{\hbar^2}{2m\sqrt{n}}\nabla^2\sqrt{n}\right) - \frac{1}{m}\nabla V. \tag{229}$$

Note that $mn = \rho_\mathrm{s}$ is the density of the superfluid. In helium-4, the superfluid component coexists with the normal fluid, whose velocity field is denoted by $\mathbf{u}_\mathrm{n}$. The equations for the superfluid and normal-fluid components are [50, 51]

$$\frac{\partial\mathbf{u}_\mathrm{s}}{\partial t} + (\mathbf{u}_\mathrm{s}\cdot\nabla)\mathbf{u}_\mathrm{s} = -\frac{1}{\rho_\mathrm{s}}\nabla p_\mathrm{s} - \frac{\rho_\mathrm{s}}{\rho}\mathbf{F}_{ns}, \tag{230}$$

$$\frac{\partial\mathbf{u}_\mathrm{n}}{\partial t} + (\mathbf{u}_\mathrm{n}\cdot\nabla)\mathbf{u}_\mathrm{n} = -\frac{1}{\rho_\mathrm{n}}\nabla p_\mathrm{n} + \frac{\rho_\mathrm{n}}{\rho}\mathbf{F}_{ns} + \mathbf{F}_\mathrm{LS} + \nu\nabla^2\mathbf{u}_\mathrm{n}, \tag{231}$$

where ρ_n is the density of the normal fluid, $\rho = \rho_\mathrm{s} + \rho_\mathrm{n}$ is the total density of the fluid, $\mathbf{F}_\mathrm{LS}$ is the large-scale force applied to the normal fluid, and $\mathbf{F}_\mathrm{ns} = (B/2)|\boldsymbol{\omega}|(\mathbf{u}_\mathrm{s} - \mathbf{u}_\mathrm{n})$ is the mutual friction. Here $\boldsymbol{\omega}$ is the superfluid vorticity, and B is a constant. Note that $p_\mathrm{n} = (\rho_\mathrm{n}/\rho)p + \rho_\mathrm{s}ST$ and $p_\mathrm{s} = (\rho_\mathrm{s}/\rho)p - \rho_\mathrm{s}ST$ are partial pressures with S, T, p as the specific entropy, temperature, and pressure respectively. Also, the relative density $\rho_\mathrm{n}/\rho_\mathrm{s}$ increases with temperature, and helium-4 becomes a normal fluid beyond the critical temperature of 2.17 K. In the following discussion, for simplification, the fluid densities are assumed to be constant.

Researchers have studied superfluid turbulence using experiments and numerical simulations ([53, 55, 211–213] and references therein). These works show that both superfluid

and normal fluid exhibit Kolmogorov-like $k^{-5/3}$ spectra and nearly constant energy fluxes [53, 211–213]. At very low temperatures, $\rho_n \approx 0$, which is observed in helium-3; for such flows, vortex reconnections and phonon coupling at small scales provide the necessary dissipation to sustain the $k^{-5/3}$ spectrum. Also refer to Arnol *et al* [214] for a recent work on energy flux in trapped Bose–Einstein condensate.

In the following discussion, we briefly look at the variable energy flux in quantum turbulence. In the turbulent regime, the nonlinear terms of the above equations, $(\mathbf{u}_s \cdot \nabla)\mathbf{u}_s$ and $(\mathbf{u}_n \cdot \nabla)\mathbf{u}_n$, induce the respective energy cascades $\Pi_{u,s}(k)$ and $\Pi_{u,n}(k)$ for the two components. These energy fluxes are affected by the mutual friction. The energy injection rates by $\mathbf{F}_{ns}$ to the normal and superfluid components are (see section 3)

$$\mathcal{F}_{u,s}(\mathbf{k}) = -\frac{\rho_s}{\rho}\Re[\mathbf{F}_{ns}(\mathbf{k}) \cdot \mathbf{u}_s^*(\mathbf{k})]; \qquad \mathcal{F}_{u,n}(\mathbf{k}) = \frac{\rho_n}{\rho}\Re[\mathbf{F}_{ns}(\mathbf{k}) \cdot \mathbf{u}_n^*(\mathbf{k})]. \tag{232}$$

Therefore, the energy fluxes for the two fluids vary with k as

$$\frac{\mathrm{d}}{\mathrm{d}k}\Pi_{u,s}(k) = \mathcal{F}_{u,s}(k); \qquad \frac{\mathrm{d}}{\mathrm{d}k}\Pi_{u,n}(k) = \mathcal{F}_{u,n}(k) - 2\nu k^2 E_n(k), \tag{233}$$

where $2\nu k^2 E_n(k)$ is the dissipation rate for the normal fluid. Roche *et al* [51] and Wacks and Barenghi [52] analyzed the above energy transfers using numerical simulations and observed that $\mathcal{F}_{u,s} < 0$ and $\mathcal{F}_{u,n} > 0$. Note however that these quantities depend on the temperature or ρ_s/ρ_n. Based on these observations, we expected that $\Pi_{u,n}$ and $\Pi_{u,s}$ vary with k. These variations can induce additional k dependence in the energy spectra over Kolmogorov's $k^{-5/3}$ spectrum. These predictions need further examination using experiments and numerical simulations.

Quantum systems are energy conserving. However, sustenance of $k^{-5/3}$ spectrum requires dissipation at small scales. It has been argued that the compressible waves produced during vortex reconnections may provide the required dissipation [53, 203, 211–213]. These issues, as well as the energy spectrum and fluxes of GP equations, have been studied using numerical simulations and experiments [53, 54, 67, 199, 211–213].

For quantum turbulence, the energy fluxes have not been studied widely. We believe that careful analysis of the fluxes will be useful for understanding quantum turbulence.

12.2. Variable energy fluxes in binary-mixture turbulence

In this section, we briefly describe the energy fluxes of binary fluid mixtures [215–218]. We consider a binary mixture with two components whose relative densities are $\zeta(\mathbf{r})$ and $1 - \zeta(\mathbf{r})$. Researchers describe the dynamics of these fields using *time-dependent Ginzburg–Landau equation* and *Cahn–Hilliard* (*CH*) *equation* [58, 59, 78]. Here we illustrate applications of energy flux for the above equations.

The time-dependent Ginzburg–Landau (TDGL) equation, also called *model A*, is [59]:

$$\frac{\partial \zeta}{\partial t} = \zeta - \zeta^3 + \nabla^2\zeta. \tag{234}$$

The equation for the spectral energy $E_\zeta(\mathbf{k}) = \frac{1}{2}|\zeta(\mathbf{k})|^2$ is

$$\frac{\mathrm{d}}{\mathrm{d}t}E_\zeta(\mathbf{k}) = -\sum_{\mathbf{k}_1,\mathbf{k}_2}\Re[\zeta(\mathbf{k}_1)\zeta(\mathbf{k}_2)\zeta(\mathbf{k}_3)\zeta^*(\mathbf{k})] + 2E_\zeta(\mathbf{k}) - 2k^2E_\zeta(\mathbf{k}), \tag{235}$$

where $\mathbf{k}_3 = \mathbf{k} - \mathbf{k}_1 - \mathbf{k}_2$. In equation (235), the second term in the right-hand-side enhances $E_\zeta(\mathbf{k})$, while the last term dissipates $E_\zeta(\mathbf{k})$. The nonlinear term, the first term in the right-hand-side of the above equation, induces the following energy flux for a wavenumber sphere of radius k_0:

$$\Pi_\zeta(k_0) = -\sum_{k\leqslant k_0}\sum_{\mathbf{k}_1,\mathbf{k}_2} \Re[\zeta(\mathbf{k}_1)\zeta(\mathbf{k}_2)\zeta(\mathbf{k}_3)\zeta^*(\mathbf{k})]. \tag{236}$$

Numerical simulation and analytical studies of TDGL equation reveal that asymptotically ($t\to\infty$), the system exhibits either a constant solution ($\zeta = 1$ or -1) or a train of domains described by $\zeta = \tanh(x/\sqrt{2})$ (see [59] and references therein). The above route to structure formation has been studied in detail, but the formalism of energy flux has not been applied to this system. In the following discussion we show how the energy flux can explain the emergence of constant ζ solutions.

The scalar energy E_ζ is dissipated strongly at small scales due to the k^2 factor in the dissipation rate. Consequently, a forward cascade of E_ζ is set up that transfers the energy of large and intermediate scales to small scales where it is dissipated. Note however that the mean energy, $E_\zeta(k=0)$, is not dissipated (due to the structure of the dissipation term). Consequently, only $k=0$ mode survives, while the rest of the modes vanish due to the forward cascade and dissipation. Therefore, the final state is either $\zeta = 1$ or -1 with zero energy flux. It will be interesting to employ flux arguments to the domain solution ($\zeta = \tanh(x/\sqrt{2})$). Thus, the energy flux provides useful insights into the dynamics of TDGL equation.

Similar analysis is applicable to *model B* or the Cahn-Hilliard (CH) equation [59], which is

$$\frac{\partial\zeta}{\partial t} = -\nabla^2(\zeta - \zeta^3 + \nabla^2\zeta). \tag{237}$$

The evolution equation for the modal energy of the CH equation is

$$\frac{\mathrm{d}}{\mathrm{d}t}E_\zeta(\mathbf{k}) = -k^2\sum_{\mathbf{k}_1,\mathbf{k}_2} \Re[\zeta(\mathbf{k}_1)\zeta(\mathbf{k}_2)\zeta(\mathbf{k}_3)\zeta^*(\mathbf{k})] + 2k^2E_\zeta(\mathbf{k}) - 2k^4E_\zeta(\mathbf{k}), \tag{238}$$

while the corresponding scalar energy flux is

$$\Pi_\zeta(k_0) = -k^2\sum_{k<k_0}\sum_{\mathbf{k}_1,\mathbf{k}_2} \Re[\zeta(\mathbf{k}_1)\zeta(\mathbf{k}_2)\zeta(\mathbf{k}_3)\zeta^*(\mathbf{k})]. \tag{239}$$

The energetics of CH equation is very similar to that of TDGL: $k^2E_\zeta(\mathbf{k})$ term feeds energy into the system, while $-k^4E_\zeta(\mathbf{k})$ term dissipates energy. The first term in the right-hand-side of equation (238) creates forward energy cascade. The cascaded energy is dissipated at small scales. Asymptotically, we obtain domains separated by domain walls [59]. Detailed characterization of energy flux is not yet explored for this system.

Inclusion of hydrodynamic effects into CH equation yields the following equations for the velocity field and ζ [58]:

$$\frac{\partial\mathbf{u}}{\partial t} + (\mathbf{u}\cdot\nabla)\mathbf{u} = -\frac{1}{\rho}\nabla\mathbf{p} + a\zeta\nabla\nabla^2\zeta + \mathbf{F}_{\mathrm{LS}} + \nu\nabla^2\mathbf{u}, \tag{240}$$

$$\frac{\partial\zeta}{\partial t} + (\mathbf{u}\cdot\nabla)\zeta = -\nabla^2(\zeta - \zeta^3 + \nabla^2\zeta), \tag{241}$$

$$\nabla\cdot\mathbf{u} = 0, \tag{242}$$

with corresponding forces as $\mathbf{F}_u = a\zeta\nabla\nabla^2\zeta$ and $F_\zeta = \nabla^2\zeta^3$. The energy spectra and fluxes of the above system have been studied in detail by many researchers (see [217, 218] and references therein).

The nonlinear terms $(\mathbf{u}\cdot\nabla)\mathbf{u}$ and $(\mathbf{u}\cdot\nabla)\zeta$ generate the respective fluxes $\Pi_u(k)$ and $\Pi_\zeta(k)$ for the kinetic and scalar energies. The force $\mathbf{F}_u$ induces variations in $\Pi_u(k)$ due to the energy injection rate:

$$\mathcal{F}_u(\mathbf{k}) = \Re[\mathbf{F}_u(\mathbf{k})\cdot\mathbf{u}^*(\mathbf{k})] = \sum_{\mathbf{p}} \Im[p^2\zeta(\mathbf{k}-\mathbf{p})\zeta(\mathbf{p})\{\mathbf{p}\cdot\mathbf{u}^*(\mathbf{k})\}]. \tag{243}$$

Refer to equation (238) for the expression of $\mathcal{F}_\zeta(\mathbf{k})$. Interestingly, hydrodynamic version of CH equation too exhibits coarsening [217, 218]. Note that the scalar field appears to exhibit forward cascade. Thus, the coarsening process in binary fluid is not due to any inverse cascade (as in 2D turbulence), but it is due to the energy injection term of the equation.

In summary, the scalar energy flux provides valuable inputs to the dynamics of coarsening. However, more work is required for definitive conclusions.

13. Field-theoretic description of energy flux

There are several field-theoretic calculations of turbulence using which we can compute the energy flux. These are first-principle calculations, typically to first order in perturbation. Field theory is a complex and vast field that is covered in many books and papers. Hence, it is impossible to summarize it in several pages. Here, we provide a brief summary of the main results of this topic.

One of first field-theoretic calculations of turbulent flow was by Kraichnan [74] who employed direct interaction approximation to compute the *effective viscosity* and energy flux. Later works in this field include those by Wyld [219], Orszag [12], Yakhot and Orszag [101], McComb [7, 220], DeDominicis [221], Zhou [222], Adzhemyan *et al* [223], Zakharov [224], Nazarenko [79], etc. These works provide renormalized viscosity as well as energy flux; here we sketch the energy flux aspects of the above works.

Most of the field-theoretic computations of energy flux are based on perturbative expansion to first order. We start with equation (19) and assume that the Fourier modes are quasi-Gaussian that yields the following to first order in perturbation [5, 14, 43, 74]:

$$\begin{aligned}\Pi_u(k_0) &= \sum_{\mathbf{p}\leqslant k_0}\sum_{k>k_0} \Im\left[\langle\{\mathbf{k}\cdot\mathbf{u}(\mathbf{q})\}\{\mathbf{u}(\mathbf{p})\cdot\mathbf{u}^*(\mathbf{k})\}\rangle\right]\\ &\sim \sum_{\mathbf{p}\leqslant k_0}\sum_{k>k_0}\int_0^t \mathrm{d}t'\, G(\mathbf{k},t-t')\,\langle\mathbf{u}(\mathbf{p},t)\cdot\mathbf{u}(-\mathbf{p},t')\rangle\,\langle\mathbf{u}(\mathbf{q},t)\cdot\mathbf{u}(-\mathbf{q},t')\rangle\\ &= \Pi_u = \text{const.},\end{aligned} \tag{244}$$

where $G(\mathbf{k},t-t')$ is the Green's function, and t, t' are two different times with $t > t'$. The quasi-Gaussian nature of the modes yields $\langle uuuu\rangle \sim \langle uu\rangle\langle uu\rangle$. The above integral converges and yields a constant, which is consistent with Kolmogorov's theory of turbulence. Interestingly, for a 3D flow, a substitution of $E(k) = k^2$ in equation (244) leads to vanishing energy flux, consistent with the theory of dissipationless turbulence [14].

It is very hard to compute the fluctuations in the energy flux or dissipation rate using field theory. These computations, if successful, would have yielded the intermittency exponents. In spite of many valiant attempts, there is no fully consistent calculation that achieves this

objective. Belinicher *et al* [225] developed a field-theoretic procedure to compute the scaling exponents ζ_q of the qth-order structure function. In a series of papers, L'vov and Procaccia [226–228] employed exact resummation of all the Feynman diagrams of hydrodynamic turbulence and derived scaling relations among the intermittency exponents. Their perturbative theory is divergence-free both in infrared and ultraviolet regime. These results are summarized as *fusion rules* [229]. Fairhall *et al* [230] showed that the predictions of the fusion rules are in good agreement with the experimental results of atmospheric turbulence. Another important and related issue is Euler singularity and dissipative anomaly, which are discussed in Onsagar [231], Frisch [8], and Eyink and Sreenivasan [232]. Using mode coupling and renormalization group method, Das and Bhattacharjee [233] computed $\langle \Pi_u(\mathbf{r})\Pi_u(\mathbf{r}+\mathbf{l})\rangle$, which is the correlation of the energy flux.

Gurarie and Migdal [234], and Apolinario *et al* [235] employed instantons to derive the exponential tails of the PDF of the velocity gradients of randomly forced Burgers equation. Similar methods are being applied to hydrodynamic turbulence. The above calculations are quite complex; the reader is referred to the original paper for details.

Field-theoretic computations have also been applied to other turbulent systems, such as MHD turbulence ([43] and references therein) and scalar turbulence [236]. These computations are more complex than its hydrodynamic counterpart due to larger number of variables. For example, for MHD turbulence, the energy flux for the Elsässer variable $\mathbf{z}^+$ is

$$\Pi_{z^+}(k_0) = S^+(\mathbf{k}'|\mathbf{p}|\mathbf{q}) = \sum_{\mathbf{p}\leqslant k_0}\sum_{k'>k_0} \Im\left[\left\langle\{\mathbf{k}\cdot\mathbf{z}^-(\mathbf{q})\}\{\mathbf{z}^+(\mathbf{p})\cdot\mathbf{z}^+(\mathbf{k}')\}\right\rangle\right]. \quad (245)$$

Verma [43] computed the above to first order in perturbation and showed that

$$\begin{aligned}\left\langle S^+(\mathbf{k}'|\mathbf{p}|\mathbf{q})\right\rangle = -\Im\int_\infty^t \mathrm{d}t' \int \mathrm{d}\mathbf{p}'\,\mathrm{d}\mathbf{q}' \Big[& k_i'(-iM_{\mathrm{jab}}(\mathbf{k}'))G^{++}(k',t-t') \\ & \times \left\langle z_i^-(\mathbf{q},t) z_a^-(\mathbf{q}',t')\right\rangle \left\langle z_j^+(\mathbf{p},t) z_{\mathrm{b}}^+(\mathbf{p}',t')\right\rangle \\ & + k_i'(-iM_{\mathrm{jab}}(\mathbf{p}))G^{++}(\mathbf{p},t-t') \left\langle z_i^-(\mathbf{q},t) z_a^-(\mathbf{q}',t')\right\rangle \\ & \times \left\langle z_j^+(\mathbf{k}',t) z_{\mathrm{b}}^+(\mathbf{p}',t')\right\rangle\Big], \end{aligned} \quad (246)$$

where $M_{\mathrm{jab}}(\mathbf{k}')$ and $M_{\mathrm{jab}}(\mathbf{p})$ are tensors involving $\mathbf{k}, \mathbf{p}, \mathbf{q}$.

The above expressions for $\Pi_{z^+}(k_0)$ and $S^+(\mathbf{k}'|\mathbf{p}|\mathbf{q})$ are general, and they are applicable to both isotropic and anisotropic situations. For the isotropic case, Verma [43] computed the energy fluxes under the assumption of Kolmogorov-like spectrum. He also computed the flux for anisotropic turbulence, which is observed in the presence of a strong external magnetic field. For simplification, it was assumed that $\langle E_{z^+}\rangle = \langle E_{z^-}\rangle$. For this case, $\langle S^+(\mathbf{k}'|\mathbf{p}|\mathbf{q})\rangle = \langle S^-(\mathbf{k}'|\mathbf{p}|\mathbf{q})\rangle$. Further details of the calculation are as follows.

In the presence of a strong external magnetic field $\mathbf{B}_0$, Green's function and correlation function are [43, 237]

$$\begin{aligned} G^{\pm\pm}(\mathbf{k}, t-t') &= \theta(t-t')\,\exp[\pm i\mathbf{k}\cdot\mathbf{B}_0(t-t')], \\ \left\langle z_i^\pm(\mathbf{k},t) z_j^\pm(\mathbf{k}',t')\right\rangle &= \theta(t-t') C_{ij}^{\pm\pm}(\mathbf{k},t,t)\exp[\pm i\mathbf{k}\cdot\mathbf{B}_0(t-t')], \end{aligned}$$

where $\theta(t)$ is the step function. The anisotropic correlation correlations $C_{ij}^{\pm\pm}(\mathbf{k},t,t)$ are approximated as

$$C_{ij}^{\pm\pm}(\mathbf{k},t,t) = (2\pi)^d\delta(\mathbf{k}+\mathbf{k}')\left[P_{ij}(\mathbf{k})C_1(k) + P'_{ij}(\mathbf{k}',\mathbf{n})C_2(k)\right] \quad (247)$$

with

$$P'_{ij}(\mathbf{k},\mathbf{n}) = \left(n_i - \frac{\mathbf{n}\cdot\mathbf{k}}{k^2}k_i\right)\left(n_j - \frac{\mathbf{n}\cdot\mathbf{k}}{k^2}k_j\right), \tag{248}$$

where $\mathbf{n}$ is the unit vector along the mean magnetic field, and $C_{11} = C_1(k) + C_2(k)\sin^2\theta$ and $C_{22} = C_1(k)$ are the poloidal and toroidal correlations respectively [43, 237].

The $\mathrm{d}t'$ integral of equation (246) is [237]

$$\int_{-\infty}^{t} \mathrm{d}t'\theta(t-t')\,\exp[i(-\mathbf{k}+\mathbf{p}-\mathbf{q})\cdot\mathbf{B}_0(t-t')] = \frac{1-\exp\, i(-q_\parallel B_0 + i\epsilon)t}{i(-2q_\parallel B_0 + i\epsilon)}$$
$$= i\,\mathrm{Pr}\,\frac{1}{2q_\parallel B_0} + \pi\delta(2q_\parallel B_0), \tag{249}$$

with Pr representing the principal value and $\epsilon > 0$ is a constant. The term $\delta(q_\parallel)$ in $\langle S^+(\mathbf{k}'|\mathbf{p}|\mathbf{q})\rangle$ implies that the energy transfer in weak MHD turbulence occurs in a plane formed by $\mathbf{p}_\perp$ and $\mathbf{k}_\perp$. Under this assumption, $\mathbf{p}'_{ij}(\mathbf{n},\mathbf{k}) = n_i n_j$, which leads to

$$\left\langle S^+(\mathbf{k}'|\mathbf{p}|\mathbf{q})\right\rangle = \frac{\pi\delta(q_\parallel)}{2B_0}k_\perp^2(1-y^2)\left[1+z^2+C_2(\mathbf{p})/C_1(q)\right]C_1(q)$$
$$\times\left[C_1(\mathbf{p}_\perp) - C_1(k_\perp)\right]. \tag{250}$$

Hence,

$$\Pi \sim \int \mathrm{d}\mathbf{k}\int \mathrm{d}\mathbf{q}\frac{\pi\delta(q_\parallel)}{2B_0}k_\perp^2(1-y^2)\left[1+z^2+C_2(\mathbf{p})/C_1(q)\right]C_1(\mathbf{q})\left[C_1(\mathbf{p}) - C_1(\mathbf{k})\right]$$
$$= k_\parallel\int \mathrm{d}\mathbf{k}_\perp\int \mathrm{d}\mathbf{q}_\perp\,\mathrm{d}q_\parallel\,\frac{\pi\delta(q_\parallel)}{2B_0}k_\perp^2(1-y^2)\left[1+z^2+C_2(\mathbf{p})/C_1(q)\right]C_1(\mathbf{q})$$
$$\times\left[C_1(\mathbf{p}) - C_1(\mathbf{k})\right], \tag{251}$$

that yields

$$\Pi \sim k_\parallel k_\perp^6 C_1^2(\mathbf{k})/B_0. \tag{252}$$

Using $C_1(k_\perp, k_\parallel) = E_1(k_\perp)/(2\pi k_\perp k_\parallel)$, we obtain

$$E_{1,2}(k_\perp) \sim (\Pi B_0)^{1/2}k_\parallel^{1/2}k_\perp^{-2}, \tag{253}$$

which is same as that derived by Galtier *et al* [237] using Zakharov transforms. Note that the above spectrum is very different from Kolmogorov's $5/3$ spectrum. Also, the above derivation uses constancy of energy flux rather than Zakharov transform, which was employed by Galtier *et al* [237].

Goldreich and Sridhar [238] performed field-theoretic computation of strong turbulence. The energy flux in this framework is [43]

$$\Pi(k_0) \sim \int \mathrm{d}\mathbf{k}'\int \mathrm{d}\mathbf{p}\,\Im\left[(-i)k_\perp^2 t_i(v,w)C(\mathbf{q})(C(\mathbf{p}) - C(\mathbf{k}))\frac{1}{-i\omega(\mathbf{k}) + \eta(\mathbf{k})}\right]$$
$$\sim \iint \mathrm{d}k_\perp\,\mathrm{d}k_\parallel\,\mathrm{d}\mathbf{p}_\perp\,\mathrm{d}\mathbf{p}_\parallel k_\perp^3\mathbf{p}_\perp C(\mathbf{q})(C(\mathbf{p}) - C(\mathbf{k}))\frac{1}{\omega}\frac{(\eta(\mathbf{k})/\omega(\mathbf{k}))}{1+(\eta(\mathbf{k})/\omega(\mathbf{k}))^2}. \tag{254}$$

with

$$\eta(\mathbf{k}) = \eta_0 k_\perp^2 \left[k_\parallel E(k,t)\right]^{1/2}, \tag{255}$$

Using $\omega \sim k_\parallel B_0$ and dimensional analysis it can be deduced that [238]

$$C(\mathbf{k}) \sim \Pi^{2/3} k_\perp^{-10/3} L^{-1/3} f\left(\frac{k_\parallel L^{1/3}}{k_\perp^{2/3}}\right). \tag{256}$$

The above arguments show that we can derive important phenomenological relations using the field-theoretic computation of energy flux. In the above derivations, the energy fluxes are constant, but the framework is expected to work for cases when the energy flux are k-dependent. Such explorations would be interesting.

14. Summary and conclusions

The energy flux is an important quantity in turbulence. The inertial-range energy flux is constant in hydrodynamic turbulence with large-scale forcing. However, in the presence of inertial-range energy injection ($\mathcal{F}_u(k)$) and dissipation ($D_u(k)$), the kinetic energy flux becomes scale-dependent and is described by $\mathrm{d}\Pi_u(k)/\mathrm{d}k = \mathcal{F}_u(k) - D_u(k)$. Due to these variations, such fluxes are referred to as *variable energy flux*. In this article, we review how the variable energy flux formalism is useful for modelling many turbulent systems, especially in determining their energy spectra and fluxes. External force can induce anisotropy in the flow. Yet, the energy flux and shell spectrum are useful tools for describing multiscale energy transfers in complex turbulent flows.

A summary of the results presented in the review is as follows.

- **Buoyancy driven turbulence**: In stably stratified turbulence with moderate stratification, the kinetic energy is transferred to the potential energy, hence $\mathcal{F}_u(k) < 0$. Therefore, $\Pi_u(k)$ decreases with k in the inertial range itself; in particular, $\Pi_u(k) \sim k^{-4/5}$ and $E_u(k) \sim k^{-11/5}$, which is steeper than $k^{-5/3}$ spectrum [19, 20]. However, $\mathcal{F}_u(k) > 0$ in turbulent thermal convection. Hence, $E_u(k)$ for thermal convection is expected to be shallower than $k^{-5/3}$. Yet, turbulent thermal convection with $\mathrm{Pr} \lessapprox 1$ has behaviour similar to hydrodynamic turbulence (nearly constant energy flux and $k^{-5/3}$ kinetic energy spectrum in the inertial range). This is due to the fact that for $\mathrm{Pr} \lessapprox 1$, $\mathcal{F}_u(k)$ decreases sharply with k and is quite weak in the inertial range, similar to that in Kolmogorov's model for hydrodynamic turbulence.
- **MHD and polymeric turbulence**: In MHD turbulence, the nonlinear interactions between the velocity and magnetic fields cause energy transfers from the velocity field to the magnetic field. This conversion mechanism is responsible for the growth of the magnetic field in astrophysical objects, and for making $\Pi_u(k)$ a decreasing function of k. Similar energy transfers are observed in turbulent flows with polymers. The suppression of $\Pi_u(k)$ or the nonlinear term $(\mathbf{u}\cdot\nabla)\mathbf{u}$ is one of the primary causes of drag reduction in such flows. Using variable energy flux formalism we also derive identities relating various fluxes.
- **Dissipation**: In turbulence, viscous dissipation suppresses the energy flux in the dissipation range. Using several assumptions, Pao [35, 113] showed that in the inertial–dissipation range of hydrodynamic turbulence, the energy flux and normalized energy spectrum vary as $\exp(-(k/k_d)^{4/3})$, where k_d is Kolmogorov wavenumber. Ekman friction that acts at all scales steepens the inertial-range energy spectrum even more than the $k^{-5/3}$

Table 3. Table illustrating 3D turbulent systems along with their forces ($\mathbf{F}_u(\mathbf{k})$), the kinetic energy injection rates by the forces ($\mathcal{F}_u(\mathbf{k})$), and the nature of kinetic energy fluxes in the inertial range. For the meaning of the symbols, refer to the discussion in the paper. IC stands for initial condition.

System	$\mathbf{F}_u(\mathbf{k})$	$\mathcal{F}_u(\mathbf{k})$	Nature of $\Pi_u(k)$
Kolmogorov's K41 law	0	0	Const.
QS MHD turbulence	$-B_0^2\cos^2\theta\mathbf{u}(\mathbf{k})$	$-2B_0^2\cos^2\theta E_u(k)<0$	Decreases
Ekman friction (3D)	$-\alpha\mathbf{u}(\mathbf{k})$	$-2\alpha E_u(\mathbf{k})<0$	Decreases
Stably stratified turbulence	$-N\zeta(\mathbf{k})$	$-N\Re[\zeta(\mathbf{k})u_z^*(\mathbf{k})]<0$	Decreases
Thermal convection	$\alpha g\zeta(\mathbf{k})$	$\alpha g\Re[\zeta(\mathbf{k})u_z^*(\mathbf{k})]>0$	Marginally increases
Unstably stratified turbulence	$g\zeta(\mathbf{k})$	$g\Re[\zeta(\mathbf{k})u_z^*(\mathbf{k})]>0$	Increases
MHD (dynamo)	$[\mathbf{J}\times\mathbf{B}](\mathbf{k})$	$\Re\{[\mathbf{J}\times\mathbf{B}](\mathbf{k})\cdot\mathbf{u}^*(\mathbf{k})\}<0$	Decreases
Dilute polymer	$\frac{\mu}{\tau_p}\partial_j(f\zeta_{ij})$	Complex convolution <0	Decreases
Shear turbulence	Shear force	Positive	Increases
Euler turbulence	0	0	Zero or mixed depending on IC

power-law. In quasi-static MHD turbulence, the Joule dissipation provides similar steepening of the kinetic energy spectrum. Pao's model has been generalized to 2D hydrodynamic turbulence with Ekman friction.

- **Energy flux of a secondary flow ζ**: The advection term of a secondary field ζ, $(\mathbf{u}\cdot\nabla)\zeta$, has an associated secondary energy flux Π_ζ. This flux too exhibits variability: $\mathrm{d}\Pi_\zeta(k)/\mathrm{d}k = \mathcal{F}_\zeta(k) - D_\zeta(k)$, where $\mathcal{F}_\zeta(k)$ is the secondary energy injection rate, and $D_\zeta(k)$ is the diffusion rate of the secondary field. Such flux variations are present in MHD turbulence, stably stratified turbulence, binary-mixture turbulence, and related complex flows.

Thus, variable energy flux is a useful diagnostic for modelling above flows, as well as shear turbulence, stably and unstably stratified turbulence, Euler turbulence, quantum turbulence, etc. Energy flux provides inputs for understanding quantum turbulence and the coarsening processes in time-dependent Ginzburg–Landau and Cahn-Hilliard equations. Interestingly, the money supply in a free market economy too exhibits a cascade across various income groups; this cascade has similarities with the energy flux in turbulence [239]. It is also important to note that the nature of variable energy flux depends on the space dimensionality. In table 3, we summarise the variable energy fluxes discussed in this review.

For a delta-correlated field as an initial condition, truncated Euler turbulence exhibits equilibrium behaviour with vanishing kinetic energy flux and nearly k^2 energy spectrum in three dimensions. However, for orderly initial condition, such as Taylor–Green vortex, Euler turbulence yields a mix of nonequilibrium and equilibrium behaviour with a combination of $k^{-5/3}$ and k^2 spectra. Asymptotically, the k^2 spectrum is expected for all k's. Dissipationless MHD turbulence and passive-scalar turbulence also exhibit similar behaviour. These features of dissipationless turbulence provide interesting clues into the thermalization processes of complex systems.

There is a large body of works on the real-space description of energy flux and its relation to the structure functions. The intermittency effects are related to the fluctuations in energy fluxes. It has been shown that the real-space and Fourier-space formalisms of energy transfers are related to each other. There are some works that describe structure functions for anisotropic turbulence. However, further investigations are required for a complete understanding of energy transfers in anisotropic turbulence.

As discussed in the review, variable energy flux provides a unifying platform for modelling many turbulent systems. Note, however, that this framework has the following limitations:

(a) In the present formalism, we assumed the flows to be steady. Equation (35) is applicable to unsteady flows, but general properties of the energy fluxes for such unsteady flows have not been studied in detail.

(b) Kolmogorov's theory [1, 2] describes the properties of average energy flux and energy spectrum of turbulent hydrodynamics. The energy flux fluctuates around the above mean. These fluctuations are related to the intermittency, which is not covered in this review. Note that the energy fluxes of buoyant flows, magnetofluids, and more complex flows exhibit variations in the energy fluxes due to intermittency effects, as well as due to the external forces.

(c) The energy transfers are anisotropic in the presence of a directional forcing or a mean field. For example, in MHD turbulence with a constant mean magnetic field, the energy exchange is dominant near the plane perpendicular to the mean magnetic field [157]. For such systems, the ring-to-ring energy transfer provides valuable insights [18]. However, the energy flux, which is the net energy transfer from the modes inside a sphere to the modes outside the sphere, is still defined for a anisotropic system. In addition, the energy flux represents over-all scale-by-scale energy transfer in such systems. Consequently, a large body of work have employed energy flux for modelling anisotropic flows. For example, Krachnan [240] and Irishnokov [241] modelled MHD turbulence using energy flux. Also, Bolgiano [19] and Obukhov [20] employed energy flux for modelling stably-stratified turbulence. In addition, the energy flux is used for characterizing rotating turbulence.

(d) In this review, we focus on strong turbulence. The energy flux of weak turbulence has not been discussed here.

As we show in this review, variable energy flux has been studied in some detail for the following systems—dissipative range of hydrodynamics, MHD and buoyancy-driven turbulence, flows with dilute polymers, Euler turbulence, etc. We believe that this formalism will also be useful for modelling anisotropic turbulence, quantum turbulence, binary-mixture turbulence, electron MHDs [242], shell model of turbulence [243], compressible turbulence [244], weak turbulence [79], and plasma turbulence [245]. We hope that the above issues will be addressed in near future.

Acknowledgments

For writing this review I drew heavily from the discussions and idea exchanges I had with my collaborators, namely, Franck Plunian, Rodion Stepanov, Ravi Samtaney, Daniele Carati, Stephan Fauve, Jai Sukhatme, Sanjay Puri, K R Sreenivasan, Alexandros Alexakis, Gaurav Dar, Vinayak Eswaran, and Bernard Knaepen. I am very grateful to them for the same. In addition, I received critical inputs and ideas from many past and present doctoral and master students—Abhishek Kumar, Shashwat Bhattacharya, Roshan Samuel, Mohammad Anas, Shadab Alam, Soumyadeep Chatterjee, Pankaj Mishra, Satyajit Barman, Manohar Sharma, Shubhadeep Sadhukhan, Olivier Debliquy, Bogdan Teaca, Thomas Lessinness, Valerii Titov, Ambrish Pandey, Sandeep Reddy, Anando Chatterjee, Arvind Ayyer, and V Avinash. I also thank J K Bhattacharjee, Peter Frick, Annick Pouquet, Arnab Rai Choudhuri, Avinash Khare, P K Yeung, Diego Donzis, Xavier Albets, Itamar Procaccia, Maurice Rossi, Andrei Teimurazov, Andrei Sukhanovskii, Marc Brachet, Gregory Eyink, Luca Moriconi, Sagar Chakraborty,

Supratik Banerjee, Sonakshi Sachdev, Akanksha Gupta, and Luca Biferale for useful discussions. I also thank the anonymous referees and an Editorial Board Member for useful suggestions. I gratefully acknowledge the support of Indo-French projects 4904-1 and 6104-1 from CEFIPRA, IFCAM project MA/IFCAM/19/90, Indo-Russian project INT/RUS/RSF/P-03 from Department of Science and Technology India, and SERB project SERB/F/3279/2013-14 that made the collaborative work and idea exchanges possible. Some of the results presented in the review have been generated using SHAHEEN II of KAUST (project K1052) and HPC2013 of IIT Kanpur.

Data availability statement

The data that support the findings of this study are available upon reasonable request from the authors.

ORCID iDs

Mahendra K Verma https://orcid.org/0000-0002-3380-4561

References

[1] Kolmogorov A N 1941 *Dokl. Akad. Nauk SSSR* **30** 301–5
[2] Kolmogorov A N 1941 *Dokl. Akad. Nauk SSSR* **32** 16–8
[3] Monin A S and Yaglom A M 2007 *Statistical Fluid Mechanics: Mechanics of Turbulence* vol 1 (New York: Dover)
[4] Monin A S and Yaglom A M 2007 *Statistical Fluid Mechanics: Mechanics of Turbulence* vol 2 (New York: Dover)
[5] Leslie D C 1973 *Developments in the Theory of Turbulence* (Oxford: Clarendon)
[6] Lesieur M 2008 *Turbulence in Fluids* (Berlin: Springer)
[7] McComb W D 1990 *The Physics of Fluid Turbulence* (Oxford: Clarendon)
[8] Frisch U 1995 *Turbulence: The Legacy of A. N. Kolmogorov* (Cambridge: Cambridge University Press)
[9] Davidson P A 2004 *Turbulence: An Introduction for Scientists and Engineers* (Oxford: Oxford University Press)
[10] Sagaut P and Cambon C 2018 *Homogeneous Turbulence Dynamics* 2nd edn (Cambridge: Cambridge University Press)
[11] Pope S B 2000 *Turbulent Flows* (Cambridge: Cambridge University Press)
[12] Orszag S A 1973 *Lectures on the Statistical Theory of Turbulence in Fluid Dynamics Les Houches Summer School of Theoretical Physics* ed R Balian and J L Peube (Gordon and Breach) p 235
[13] McComb W D 1995 *Rep. Prog. Phys.* **58** 1117–205
[14] Verma M K 2019 *Energy Transfers in Fluid Flows: Multiscale and Spectral Perspectives* (Cambridge: Cambridge University Press)
[15] Landau L D and Lifshitz E M 1987 *Fluid Mechanics* (*Course of Theoretical Physics*) 2nd edn (Amsterdam: Elsevier)
[16] Meneveau C and Sreenivasan K R 1987 *Phys. Rev. Lett.* **59** 1424–7
[17] Stolovitzky G and Sreenivasan K R 1994 *Rev. Mod. Phys.* **66** 229–40
[18] Teaca B, Verma M K, Knaepen B and Carati D 2009 *Phys. Rev.* E **79** 046312
[19] Bolgiano R 1959 *J. Geophys. Res.* **64** 2226–9
[20] Obukhov A M 1959 *Dokl. Akad. Nauk SSSR* **125** 1246
[21] Kumar A, Chatterjee A G and Verma M K 2014 *Phys. Rev.* E **90** 023016
[22] Verma M K, Kumar A and Pandey A 2017 *New J. Phys.* **19** 025012

[23] Verma M K 2018 *Physics of Buoyant Flows: From Instabilities to Turbulence* (Singapore: World Scientific)
[24] Moffatt H K 1978 *Magnetic Field Generation in Electrically Conducting Fluids* (Cambridge: Cambridge University Press)
[25] Brandenburg A, Subramanian K, Subramanian K and Subramanian K 2005 *Phys. Rep.* **417** 1–209
[26] Moreau R J 1990 *Magnetohydrodynamics* (Berlin: Springer)
[27] Knaepen B and Moreau R 2008 *Annu. Rev. Fluid Mech.* **40** 25–45
[28] Verma M K 2017 *Rep. Prog. Phys.* **80** 087001
[29] Anas M and Verma M K 2019 *Phys. Rev. Fluids* **4** 104611
[30] Tchen C M 1952 *J. Res. Natl Bur. Stand.* **50** 51–62
[31] Matthaeus W H and Goldstein M L 1986 *Phys. Rev. Lett.* **57** 495–8
[32] Pereira M, Gissinger C and Fauve S 2019 *Phys. Rev.* E **99** 023106
[33] Boffetta G, Cenedese A, Espa S and Musacchio S 2005 *Europhys. Lett.* **71** 590–6
[34] Verma M K 2012 *Europhys. Lett.* **98** 14003
[35] Pao Y-H 1965 *Phys. Fluids* **8** 1063–75
[36] Chen S, Doolen G, Herring J R, Kraichnan R H, Orszag S A and She Z S 1993 *Phys. Rev. Lett.* **70** 3051–4
[37] Martínez D O, Chen S, Doolen G D, Kraichnan R H, Wang L-P and Zhou Y 1997 *J. Plasma Phys.* **57** 195–201
[38] Gupta A, Jayaram R, Chaterjee A G, Sadhukhan S, Samtaney R and Verma M K 2019 *Phys. Rev.* E **100** 053101
[39] Falkovich G 1994 *Phys. Fluids* **6** 1411–4
[40] Verma M K and Donzis D 2007 *J. Phys. A: Math. Theor.* **40** 4401–12
[41] Küchler C, Bewley G and Bodenschatz E 2019 *J. Stat. Phys.* **175** 617–39
[42] Dar G, Verma M K and Eswaran V 2001 *Physica* D **157** 207–25
[43] Verma M K 2004 *Phys. Rep.* **401** 229–380
[44] Alexakis A, Mininni P D and Pouquet A G 2005 *Phys. Rev.* E **72** 046301
[45] de Gennes P G 1990 *Introduction to Polymer Dynamics* (Cambridge: Cambridge University Press)
[46] Valente P C, da Silva C B and Pinho F T 2014 *J. Fluid Mech.* **760** 39–62
[47] Valente P C, da Silva C B and Pinho F T 2016 *Phys. Fluids* **28** 075108
[48] Verma M K, Alam S and Chatterjee S 2020 *Phys. Plasmas* **27** 052301
[49] Sharma M K, Kumar A, Verma M K and Chakraborty S 2018 *Phys. Fluids* **30** 045103
[50] L'vov V S, Nazarenko S V and Skrbek L 2006 *J. Low Temp. Phys.* **145** 125–42
[51] Roche P-E, Barenghi C F and Leveque E 2009 *Europhys. Lett.* **87** 54006
[52] Wacks D H and Barenghi C F 2011 *Phys. Rev.* B **84** 216–8
[53] Madeira L, Caracanhas M A, dos Santos F E A and Bagnato V S 2020 *Annu. Rev. Condens. Matter Phys.* **11** 37–56
[54] Krstulovic G and Brachet M E 2011 *Phys. Rev.* E **83** 132506
[55] Tsatsos M C, Tavares P E S, Cidrim A, Fritsch A R, Caracanhas M A, dos Santos F E A, Barenghi C F and Bagnato V S 2016 *Phys. Rep.* **622** 1–52
[56] Berti S, Boffetta G, Cencini M and Vulpiani A 2005 *Phys. Rev. Lett.* **95** 224501
[57] Perlekar P, Pal N and Pandit R 2017 *Sci. Rep.* **7** 44589
[58] Cahn J W and Hilliard J E 2004 *J. Chem. Phys.* **28** 258–67
[59] Puri S and Wadhawan V (ed) 2009 *Kinetics of Phase Transitions* (Boca Raton, FL: CRC Press)
[60] Lee T D 1952 *Q. Appl. Math.* **10** 69–74
[61] Kraichnan R H 1973 *J. Fluid Mech.* **59** 745–52
[62] Cichowlas C, Bonaïti P, Debbasch F and Brachet M 2005 *Phys. Rev. Lett.* **95** 264502
[63] Verma M K 2020 *Phil. Trans. R. Soc.* A **378** 20190470
[64] Verma M K, Bhattacharya S and Chatterjee S 2020 arXiv:2004.09053
[65] Frisch U, Pouquet A, LÉOrat J and Mazure A 1975 *J. Fluid Mech.* **68** 769–78
[66] Stribling T and Matthaeus W H 1991 *Phys. Fluids* B **3** 1848–64
[67] Davis M J, Morgan S A and Burnett K 2001 *Phys. Rev. Lett.* **87** 160402
[68] Krstulovic G and Brachet M 2011 *Phys. Rev. Lett.* **106** 115303
[69] Frisch U, Kurien S, Pandit R, Pauls W, Ray S S, Wirth A and Zhu J-Z 2008 *Phys. Rev. Lett.* **101** 144501
[70] Alexakis A and Biferale L 2018 *Phys. Rep.* **767–769** 1–101
[71] L'vov V S 1991 *Phys. Rev. Lett.* **67** 687–90
[72] L'vov V S and Falkovich G 1992 *Physica* D **57** 85–95

[73] Rubinstein R 1994 Renormalization group theory of Bolgiano scaling in Boussinesq turbulence *Technical Report ICOM-94-8; CMOTT-94-2*
[74] Kraichnan R H 1959 *J. Fluid Mech.* **5** 497–543
[75] Alexakis A, Mininni P D and Pouquet A 2005 *Phys. Rev. Lett.* **95** 264503
[76] Verma M K, Roberts D A, Goldstein M L, Ghosh S and Stribling W T 1996 *J. Geophys. Res.* **101** 21619–25
[77] Amit D J 1978 *Field Theory, the Renormalization Group, and Critical Phenomena* (*International Series in Pure and Applied Physics*) (Singapore: World Scientific)
[78] Chaikin P M and Lubensky T C 2000 *Principles of Condensed Matter Physics* (Cambridge: Cambridge University Press)
[79] Nazarenko S V 2011 *Wave Turbulence* (Berlin: Springer)
[80] Verma M K, Ayyer A, Debliquy O, Kumar S and Chandra A V 2005 *Pramana J. Phys.* **65** 297–310
[81] Verma M K, Kumar A, Kumar P, Barman S, Chatterjee A G, Samtaney R and Stepanov R 2018 *Fluid Dyn.* **53** 728–39
[82] Sharma M K, Verma M K and Chakraborty S 2019 *Phys. Fluids* **31** 085117
[83] Teaca B, Carati D, Knaepen B and Verma M K 2009 Spectral analysis of energy transfers in anisotropic MHD turbulence *Advances in Turbulence XII: Proceedings of the 11th EUROMECH European Turbulence Conference XII* (Berlin: Springer) pp 841–4
[84] De Karman T and Howarth L 1938 *Proc. R. Soc.* A **164** 192–215
[85] Batchelor G K 1953 *The Theory of Homogeneous Turbulence* (Cambridge: Cambridge University Press)
[86] Verma M K 2005 arXiv:nlin/0510069
[87] Boffetta G, de Lillo F, Mazzino A and Musacchio S 2011 *Europhys. Lett.* **95** 34001
[88] Falkovich G and Kritsuk A G 2017 *Phys. Rev. Fluids* **2** 092603
[89] Domaradzki J A and Rogallo R S 1990 *Phys. Fluids* A **2** 414–26
[90] Eyink G L 2005 *Physica* D **207** 91–116
[91] Kolmogorov A N 1962 *J. Fluid Mech.* **13** 82–5
[92] Saddoughi S G and Veeravalli S V 1994 *J. Fluid Mech.* **268** 333–72
[93] Buaria D and Sreenivasan K R 2020 *Phys. Rev. Fluids* **5** 092601
[94] Grant H L, Stewart R W and Moilliet A 1962 *J. Fluid Mech.* **12** 241–68
[95] Ishihara T, Morishita K, Yokokawa M, Uno A and Kaneda Y 2016 *Phys. Rev. Fluids* **1** 082403
[96] Spyksma K, Magcalas M and Campbell N 2012 *Phys. Fluids* **24** 125102
[97] Donzis D A and Sreenivasan K R 2010 *J. Fluid Mech.* **657** 171–88
[98] Sheremet A, Qin Y, Kennedy J P, Zhou Y and Maurer A P 2019 *Front. Syst. Neurosci.* **12** 62
[99] Duguid C D, Barker A J and Jones C A 2020 *Mon. Not. R. Astron. Soc.* **497** 3400–17
[100] Heisenberg W 1948 *Proc. R. Soc.* A **195** 402–6
[101] Yakhot V and Orszag S A 1986 *J. Sci. Comput.* **1** 3–51
[102] Sain A, Manu and Pandit R 1998 *Phys. Rev. Lett.* **81** 4377–80
[103] Taylor G I 1954 *Proc. R. Soc.* A **223** 446–68
[104] Lohse D and Xia K-Q 2010 *Annu. Rev. Fluid Mech.* **42** 335–64
[105] Kumar A and Verma M K 2018 *R. Soc. Open Sci.* **5** 172152
[106] Verma M K, Kumar A and Gupta A 2020 *Trans. Indian Natl. Acad. Eng.* **5** 649–62
[107] Dutta P and Horn P M 1981 *Rev. Mod. Phys.* **53** 497–516
[108] Banerjee J, Verma M K, Manna S and Ghosh S 2006 *Europhys. Lett.* **73** 457–63
[109] Verma M K, Manna S, Banerjee J and Ghosh S 2006 *Europhys. Lett.* **76** 1050–6
[110] Verma M K 2001 *Int. J. Mod. Phys.* B **15** 3419–28
[111] Yeung P K, Donzis D A and Sreenivasan K R 2005 *Phys. Fluids* **17** 081703
[112] Sreenivasan K R 2019 *Proc. Natl Acad. Sci.* **116** 18175–83
[113] Pao Y-H 1968 *Phys. Fluids* **11** 1371–2
[114] Gotoh T and Yeung P K 2013 Passive scalar transport turbulence: a computational perspective *Ten Chapters in Turbulence* ed P A Davidson, Y Kaneda and K R Sreenivasan (Cambridge: Cambridge University Press) pp 87–131
[115] Donzis D A, Sreenivasan K R and Yeung P K 2010 *Flow Turbul. Combust.* **85** 549–66
[116] Waleffe F 1992 *Phys. Fluids* A **4** 350–63
[117] Tritton D J 1988 *Physical Fluid Dynamics* (Oxford: Clarendon)
[118] Davidson P A 2013 *Turbulence in Rotating, Stratified and Electrically Conducting Fluids* (Cambridge: Cambridge University Press)
[119] Verma M K 2019 *Phys. Scr.* **94** 1–10

[120] Lindborg E 2006 *J. Fluid Mech.* **550** 207–42
[121] Alam S, Guha A and Verma M K 2019 *J. Fluid Mech.* **875** 961–73
[122] Kimura Y and Herring J R 1996 *J. Fluid Mech.* **328** 253–69
[123] Rosenberg D, Pouquet A, Marino R and Mininni P D 2015 *Phys. Fluids* **27** 055105
[124] Kumar A, Verma M K and Sukhatme J 2017 *J. Turbul.* **18** 219–39
[125] Chandrasekhar S 1981 *Hydrodynamic and Hydromagnetic Stability* (New York: Dover)
[126] Procaccia I and Zeitak R 1990 *Phys. Rev.* A **42** 821–30
[127] Pandey A, Verma M K and Mishra P K 2014 *Phys. Rev.* E **89** 023006
[128] Bhattacharya S, Sadhukhan S, Guha A and Verma M K 2019 *Phys. Fluids* **31** 115107
[129] Nath D, Pandey A, Kumar A and Verma M K 2016 *Phys. Rev. Fluids* **1** 064302
[130] Boffetta G and Mazzino A 2017 *Annu. Rev. Fluid Mech.* **49** 119–43
[131] Lakkaraju R, Stevens R J A M, Oresta P, Verzicco R, Lohse D and Prosperetti A 2013 *Proc. Natl Acad. Sci. USA* **110** 9237–42
[132] Lewis G S and Swinney H L 1999 *Phys. Rev.* E **59** 5457–67
[133] Grossmann S, Lohse D and Sun C 2016 *Annu. Rev. Fluid Mech.* **48** 53–80
[134] Banerjee A, Kraft W N and Andrews M J 2010 *J. Fluid Mech.* **659** 127–90
[135] Akula B and Ranjan D 2016 *J. Fluid Mech.* **795** 313–55
[136] Cowling T G 1976 *Magnetohydrodynamics* (Bristol: Hilger)
[137] Davidson P A 2017 *An Introduction to Magnetohydrodynamics* 2nd edn (Cambridge: Cambridge University Press)
[138] Biskamp D 2003 *Magnetohydrodynamic Turbulence* (Cambridge: Cambridge University Press)
[139] Goldstein M L, Roberts D A and Matthaeus W H 1995 *Annu. Rev. Astron. Astrophys.* **33** 283–325
[140] Debliquy O, Verma M K and Carati D 2005 *Phys. Plasmas* **12** 042309
[141] Batchelor G K 1950 *Proc. R. Soc.* A **201** 405–16
[142] Verma M, Sharma M, Chatterjee S and Alam S 2021 *Fluids* **6** 225
[143] Zeldovich Y B, Ruzmaikin A A and Sokoloff D D 1983 *Magnetic Fields in Astrophysics* (London: Gordon and Breach)
[144] Marsch E 1991 Turbulence in the solar wind *Reviews in Modern Astronomy* ed G Klare (Berlin: Springer) pp 145–56
[145] Alemany A, Moreau R and Frisch U 1979 *J. Mec.* **18** 277–312
[146] Eckert S, Gerbeth G, Witke W and Langenbrunner H 2001 *Int. J. Heat Fluid Flow* **22** 358–64
[147] Kolesnikov Y B and Tsinober A B 1976 *Fluid Dyn.* **9** 621–4
[148] Kit L G and Tsinober A B 1971 *Magn. Gidrodin.* **7** 27–34
[149] Sreenivasan B and Alboussière T 2000 *Eur. J. Mech.* B **19** 403–21
[150] Boeck T, Krasnov D, Thess A, Zikanov O, Thess A and Zikanov O 2008 *Phys. Rev. Lett.* **101** 244501
[151] Pothérat A and Klein R 2014 *J. Fluid Mech.* **761** 168–205
[152] Reddy K S and Verma M K 2014 *Phys. Fluids* **26** 025109
[153] Reddy K S, Kumar R and Verma M K 2014 *Phys. Plasmas* **21** 102310
[154] Moffatt H K 1967 *J. Fluid Mech.* **28** 571–92
[155] Schumann U 1976 *J. Fluid Mech.* **74** 31–58
[156] Verma M K and Reddy K S 2015 *Phys. Fluids* **27** 025114
[157] Sundar S, Verma M K, Alexakis A and Chatterjee A G 2017 *Phys. Plasmas* **24** 022304
[158] de Gennes P G 1979 *Scaling Concepts in Polymer Physics* (Ithaca, NY: Cornell University Press)
[159] Tabor M and Gennes P G d 1986 *Europhys. Lett.* **2** 519–22
[160] Sreenivasan K R and White C M 2000 *J. Fluid Mech.* **409** 149–64
[161] Benzi R, Ching E S C, De Angelis E and Procaccia I 2008 *Phys. Rev.* E **77** 046309
[162] Benzi R 2010 *Physica* D **239** 1338–45
[163] Benzi R and Ching E S C 2018 *Annu. Rev. Condens. Matter Phys.* **9** 163–81
[164] Fouxon A and Lebedev V 2003 *Phys. Fluids* **15** 2060–72
[165] Perlekar P, Mitra D and Pandit R 2006 *Phys. Rev. Lett.* **97** 264501
[166] Sadhukhan S, Samuel R, Plunian F, Stepanov R, Samtaney R and Verma M K 2019 *Phys. Rev. Fluids* **4** 084607
[167] Müller W-C, Malapaka S K and Busse A 2012 *Phys. Rev.* E **85** 015302
[168] Plunian F, Stepanov R and Verma M K 2019 *J. Plasma Phys.* **85** 905850507
[169] Zhou Y and Vahala G 1993 *Phys. Rev.* E **47** 2503–19
[170] Avinash V, Verma M K and Chandra A V 2006 *Pramana J. Phys.* **66** 447–53

[171] Teimurazov A, Stepanov R, Verma M K, Barman S, Kumar A and Sadhukhan S 2017 *Comput. Contin. Mech.* **10** 474
[172] Kessar M, Plunian F, Stepanov R and Balarac G 2015 *Phys. Rev.* E **92** 031004
[173] Sahoo G and Biferale L 2018 *Fluid Dyn. Res.* **50** 011420
[174] Craya A 1958 Contribution à l'analyse de la turbulence associée à des vitesses moyennes *PhD Thesis* Université de Granoble
[175] Herring J R 1974 *Phys. Fluids* **17** 859–72
[176] Biferale L, Musacchio S and Toschi F 2012 *Phys. Rev. Lett.* **108** 164501
[177] Sahoo G, Alexakis A and Biferale L 2017 *Phys. Rev. Lett.* **118** 164501
[178] Plunian F, Teimurazov A, Stepanov R and Verma M K 2020 *J. Fluid Mech.* **895** 229–314
[179] Buzzicotti M, Aluie H, Biferale L and Linkmann M 2018 *Phys. Rev. Fluids* **3** 034802
[180] Biferale L, Gustavsson K and Scatamacchia R 2019 *J. Fluid Mech.* **869** 646–73
[181] Kraichnan R H 1967 *Phys. Fluids* **10** 1417–23
[182] Gotoh T 1998 *Phys. Rev.* E **57** 2984–91
[183] Belmonte A, Goldburg W I, Kellay H, Rutgers M A, Martin B and Wu X L 1999 *Phys. Fluids* **11** 1196–200
[184] Rutgers M A 1998 *Phys. Rev. Lett.* **81** 2244–7
[185] Rivera M, Vorobieff P and Ecke R E 1998 *Phys. Rev. Lett.* **81** 1417–20
[186] Tabeling P 2002 *Phys. Rep.* **362** 1–62
[187] Boffetta G and Ecke R E 2012 *Annu. Rev. Fluid Mech.* **44** 427–51
[188] Godeferd F S and Moisy F 2015 *Appl. Mech. Rev.* **67** 030802
[189] Alexakis A 2015 *J. Fluid Mech.* **769** 46–78
[190] Sharma M K, Verma M K and Chakraborty S 2018 *Phys. Fluids* **30** 115102
[191] Sommeria J and Moreau R 1982 *J. Fluid Mech.* **118** 507
[192] Shebalin J V, Matthaeus W H and Montgomery D 1983 *J. Plasma Phys.* **29** 525–47
[193] Bandyopadhyay R, Matthaeus W H, Oughton S and Wan M 2019 *J. Fluid Mech.* **876** 5–18
[194] Bartello P 1995 *J. Atmos. Sci.* **52** 4410–28
[195] Biferale L, Buzzicotti M and Linkmann M 2017 *Phys. Fluids* **29** 111101
[196] Alexakis A, Petrelis F, Benavides S J and Seshasayanan K 2021 *Phys. Rev. Fluids* **6** 024605
[197] D'Alessio L, Kafri Y, Polkovnikov A and Rigol M 2016 *Adv. Phys.* **65** 239–362
[198] Connaughton C and Nazarenko S V 2004 *Phys. Rev. Lett.* **92** 044501
[199] Shukla V, Dubrulle B, Nazarenko S V, Krstulovic G and Thalabard S 2019 *Phys. Rev.* E **100** 043104
[200] Ganga Prasath S G, Fauve S and Brachet M 2014 *Europhys. Lett.* **106** 29002
[201] Dallas V, Fauve S and Alexakis A 2015 *Phys. Rev. Lett.* **115** 204501
[202] Alexakis A and Brachet M-E 2019 *J. Fluid Mech.* **872** 594–625
[203] Verma M K 2019 *Eur. Phys. J.* B **92** 190
[204] Ray S S, Frisch U, Nazarenko S V and Matsumoto T 2011 *Phys. Rev.* E **84** 016301
[205] Burgers J M 1948 *Adv. Appl. Mech.* **1** 171–99
[206] Verma M K 2000 *Physica* A **277** 359–88
[207] Fermi E, Pasta J and Ulam S 1955 Studies of nonlinear problems *Technical Report LA-1940* http://users.mat.unimi.it/users/galgani/arch/FPU.pdf
[208] Arnold V I, Kozlov V V and Neishtadt A I 2006 *Mathematical Aspects of Classical and Celestial Mechanics* 3rd edn (Berlin: Springer)
[209] Christodoulidi H and Efthymiopoulos C 2019 *Math. Eng.* **1** 359–77
[210] Benettin G, Livi R and Ponno A 2008 *J. Stat. Phys.* **135** 873–93
[211] Barenghi C F and Parker N G 2016 arXiv:1605.09580
[212] Barenghi C F, Skrbek L and Sreenivasan K R 2014 *Proc. Natl Acad. Sci.* **111** 4647
[213] Sasa N, Kano T, Machida M, L'vov V S, Rudenko O and Tsubota M 2011 *Phys. Rev.* B **84** 054525
[214] Daniel García-Orozco A, Madeira L, Galantucci L, Barenghi C F and Bagnato V S 2020 *Europhys. Lett.* **130** 46001
[215] Hohenberg P C and Halperin B I 1977 *Rev. Mod. Phys.* **49** 435–79
[216] Novick-Cohen A and Segel L A 1984 *Physica* D **10** 277–98
[217] Ruiz R and Nelson D R 1981 *Phys. Rev.* A **23** 3224–46
[218] Perlekar P 2019 *J. Fluid Mech.* **873** 459–74
[219] Wyld H W J 1961 *Ann. Phys., NY* **14** 143–65
[220] McComb W D 2014 *Homogeneous, Isotropic Turbulence: Phenomenology, Renormalization and Statistical Closures* (Oxford: Oxford University Press)

[221] DeDominicis C and Martin P C 1979 *Phys. Rev.* A **19** 419–22
[222] Zhou Y 2010 *Phys. Rep.* **488** 1–49
[223] Adzhemyan L T, Antonov N V and Vasiliev A N 1999 *Field Theoretic Renormalization Group in Fully Developed Turbulence* (Boca Raton, FL: CRC Press)
[224] Zakharov V E, Falkovich G and Falkovich G 1992 *Kolmogorov Spectra of Turbulence I* (Berlin: Springer)
[225] Belinicher V I, L'vov V S, Pomyalov A and Procaccia I 1998 *J. Stat. Phys.* **93** 797–832
[226] L'vov V and Procaccia I 1995 *Phys. Rev.* E **52** 3840–57
[227] L'vov V and Procaccia I 1995 *Phys. Rev.* E **52** 3858–75
[228] L'vov V and Procaccia I 1996 *Phys. Rev.* E **53** 3468–90
[229] L'vov V and Procaccia I 1996 *Phys. Rev. Lett.* **77** 3541–4
[230] Fairhall A L, Dhruva B, L'vov V S, Procaccia I and Sreenivasan K R 1997 *Phys. Rev. Lett.* **79** 3174–7
[231] Onsager L 1949 *Nuovo Cimento* **6** 279–87
[232] Eyink G L and Sreenivasan K R 2006 *Rev. Mod. Phys.* **78** 87–135
[233] Das A and Bhattacharjee J K 1994 *Europhys. Lett.* **26** 527–32
[234] Gurarie V and Migdal A 1996 *Phys. Rev.* E **54** 4908–14
[235] Apolinario G B, Moriconi L and Pereira R M 2019 *Phys. Rev.* E **91** 033104
[236] Falkovich G, Gawędzki K and Vergassola M 2001 *Rev. Mod. Phys.* **73** 913–75
[237] Galtier S, Nazarenko S V, Newell A C and Pouquet A 2000 *J. Plasma Phys.* **63** 447–88
[238] Goldreich P and Sridhar S 1995 *Astrophys. J.* **438** 763–75
[239] Verma M K 2019 Hierarchical financial structures with money cascade *New Perspectives and Challenges in Econophysics and Sociophysics* ed F Abergel, B Chakrabarti, A Chakraborti, N Deo and K Sharma (Berlin: Springer)
[240] Kraichnan R H 1965 *Phys. Fluids* **8** 1385–7
[241] Iroshnikov P S 1964 *Sov. Astron.* **7** 566–71
[242] Biskamp D, Schwarz E and Drake J F 1996 *Phys. Rev. Lett.* **76** 1264–7
[243] Plunian F, Stepanov R and Frick P 2012 *Phys. Rep.* **523** 1–60
[244] Galtier S and Banerjee S 2017 *Phys. Rev.* E **96** 053116
[245] Teaca B, Jenko F and Told D 2017 *New J. Phys.* **19** 045001